NIST Special Publication 996

# On the Fractographic Analysis of Machining Cracks in Ground Ceramics:

## A Case Study on Silicon Nitride

George D. Quinn
Lewis K. Ives
Said Jahanmir

National Institute of Standards and Technology • Technology Administration • U.S. Department of Commerce

# *NIST* Technical Publications

## *Periodical*

**Journal of Research of the National Institute of Standards and Technology**—Reports NIST research and development in those disciplines of the physical and engineering sciences in which the Institute is active. These include physics, chemistry, engineering, mathematics, and computer sciences. Papers cover a broad range of subjects, with major emphasis on measurement methodology and the basic technology underlying standardization. Also included from time to time are survey articles on topics closely related to the Institute's technical and scientific programs. Issued six times a year.

## *Nonperiodicals*

**Monographs**—Major contributions to the technical literature on various subjects related to the Institute's scientific and technical activities.

**Handbooks**—Recommended codes of engineering and industrial practice (including safety codes) developed in cooperation with interested industries, professional organizations, and regulatory bodies.

**Special Publications**—Include proceedings of conferences sponsored by NIST, NIST annual reports, and other special publications appropriate to this grouping such as wall charts, pocket cards, and bibliographies.

**National Standard Reference Data Series**—Provides quantitative data on the physical and chemical properties of materials, compiled from the world's literature and critically evaluated. Developed under a worldwide program coordinated by NIST under the authority of the National Standard Data Act (Public Law 90-396). NOTE: The Journal of Physical and Chemical Reference Data (JPCRD) is published bimonthly for NIST by the American Institute of Physics (AIP). Subscription orders and renewals are available from AIP, P.O. Box 503284, St. Louis, MO 63150-3284.

**Building Science Series**—Disseminates technical information developed at the Institute on building materials, components, systems, and whole structures. The series presents research results, test methods, and performance criteria related to the structural and environmental functions and the durability and safety characteristics of building elements and systems.

**Technical Notes**—Studies or reports which are complete in themselves but restrictive in their treatment of a subject. Analogous to monographs but not so comprehensive in scope or definitive in treatment of the subject area. Often serve as a vehicle for final reports of work performed at NIST under the sponsorship of other government agencies.

**Voluntary Product Standards**—Developed under procedures published by the Department of Commerce in Part 10, Title 15, of the Code of Federal Regulations. The standards establish nationally recognized requirements for products, and provide all concerned interests with a basis for common understanding of the characteristics of the products. NIST administers this program in support of the efforts of private-sector standardizing organizations.

*Order the* **following** *NIST publications—FIPS and NISTIRs—from the National Technical Information Service, Springfield, VA 22161.*

**Federal Information Processing Standards Publications (FIPS PUB)**—Publications in this series collectively constitute the Federal Information Processing Standards Register. The Register serves as the official source of information in the Federal Government regarding standards issued by NIST pursuant to the Federal Property and Administrative Services Act of 1949 as amended, Public Law 89-306 (79 Stat. 1127), and as implemented by Executive Order 11717 (38 FR 12315, dated May 11, 1973) and Part 6 of Title 15 CFR (Code of Federal Regulations).

**NIST Interagency or Internal Reports (NISTIR)**—The series includes interim or final reports on work performed by NIST for outside sponsors (both government and nongovernment). In general, initial distribution is handled by the sponsor; public distribution is handled by sales through the National Technical Information Service, Springfield, VA 22161, in hard copy, electronic media, or microfiche form. NISTIR's may also report results of NIST projects of transitory or limited interest, including those that will be published subsequently in more comprehensive form.

# On the Fractographic Analysis of Machining Cracks in Ground Ceramics:

# A Case Study on Silicon Nitride

George D. Quinn
Lewis K. Ives
Said Jahanmir
*Materials Science and Engineering Laboratory*

May 2003

Certain commercial entities, equipment, or materials may be identified in this document
in order to describe an experimental procedure or concept adequately. Such
identification is not intended to imply recommendation or endorsement by the National
Institute of Standards and Technology, nor is it intended to imply that the entities,
materials, or equipment are necessarily the best available for the purpose.
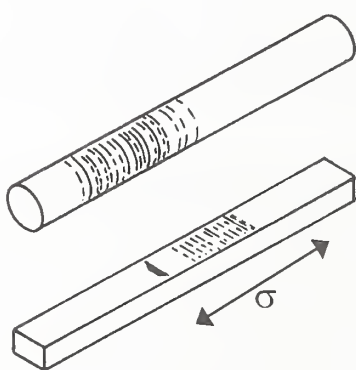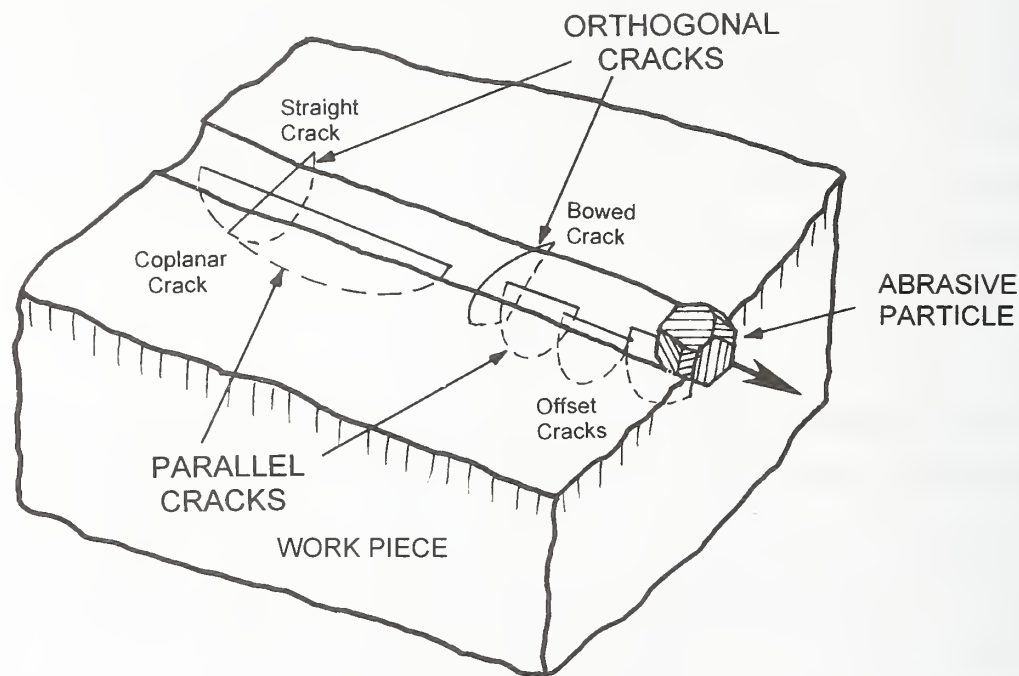
# TABLE OF CONTENTS

# ABSTRACT

Meticulous fractographic analysis of broken flexural strength specimens was used to characterize the size, shape, and severity of grinding flaws in a commercial silicon nitride. The cylindrical rods and rectangular bars were prepared by a variety of grinding procedures. Grinding flaw size correlated strongly with grinding direction and wheel grit size. Cracks depths from as small as 12 μm to as large as 80 μm were measured. Copious illustrations of machining cracks are provided. Some grinding treatments had no deleterious effect on strength since the machining cracks were very small and fracture occurred from the material's inherent flaws. Telltale signs of machining damage were found with conventional low power optical microscopy using simple fractographic techniques. The telltale signs are summarized in a new series of schematic drawings that will aid pattern recognition for engineers and fractographers. These schematics will make detection of machining cracks much easier. Machining damage maps for silicon nitride are presented.

# INTRODUCTION

Micro crack formation in the work piece is an integral part of the process of diamond abrasive surface grinding of ceramics. Residual surface cracks may act as strength limiting flaws that degrade the strength of the ceramic component or test piece. **Figures 1-3** show several depictions of these machining cracks. Optimal machining procedures for ceramics allow rapid, cost effective material removal while minimizing or controlling the residual damage in the work piece. Surface grinding processes often feature several grinding stages. Rough and intermediate grinding is done with coarse or medium grit wheels and aggressive removal rates to bring the part close to final dimensions. Finish machining then is applied to remove the prior damage, to obtain correct final part dimension and finish, and to avoid or minimize introduction of deleterious cracks or residual stresses.

The present study was initiated as part of a NIST Consortium program to optimize ceramic machining practices. Findings from earlier phases of the Consortium program have been presented previously.[1,2,3,4,5,6,7] One component of this program was to investigate machining damage in ground ceramics. Flexural strength specimens are ideal for the study of machining flaws in as much as they are very sensitive to surface flaws. Both conventional rectangular bar and cylindrical rod specimens were evaluated in the study. The bar specimens were tested in accordance with well-known standard test methods. Analogous standards for rod specimens do not yet exist, and the present study was undertaken as part of a prestandization effort to prepare just such a standard test method. Cylindrical test pieces are preferred to rectangular beam specimens in many instances, particularly if the material is fabricated in

1

*Figure 1* Schematic of flaws introduced by machining or scratching a ceramic or glass surface. An abrasive grit particle moves from left to right. Long coplanar or short overlapping semi-elliptical parallel cracks form in the direction of abrasive motion. Short orthogonal cracks form perpendicular to the abrasive motion direction. Orthogonal cracks are either similar in depth or shallower than the parallel cracks. The parallel cracks are especially severe due to their greater length and stress intensity shape factor. This causes a dependence of specimen strength on the direction of machining if machining cracks are strength limiting.



ORTHOGONAL CRACKS

Straight Crack

Bowed Crack

Coplanar Crack

ABRASIVE PARTICLE

Offset Cracks

PARALLEL CRACKS

WORK PIECE

Transversely-ground specimens

Flexure testing activates the parallel machining cracks
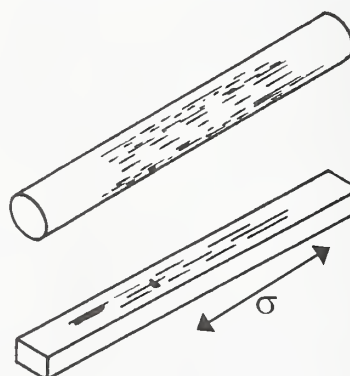
Longitudinally-ground specimens

Flexure testing activates the orthogonal machining cracks

2

*Figure 2* Schematic of machining cracks as they may appear when viewing the fracture surface. The cracks may link (a); link and extend (b); or overlap (c).
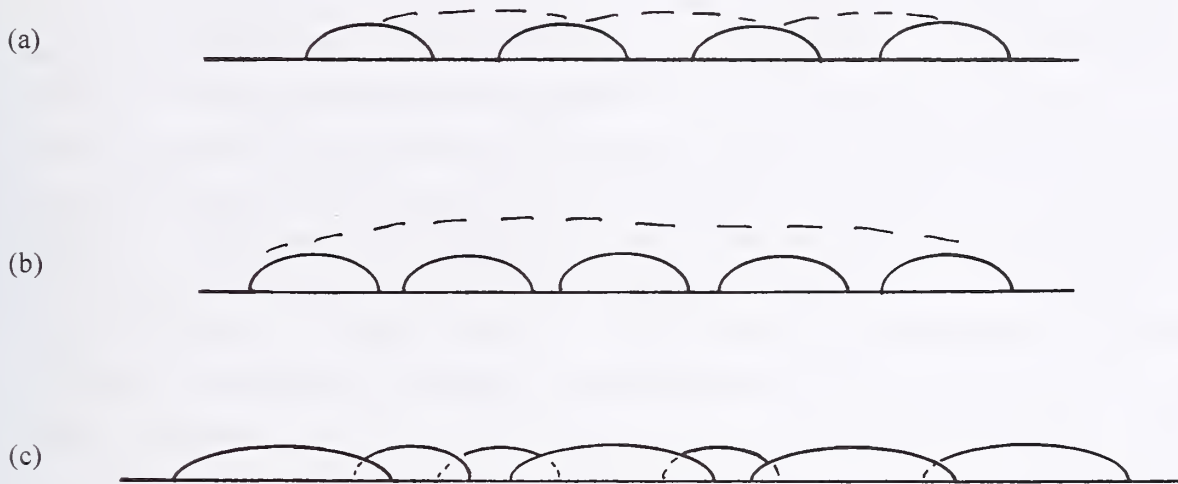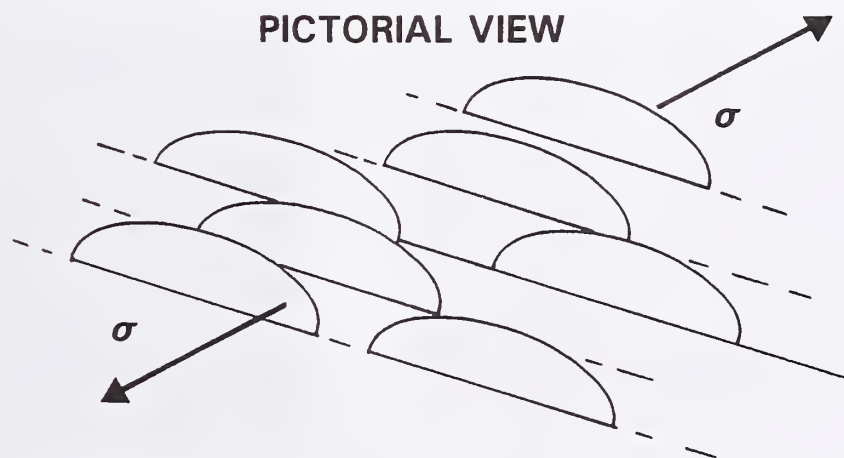
(a)

(b)

(c)

*Figure 3* Schematic of machining cracks in a ground surface with a stress applied as shown. The cracks may interact or link in various ways depending upon their density, relative sizes, locations and orientations.

**PICTORIAL VIEW**

$\sigma$

$\sigma$

cylindrical shape or the application is for a cylindrical component. The rods also do not have edges which are vulnerable damage sites in rectangular beam specimens. One might expect that for cylindrical component reliability analysis, the strength data from rod shaped specimens would be more useful than data from rectangular beam specimens

Many studies have investigated the effects of surface grinding and heat treatments on flexure strength of cylindrical rods (e.g., [8,9,10,11]) or rectangular beam specimens (e.g., [12,13,14,15,16,17, 18,19,20,21,22,23,24,25,26,27]). Although some of these studies have shown a few illustrative machining flaws, more often than not a detailed characterization of the machining flaws such as their size, shape, and morphology, and density has been lacking. Correlations of flaw characteristics with grinding conditions are rare. The usual approach is to use several grinding procedures to prepare many test specimens that are then fractured in a bend strength test. Results are shown as Weibull distribution curves or data tables and machining effects are inferred from strength degradations. Little or no corroborative fractographic information is given. Notable exceptions to this approach have been the studies of Hollstein et al.[28]; Rice, Mecholsky and colleagues [29,30,31,32]; and Foley, Pujari and colleagues [33,34] wherein the sizes and shapes of machining cracks in many specimens were reported. Nonetheless, very little work has been done to systematically correlate the size and severity of machining flaw cracks to the grinding conditions that created them. Very little work has been done to compare the machining flaws created by different machine shops attempting to grind to the same specifications [Refs. 15,18,35,36].[a] How consistent is the machining damage from shop to shop?

One important reason for the paucity of good fractographic characterization of machining flaws is that machining flaws *are* elusive in many ceramics. They are relatively easy to detect in homogeneous materials such as glasses, very fine-grained fully dense ceramics, or some very coarse-grained materials wherein the machining crack may be entirely within one grain. Machining flaws may be quite small; of the order of 10 μm to 50 μm in size, and careful microscopy is required to find them in many polycrystalline ceramics since they often blend into the background microstructural features. It is not uncommon for a fractographer to readily find a fracture mirror centered on a surface origin location, but not find an obvious defect at the origin. This has led some fractographers to *guess* that the origin must be machining damage.[b] Sometimes machining cracks are confused with other fracture origin types such as scratches or handling damage.

---

[a]   Quinn [35] found significant variability in the quality and strengths of rectangular bend specimens prepared by five machine shops to the requirements of Military Standard 1942(MR) test method. The variability was traced to billet-to-billet differences in the material flaws, however, and not to variations in the machining flaws. Allor et al. [15] similarly observed billet-to-billet variations in hot pressed silicon nitride, but crucial differences between the procedures used in five different machine shops also contributed to variability. Richter [36] was concerned that five different shops could not produce bend specimens with comparable strengths when working to specifications in a European standard. Breder et al. [18] observed strength variability of as much as 200 MPa with repeated batches from one shop, and batches from different shops. On the other hand, Ives et al. [3,4] observed fairly consistent strength results for bars prepared by eight machine shops, both with repeated sample batches from one shop and batches from different shops.

[b]   The origin could be a seam of microporosity, a delamination from a crack in the green state, a contact damage crack, a scratch, or some other flaw the fractographer does not recognize. A fracture origin located directly on the surface *may* be machining damage.

An ASTM standard [37] for fractographic characterization of fracture origins in ceramics facilitates machining damage crack identification. Nonetheless, it cannot be denied that machining cracks are difficult to detect against the background microstructural features in some ceramics, even for experienced fractographers. These difficulties were underscored in a Versailles Advanced Materials and Standards (VAMAS) international fractography round robin project that, as one task, asked participants to identify and characterize machining cracks [38,39].

One objective of the present study was to refine techniques to find machining cracks and to make their identification easier for engineers and fractographers. Fractographic analysis entails pattern recognition. Fracture surfaces and fracture origins have tell tale markings which may be interpretable by the fractographer. As we will show, machining cracks do have distinctive features that can aid their detection and interpretation. Some simple techniques with conventional optical microscopy are effective. Copious illustrations and schematic drawings are furnished of several important classes of machining cracks in this paper.

Residual stress determinations were unfortunately not part of the study. As will be discussed in the results section, their influence was thought to be of secondary importance as inferred from fracture mechanics analysis of the machining crack origins.

This program included testing of glass, alumina, silicon carbide, and several silicon nitrides. In this paper we present detailed results for one particular sintered reaction-bonded silicon nitride with primary emphasis on the fractographic findings. Results are compared to findings from other silicon nitrides. How severe are machining cracks, when do they control strength, and how can fractographers find them more easily?



2µm 10000X

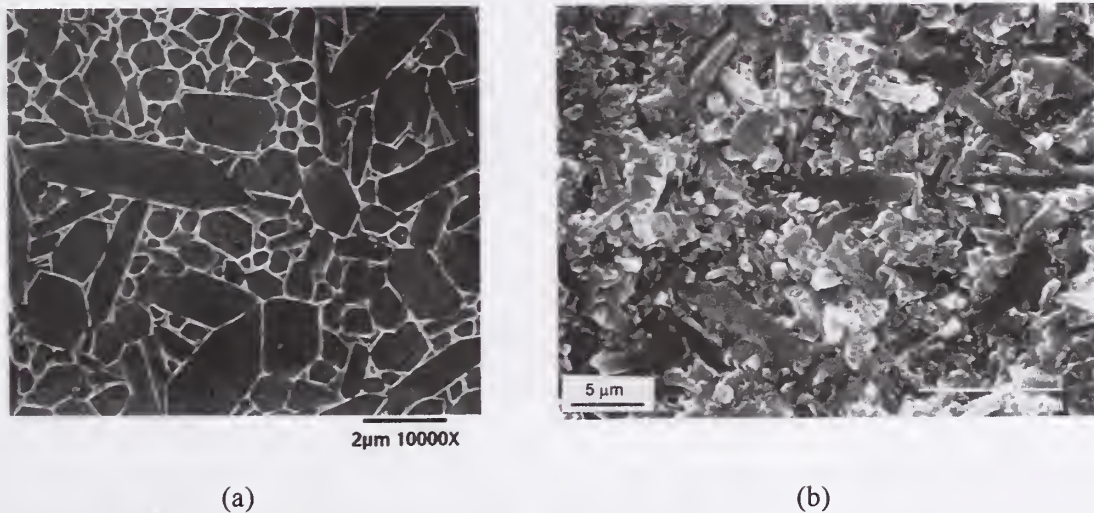(a)                                                                                    (b)

*Figure 4*   Microstructure of the SRBSN in this study. (a) shows a polished and etched section.
(b) shows an SEM photo from a region inside a specimen fracture mirror, but not at the origin.

# MATERIAL

A sintered reaction-bonded silicon nitride (SRBSN)[c,d] containing yttria and alumina was used in this study. The material is in full-scale production for several applications including cam roller followers in a diesel engine and pump valve components for the oil extraction industry. This SRBSN has needle-like beta silicon nitride grains, 0.5 μm to 3 μm wide by up to 10 μm long, bonded by a second phase as illustrated in **Figure 4**. The material was designed to have enhanced fracture toughness as discussed below. The manufacturer lists the elastic modulus as 310 GPa - 320 GPa, the strength as > 700 MPa, density as 3.21 $g/cm^3$, and the Vickers hardness as 17.6 GPa and 15.4 GPa at 2.9 N (0.3 kgf) and 49 N (5 kgf) indentation loads, respectively. Silicon starting powders were isopressed into oversized green-body rods that were nitrided and then gas-pressure sintered. The rods were nominally 7.5 mm in diameter by 111 mm long after sintering. The material was received in two lots in 1999. Two rods were sectioned, mounted and polished in order to search for any evidence of microstructural gradients. The polished sections were examined with a reflected-light microscope[e] and photographed in bright field, dark field, differential interference contrast, and fluorescence modes at up to 1000X. A fluorescent dye penetrant was used to search for microporosity. Slight variations in the microstructure were hinted at by differences in the reflectivity and translucency of polished specimens as shown in **Figure 5**.
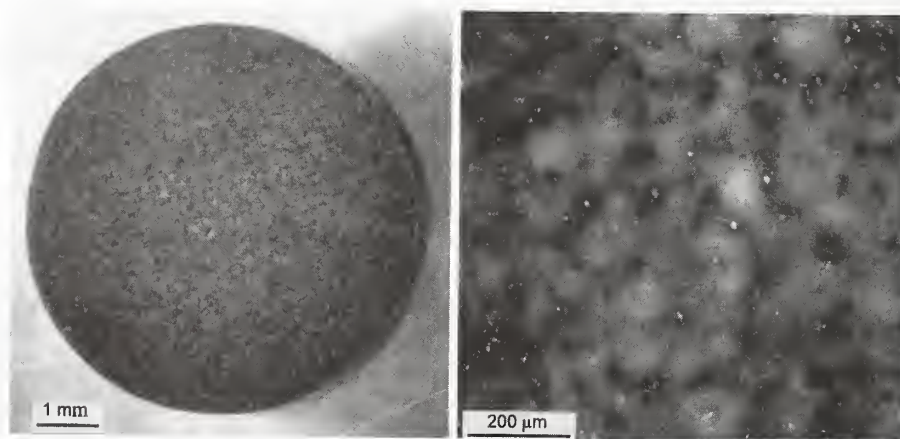


*Figure 5* Reflected light micrographs of a rod cross section showing some minor reflectivity and transparency variations. (b) is a close up of (a). The white specks are inclusions which have a slightly greater concentration in the outer 1 mm of the rod

---

No obvious gradient in microstructure was detected with the sole exception that within the outer 0.8 mm to 1.2 mm of the 6 mm diameter specimens, a few more reflective spots were detected, probably from a slightly greater inclusion content.

For comparative purposes, we include data from two sets of rectangular bend specimens that were cut from SRBSN plates. These specimens were prepared for an earlier phase of the Consortium program.

The fracture toughness of this material has been measured by the three methods in ASTM C 1421 [40] and virtually identical outcomes were obtained. The surface crack in flexure (SCF) and single-edged precracked beams (SEPB) methods gave values of 5.4 MPa√m ± 0.4 MPa√m and 5.6 MPa√m ± 0.2 MPa√m, respectively [41].[f] Chevron notch (CN) testing [42] produced 5.3 MPa√m ± 0.2 MPa√m. The small SCF precracks (50 μm – 70 μm) that were created by the 49 N indentation load prescribed in C 1421 were difficult to detect and required stereo SEM photos. Larger precracks made at indentation loads of 98 N or greater were much easier to detect since the precracks stood out clearly against the microstructure. Small amounts of stable crack extension may have occurred in several specimens. Although these three methods produce converging results for a very broad range of crack sizes (50 μm – 2 mm), there is evidence that the material does have a rising R-curve. [43,44,45]
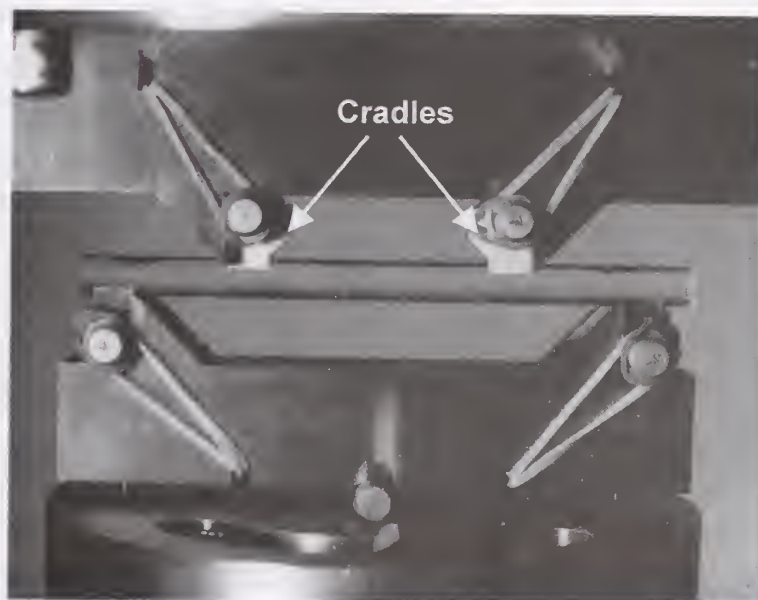


**Cradles**

*Figure 6* The four-point fixtures used for the rod flexural strength tests. Cradles on the top (arrows) and bottom apply the load evenly to the specimens on the top and bottom.

---

[f]    One standard deviation.

## EXPERIMENTAL PROCEDURES

### Flexural Strength Tests

Flexure testing is an ideal method to accentuate surface machining flaws in rod or rectangular bar specimens. Sample sets of 10 or 30 rod or bar specimens were prepared and tested per grinding condition. All cylindrical rods were 6.0 mm in diameter by 100 mm long and were transversely- or longitudinally ground as described below. Rods were tested on a four-point flexure fixture specifically designed for cylindrical rod specimens **(Figure 6)**. The spans were nominally 40 mm x 80 mm and the crosshead rate was 1.3 mm/min. The fixture is a typical semi-articulating design with the key exception that it has four cradles at the load distribution points.[7] These cradles distribute the load evenly onto a test piece and avoid severe contact stresses or wedging stresses that would otherwise occur with crossed cylinders if the rod specimens were placed directly on loading rollers as is normally done with rectangular bars. The loading geometry is equivalent to the classic four-point configuration and the stress state is identical except in the immediate vicinity of the cradles. The loading rollers are free to roll to eliminate frictional constraint forces. In keeping with customary practice, the flexural strengths reported are the maximum ("outer-fiber") stresses that existed in the rod specimen at the instant of fracture even though the rods experience the maximum stress only on a very small region (a line) on the specimen bottom. [g]

All rectangular bars were "B" sized (3 mm x 4 mm x 45 mm) four-point flexure specimens prepared in accordance with ASTM C 1161 [46]. Specimens were either longitudinally- or transversely ground as described below. The four long edges were chamfered in accordance with C 1161. Only a few specimens fractured from edge damage in this entire study. Specimens were tested with fully-articulating four-point fixtures with 20 mm and 40 mm spans under laboratory ambient testing conditions (21°C – 25°C; 40 % - 70 % R.H.) with a crosshead displacement rate of 0.5 mm/min as per ASTM C 1161.

The rods and bars were different in size but the Weibull effective volumes and effective surfaces were actually quite similar.[47,48] In fact, the bars had greater effective surfaces since they had a large surface region (4 mm wide x 20 mm long) within the inner fixtures spans whereas the rods only had a tiny surface region (a line) that experienced the maximum tensile stresses within the inner span. For example, using a Weibull modulus of 16, the rods and bars had effective volumes of 13.1 mm$^3$ and 7.5 mm,$^3$ respectively. Effective surfaces were 77.4 mm$^2$ and 88.4 mm,$^2$ respectively. Weibull strength scaling predicts the strengths should agree within a few percent for these volume or surface ratios.[h] Hence, any major differences in strengths must have been due to differences in flaw type, severity, or density and not Weibull size scaling effects.

---

[g] The maximum stress in the rod is also required for Weibull analyses. The only instances that the stress should be adjusted for the location of fracture are when computing fracture mirror constants and when performing fracture mechanics analysis of the flaw at the origin.

[h] Using different Weibull moduli alters the effective surfaces and volumes, but does not change the overall conclusion that the strength differences should be very small. For example, for an m of 27, the effective volumes are 6.0 mm$^3$ and 4.4 mm$^3$ for rods and bars, respectively. The effectives surfaces are 58.8 mm$^2$ and 85.0 mm$^2$, respectively.

The fracture origin locations were monitored in every instance. Origin locations were usually evenly distributed within the inner gage section with no tendency to cluster at the loading rollers or loading cradles in the case of the rods. An occasional primary fracture did occur at or near an inner loading point or cradle. Secondary breakages were quite common at the loading points, but a careful inspection of specimens with multiple fractures usually confirmed that the primary fracture origin was in the inner gage section. Interpretation of primary and secondary breakage patterns in flexural specimens is reviewed in ASTM standards C 1322 and C 1161.[i]

**Fractographic Analysis**

The overall fractographic analysis was performed in accordance with ASTM C 1322. All fracture surfaces of every specimen in this study were examined with a stereo binocular microscope[j] at magnifications up to 205X. It was initially felt that optical microscopy would not be effective in finding and characterizing the machining cracks, but experience proved this notion was wrong. A video camera fed images to a printer that could make hard copies of the images. Part way through the program, a newer high-resolution digital camera[k] and a computer replaced the video camera and printer. The newer digital camera recorded very sharp images. We discovered that proper illumination was crucial to finding and characterizing the machining cracks. It was essential to illuminate the specimen fracture surface from the *side or rear with a bright, low incident angle* (vicinal) illumination source as shown in **Figure 7**. This low angle illumination accentuated many crucial, tell tale features of machining damage, as the pictures in this paper will demonstrate. Illumination from directly above the specimen fracture surface washed out many key features. Contrast was reduced and helpful shadows lost. Low angle illumination from the same side of the specimen that contained the machining cracks was also inadvisable, since the illumination blurred key fracture surface features on the specimen edge at the origin and the material was partial translucent. Although we used an elaborate discussion stereomicroscope for these examinations **(Figure 7a),** the same image quality is obtainable with simpler stereomicroscopes as shown in **Figure 7b.** The key to success was having a stereomicroscope that was capable of 100 X –200 X magnifications and a bright directional illumination source. Simple specimens holders such as shown in **Figure 7c** were also helpful in aiding the examination.

Selected specimens (as many as one-half of a sample set) were examined with a scanning electron microscope (SEM).[l] Multiple photos were taken with the SEM to ensure that both the fracture mirror and

---

[i] Secondary fracture planes often were not quite perpendicular to the specimen's long axis or the symmetry of a typical primary fracture plane was missing. The tilts and asymmetries are due to elastic energy reverberations in the specimen. In some instances, the secondary fracture origins were located on the top side of the specimen, in what was originally the compression side of the specimen since elastic wave reverberations changed the phase of the stress field. With a little experience, secondary fractures can often be identified within seconds, especially if the loading points and tensile and compressive surfaces have been marked before testing.
[j] Wild Model M-10 discussion stereomicroscope that allowed two viewers to simultaneously view a fracture surface.
[k] Spot Insight, 1600 x 1200 color pixels, Media Diagnostics, Sterling Heights, MI.
[l] Hitachi Model S-530.

**Figure 7** Stereo optical microscopes used to find the fracture origins. (a) shows the Wild M10 discussion stereo microscope used in the study. (b) shows a more common stereomicroscope. Notice the intense, directional, low angle illumination applied to the specimens. Machining cracks may be highlighted by such illumination from the specimen side. (c) shows simple specimen holders such as the alligator clip mount on the left that enabled specimens to be quickly mounted and tilted around while viewing through the microscope. The other holders enabled a fractured specimen to be assembled and lined up in convenient grooves for examination of the ground surfaces. (d) shows low angle grazing (vicinal) illumination.
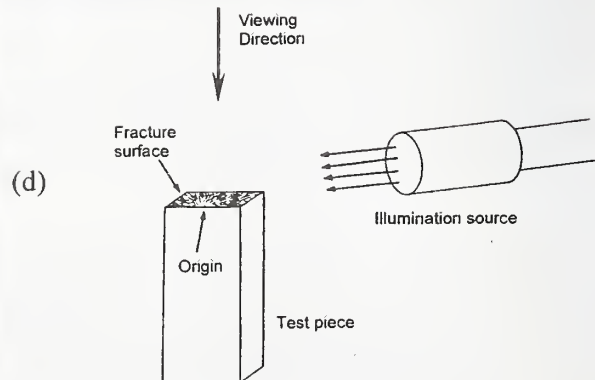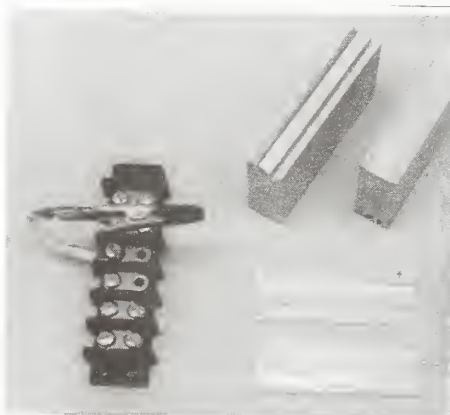
(a)

(b)

(c)

(d)

Viewing Direction

Fracture surface

Origin

Illumination source

Test piece
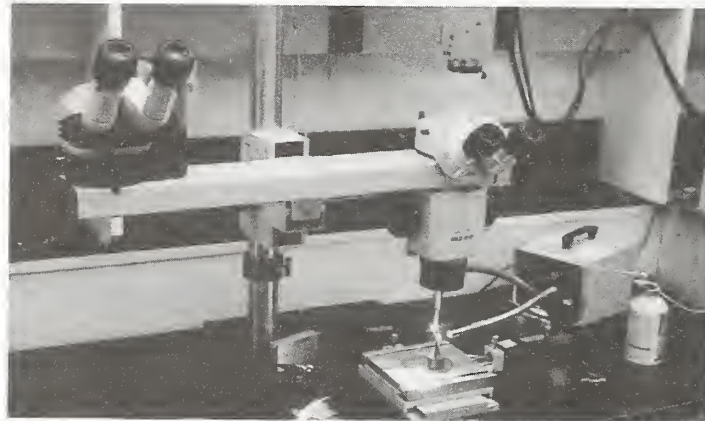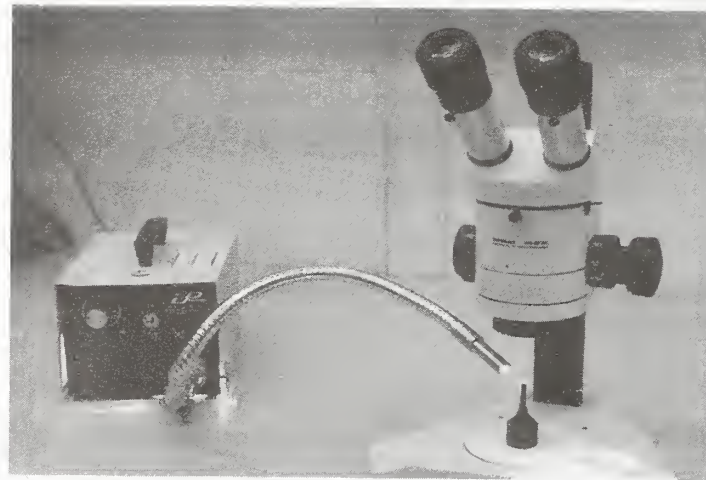
the fracture origin were recorded. Matching fracture halves were frequently examined in the SEM. Stereo pairs of SEM photos were sometimes taken and were especially valuable in ascertaining the topography of the machining cracks. This intensive level of fractographic study is warranted for machining damage, which as we have noted above, can be difficult to discern against the background microstructure. Not every specimen was examined this thoroughly, but within a give set, it was common to examine as many as 30% of the specimens in the SEM.

As the study progressed, and we gained greater experience in detecting the tell tale features of machining damage cracks, we were able to speed up our inspection process and optimize photo taking. By the end of the study, we could immediately identify transverse grinding machining damage on the first inspection with the stereomicroscope in this SRBSN material. We often followed the guidance of ASTM C 1322 and took a full suite of three or more photos from each fracture surface showing the entire fracture surface, the fracture mirror, and the fracture origin.

Fracture mirrors were invaluable in leading attention to the fracture origins. The angular location of the fracture origin relative to bottom dead center (where the tensile stress was a maximum) was measured in all the rod specimens. This enabled the stress at the exact fracture location to be calculated for fracture mirror and fracture mechanics analysis. Details of this procedure and two maps showing the distribution of fracture origin locations in rod specimens are in **Appendix A**. Fracture mirror sizes were measured with the stereo binocular microscope, while viewing at 30X – 63X through the eyepieces. In general, we found it convenient to view the fracture surface with a magnification such that the mirror region covered one-third to one-half the field of view. Mirrors were plainly evident at low magnifications, but accurate assessment of their size was difficult. The mirror region was somewhat bumpy in this self-reinforced silicon nitride, so some judgment as to what was the mirror boundary was necessary. The criterion used in the present study was that the mirror boundary occurred at the point where hackle commenced and there was an obvious roughness change relative to the mirror. Full details on the mirror measurements are in **Appendix A**.

Hereafter in this paper, we will refer to machining cracks as either *parallel* cracks or *orthogonal* cracks. The qualifier denotes the orientation of the crack plane relative to the *grinding direction*. **Figure 1**, which is adapted from a figure by Rice and Mecholsky [29],[m] is a schematic of flaws introduced by machining or scratching a ceramic or glass surface. Semi-elliptical *parallel cracks* form parallel to the abrasive motion direction. These may either be long coplanar cracks or shorter overlapping cracks. Short *orthogonal cracks* form perpendicular to the abrasive motion direction. Orthogonal cracks are either

---

[m] There are two primary changes to their figure. First, the bowed orthogonal cracks are corrected to bow in the *direction of the abrasive motion*. Secondly, Rice and Mecholsky used the terms "longitudinal" and "transverse" in a manner that caused some confusion. They used the terms to describe the cracks with respect to the grinding direction. The long cracks parallel to the machining direction were called "longitudinal cracks", and the shorter orthogonal cracks were called "transverse cracks." Using their nomenclature, flexure testing of *longitudinally*-ground bend bars would activate *transverse* cracks and vice versa. The new nomenclature shown in Figure 1 eliminates this confusion.

*Figure 8* Orthogonal machining cracks. (a) and (b) show a machining crack in a fine grained hot-pressed silicon nitride. The specimen has been tilted back to show the ground surface, labeled "T" for tensile surface. The machining crack (white arrows) is much deeper than the striations. (c) shows a crack in a hot-pressed silicon carbide. The single striation (black arrow) is helpful in making the interpretation.
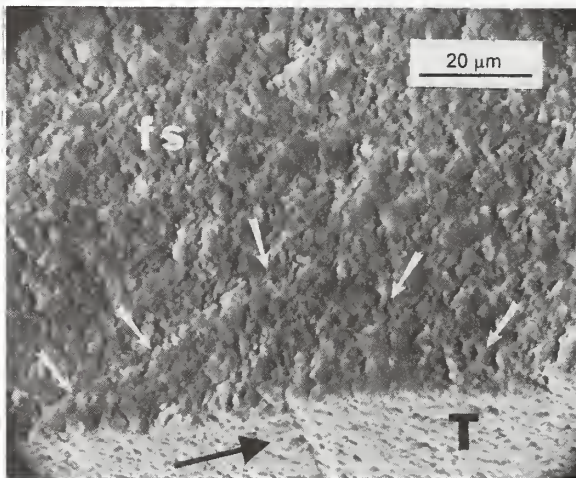
(a)
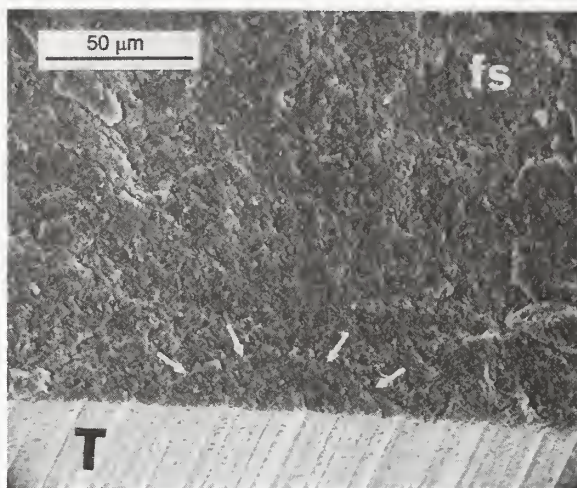
(b)
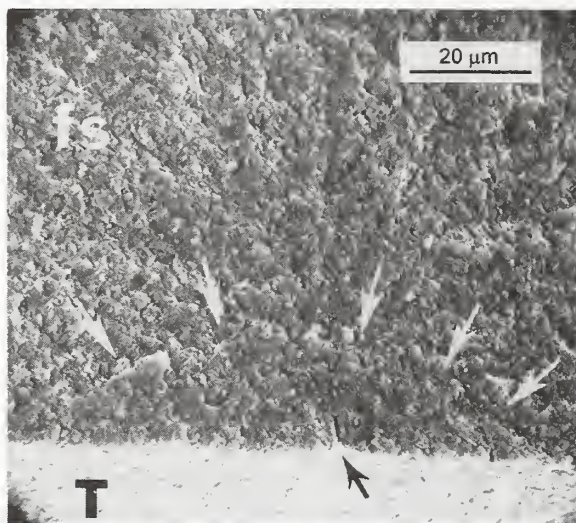
(c)

similar in depth or deeper than parallel cracks for a given grinding condition [29-31], but the parallel cracks are much severer due to their greater length and stress intensity shape factor [49]. The difference in size and shape of the orthogonal and parallel cracks usually causes a dependence of specimen strength on the direction of machining *if* machining cracks are strength limiting. Transversely ground specimens are usually weaker than longitudinally ground specimens.

Parallel machining cracks were not too difficult to detect on fracture surfaces when they were strength limiting, no matter how small they were. With some experience, we could routinely detect them even with the stereo optical microscope. Orthogonal cracks may be easy to detect in glasses, some very fine-grained materials, single crystals, or in very coarse-grained materials in which the crack is within a single grain. On the other hand, they are very difficult to detect in materials in which the microstructure masks the cracks, e.g., materials with medium to coarse grain sizes, some toughened ceramics, and composites. **Figure 8** shows orthogonal cracks in fine-grained hot-pressed silicon nitride and silicon carbide. Unfortunately such cracks, which are typically of the order of 10 μm to 50 μm in size (depending upon the grinding conditions), blended in or "hid" very well on the SRBSN fracture surfaces. The SRBSN has rough fracture surfaces even in the mirror region. In any event, only a few sets of longitudinally prepared specimens were studied in the final phase of the NIST Machining Consortium program since earlier work had shown that longitudinal grinding had little or no effect upon strength of this SRBSN.[1-6]

To improve our fractographic skills at detecting small semicircular cracks in this SRBSN, we tried a series of fracture toughness experiments using artificially created tiny SCF precracks. In this test, which is one of the methods in the ASTM standard C 1421, a Knoop indenter is used to create an artificial semicircular or semielliptical flaw in a bend bar. The exact fracture location is controlled and subsequent fractographic analysis can concentrate on finding the markings and features that distinguish the crack from the background microstructure.[50] The artificial flaw size was controlled by changing the indentation load. Semielliptical or semicircular precracks made at loads of 98 N or greater ($\approx 100 - 150$ μm deep) were relatively easy to detect in this SRBSN as shown in **Figure 9b**. Precracks made with 49 N ($\approx 60$ μm deep) were very difficult to discern and required meticulous stereo SEM microscopy. Artificial cracks made at 29.6 N load ($< 50$ μm deep) could not be detected.

Size estimates of the parallel crack and material flaw origins were made with the 1 μm resolution precision traversing stage in the stereomicroscope **(Figure 7a)** and from SEM photo analysis. Crack depths (a) could often be measured to within 5 μm or better, although in some problematic specimens the uncertainty was as much as 10 μm. The crack width (2c, the length along the ground surface) dimensions had greater uncertainties. Uncertainties of 20 μm - 40 μm were common, and in some instances the uncertainty for parallel cracks was as much as 50 μm –100 μm. The uncertainty in the width dimension is of less concern, since the depth dimension is the controlling dimension for determining the stress intensity, $K_1$ for a long surface crack.[49] Once a crack surface length becomes long, the stress intensity

*Figure 9* SEM photos of artificially introduced Knoop semielliptical flaws. (a) shows a $\approx 50$ μm deep crack made in a fine-grained hot-pressed silicon nitride (NC 132) with the 25 N Knoop indentation still intact (smaller arrows). (b) shows a 135 μm deep crack in the SRBSN introduced by 144 N Knoop indentation (white arrows), with the indentation and residual stress damage zone removed. Despite the greater surface roughness, the large semielliptical precrack is detectable. Changes in direction of micro hackle at the boundary (small black arrows) helped identify the critical crack size. Knoop flaws (< 5 N load, < 50 μm deep) could not be detected in this material.

(a)                                                    (b)
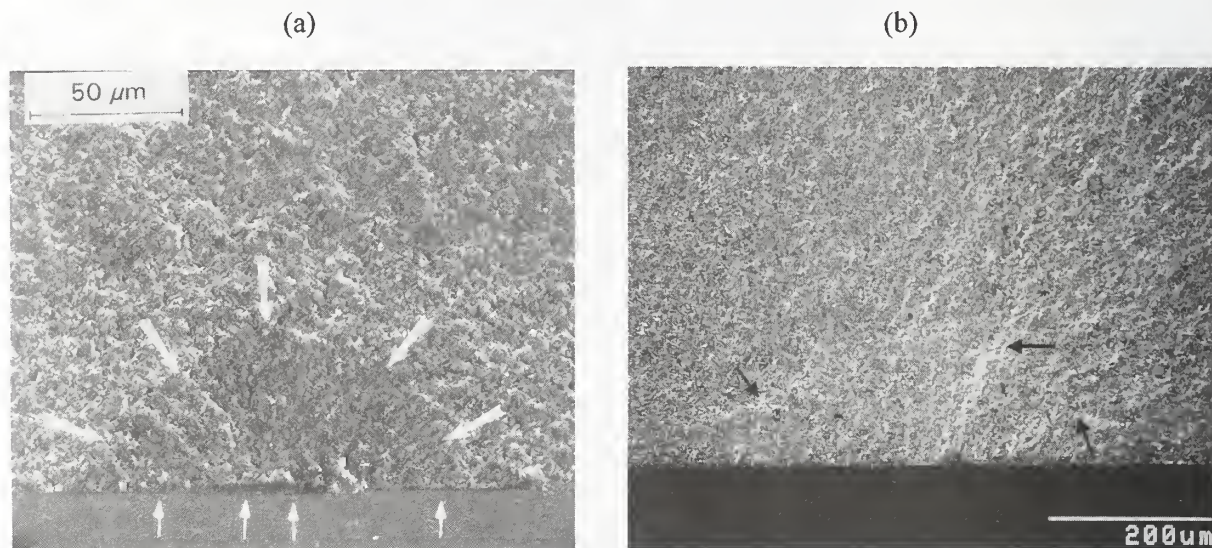


shape factor Y approaches 1.99 for the case of a long surface crack and additional length increases along the surface have negligible effect on the stress intensity factor.

**Specimen Machining Preparation**

The rods and bars were ground with conventional resin bond diamond abrasive grinding wheels. Bar specimens were surface ground either perpendicularly (transversely) to or longitudinally to the bar long axis. Rods were primarily transverse centerless or cylindrical ground, although in one instance, longitudinal grinding was applied. The well known rectangular *bar* flexure strength *standard test methods* specify longitudinal grinding to control the orientation of machining damage cracks and minimize the chance that the machining cracks will control strength.

Groups of 10 or 30 specimens were prepared by several shops, designated C, F, N, S, and W, which participated in the consortium program.[n] Key preparation steps are summarized below, but more details of the grinding conditions are in **Appendix B**.

---

[n]    NIST was "shop N."

Rod specimens were ground down from the 7.5 mm diameter blank rods to 6.00 mm diameter x 100 mm long in several steps. As we will show, the inherent strengths were obtained with one set prepared by Shop C which used longitudinal centerless finish grinding with a wheel depth of cut of 0.005 mm for 5 passes at an axial feed rate of 3.6 mm/s with a 2000 rpm work piece rotational speed. For comparison, this shop also prepared one set of 30 specimens with conventional centerless grinding with a 320 grit, 203 mm diameter wheel with 0.05 mm wheel depth of cut to initially grind the rods to 6.025 mm. Rods were then finished down to 6.00 mm by conventional transverse centerless grinding with a 0.005 mm wheel depth of cut for 5 passes at a slow axial feed rate of 2.54 mm/s at a 680 rpm work piece rotational speed. The work piece rotational speeds were set to approximately match the volumetric rates of material removal obtained in comparable sets of rectangular *bars* described below.

Other shops also prepared rods by transverse or centerless grinding with various wheel grits. Three shops used 600 grit centerless or transverse cylindrical finish grinding in order to minimize the machining crack severity. As we will show, they obtained similar results. Shop F prepared one set by transverse centerless grinding. Shop N used a three-step procedure, starting with centerless grinding with a 180 grit, 254 mm diameter wheel with an in feed of 0.050 mm per pass down to 7.05 mm diameter, then switching to an intermediate step of 400 grit, 250 mm wheel with 0.013 mm/pass down to 6.3 mm specimen diameter, then finishing the specimens down to 6.00 mm with a 600 grit, 203 mm diameter wheel with 0.005 mm/pass. Shop W used a two-step process, starting with a 320 grit, 203 mm wheel with rods mounted on centers, plunge grinding down to 6.30 mm – 6.35 mm diameter, then finish grinding with a chuck cylindrical grinder and a 600 grit, 203 mm wheel with 0.025 mm/pass and a longitudinal feed (work piece) of 254 – 305 mm/min.

Shop N prepared one set of 10 transverse centerless ground rods with a 220-grit wheel.

Shop F prepared one set by transverse centerless grinding, but with an unknown, apparently very coarse grit wheel that was subsequently estimated to have been 150 grit or 180 grit judging by the surface roughness. This set probably was prepared with the shop's normal rough grinding procedure and the finish-grinding step was inadvertently omitted. The data were useful nonetheless, since they represent the severe damage that may occur with rough grinding.

In contrast with the grinding processes described above, one shop finished their rod specimens by lapping. Shop S rough ground their rods by an unidentified procedure, but evidently centerless or cylindrical transverse grinding. Two separate groups of three specimens were then carefully lapped (with an unspecified amount of material removed) in an attempt to remove the surface damage.

Several rectangular bend *bar* sets were ground for comparison to the rod data. Most 3 mm x 4 mm x 50 mm cross-section rectangular bars were cut from the 7.5 mm diameter rod blanks. Shop C prepared two lots of 30 standard "B" rectangular bar*s,* one group ground transversely and one group ground longitudinally in accordance with the ASTM C 1161 "baseline" procedure. Shop F produced one

batch of 30 rectangular bars ground transversely with a 600-grit wheel using procedures that closely matched the transversely ground rods that they also prepared.

Two rectangular bar sets, which were from an earlier phase of this study, are included here for comparison. Shops C and F prepared rectangular bars by transverse grinding with 150 grit and 80 grit wheels, respectively. These specimens were cut from SRBSN plates, unlike all other specimens described in this paper.

Surface roughness was measured with a diamond stylus profilometer, perpendicular to the grinding direction, on at least three specimens per sample set.

## RESULTS

We present a brief discussion of the strength outcomes and the Weibull statistical analyses. Our primary goal is to not to dwell on the strength or statistics issues, but to document the key fractographic findings. What did the machining cracks look like? How large and how severe were they?

Each specimen set revealed crucial information about the nature of the strength limiting flaws, and machining damage cracks in particular. Different types of machining cracks are described below, and our objectives are to illustrate these machining cracks, correlate them to the machining conditions, and characterize and document the tell tale features so that other investigators can find them. Our primary emphases will be on the grinding wheel grit size and the grinding direction since these parameters proved to be the dominant factors in the creation of the machining cracks.

One set of 320 grit longitudinally ground rods furnished the inherent or "baseline" strength of this material, which is to say, the strength of the material as controlled by material flaws with negligible or no influence of machining cracks. Results for all other grinding treatments are compared to this baseline set. **Table 1** lists all flexural strength results for 116 rods and 70 bars from the rod blanks, and 60 bars cut from plates. Weibull parameters were computed by maximum likelihood analysis in accordance with ASTM C 1239.[51] **Tables 2 and 3** show a more reader-friendly summary of the effect of machining in each case with key fractographic findings. The rod results are reviewed first.

### Ground Rod Strengths

The seven data sets and the fractographic findings are discussed in order, starting with the strongest set shown in **Figure 10**. Shop C prepared thirty 320 grit longitudinally ground rod specimens that fractured almost exclusively from material flaws. Hence this set will hereafter be termed the *"baseline set."* The material flaws were inclusions (Fe and Ti with a red tinge) **Figure 11 – 12**, second-phase compositional inhomogeneities, **Figure 13**; large grains; and porous regions, **Figure 14**. A large subset of these specimens was examined in the SEM. Many of the origins were well beneath the surface as shown in **Figures 11 - 14** and in the origin location distribution map, **Figure A1** in the Appendix. The material

*Table 1* Flexural Strength Results for cylindrical rods and rectangular bars. Weibull parameters estimates are from the maximum likelihood analysis in accordance with ASTM C 1239. n is the numbers of specimens per test set.

| Grinding Conditions | | | | Rods | | | | Bars | | | |
|---|---|---|---|---|---|---|---|---|---|---|---|
| Shop | Wheel | Direction | n | Avg (MPa) | S. dev. (MPa) | Char. Str. (MPa) | Weibull Modulus m | Avg (MPa) | S. dev. (MPa) | Char. Str. (MPa) | Weibull Modulus m |
| C | 320 grit | Longitudinal | 30 | 816 | 59 | 843 | 14.6 | 655 | 51 | 677 | 15.0 |
| C | 320 grit | Transverse | 30 | 670 | 32 | 686** | 21.9 | 550 | 42 | 570** | 12.5 |
| W | 600 grit | Transverse | 10 | 764 | 59 | 789 | 13.3 | | | | |
| N | 600 grit | Transverse Centerless | 10 | 806 | 49 | 827 | 17.6 | | | | |
| F | 600 grit | Transverse | 10 | 735 | 47 | 754 | 18.9 | 726 | 19 | 735 | 35.9 |
| N | 220 grit | Transverse Centerless | 10 | 589 | 22 | 600 | 21.3 | | | | |
| C * | 150 grit | Transverse | 30 | | | | | 458 | 72 | 488 | 6.8* |
| F | 150/180 grit | Transverse | 10 | 427 | 14 | 433 | 28.1 | | | | |
| F * | 80 grit | Transverse | 30 | | | | | 430 | 62 | 443 | 8.2* |
| S | lapped | | 6 | 628 | 76 | ≈ 660 | ≈ 7 | | | | |

\*    Specimens cut from 2 sets of plates, not rods. Strengths of the two sets differed, accounting for the atypically low Weibull modulus for this material.

\*\*    Threshold strength > 0.

flaws had a wide range of sizes, which is not surprising since there were four different types. The porous regions ranged from equiaxed shapes with sizes of 25 μm – 35 μm diameter to elongated shapes of the order of 20 μm wide by 75 μm long. The inclusions and compositional inhomogeneities were often larger and were sometimes equiaxed with 80 μm – 90 μm diameter or elongated with sizes up to 20 μm X 100 μm. Several origins at the surface may have had small orthogonal machining cracks that interacted with the material flaws, but overall, machining damage was a minor factor in these specimens. The Weibull modulus was respectable (≈ 15) in these longitudinally ground 320 grit rods even though there were four active flaw populations. These flaw types were uniformly distributed along the strength distribution curve.

Three shops applied 600 grit transverse grinding (centerless or cylindrical). Strengths matched or nearly matched the baseline strength distribution. Hence controlled 600 grit transverse grinding has minimal or no deleterious effect upon strength in this material. Shop N's data virtually overlaps the baseline strength distribution as shown in **Figure 10.** Shop N and W specimens were only inspected with the stereo optical microscope, and although red inclusions were detected in a few of the specimens, nearly all fractured from origins located right at or immediately beneath the ground surface. Specimens from the shop F set, which was 10% weaker on average than the baseline set, were examined with both optical and scanning electron microscopes. The fracture origins were shallow 13 μm – 20 μm deep **parallel machining cracks** that interacted with material flaws.

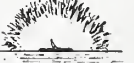## *Table 2*  Rod strengths and fracture origins.

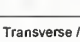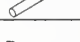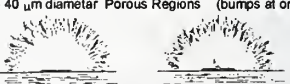| SHOP | Speciman Preparation | Wheel Grit Depth of Cut Surface finish | Effect on Strength Average ± std dev. (MPa) | Waibull paramatars Char. Str. (MPa) Modulus, m | Primary Fracture Origins |
|---|---|---|---|---|---|
| C | Longitudinal (Canterless) | 320 grit 5 μm 0.45 μm ± 0.04 μm | No affect "Baseline Strength" 816 ± 59 | 843 m = 14.6 | Inharant Volume Sintaring Flaws: Inclusions, Compositional Inhomogeneities, Porous Ragions, Larga Grains |
| N | Transvarsa | 600 grit 5 μm 0.054 μm ± 0.002 μm | No affect. 806 ± 49 | 827 m = 17.6 | Parallal machining cracks Minor interaction with inharant flaws |
| W | Transvarsa (cylindrical) | 600 grit 25 μm 0.14 μm ± 0.02 μm | 6% Reduction 764 ± 55 | 789 m = 13.3 | Parallal machining cracks Minor intaraction with inharant flaws |
| F | Transvarsa | 600 grit - 0.14 μm ± 0.02 μm | 10% Raduction 735 ± 47 | 754 m = 18.9 | Parallel machining cracks 13 - 20 μm daep Interaction with some inharant flaws |
| C | Transvarsa | 320 grit 5 μm 0.24 μm ± 0.02 μm | 18% Reduction 670 ± 32 | 686 m = 21.9 | Flat coplanar parallel machining cracks 16 - 34 μm daap |
| N | Transvarse | 220 grit 5 μm - | 28% reduction 589 ± 22 | 600 m = 21.3 | Long, parallal machining cracks 25 - 40 μm daap |
| S | Transverse / Lapped | 30 μm grit - 0.074 μm ± 0.05 μm | 15-30% Raduction 628 ± 76 | ? 660 m ? 7 | "V" machining cracks from prior grinding 20 – 35 μm daap |
| F | Transversa | 150 or 180 grit - 0.80 μm ± 0.06 μm | 48% reduction 427 ± 14 | 433 m = 28.1 | Coplanar parallel machining cracks; 40 - 80 μm deep; some V cracks |

## *Table 3*  Bar strengths and fracture origins
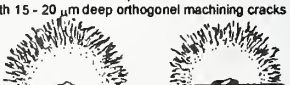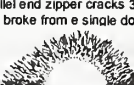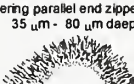
| SHOP | Specimen Praparation | Wheel Grit Depth of cut Surface finish | Effect on Strength Average, std. dev. (MPa) | Weibull parameters Char. Str. (MPa) Modulus, m | Primary Fracture Origins |
|---|---|---|---|---|---|
| F | Transversa | 600 grit 5 μm ? 0.09 μm ± 0.01 μm | 10% less then best rod strengths same strengths as thair 800 grit rods. 728 ± 19 | 735 m = 36 | 12 – 18 μm daap parallel machining cracks, or 20 - 40 μm diametar Porous Regions    (bumps at origin) |
| C | Longitudinal | 320 grit ASTM C 1161 standerd multi-step 5 μm 0.27 μm ± 0.01 μm | 10% less then 800 grit, trensverse bars above 20% less than best rods 855 ± 51 | 677 m = 15 | Pores/Porous ragions/Collapsed Agglomeretes "linear or plener flaws" with 15 - 20 μm deep orthogonel machining cracks |
| C | Transversa | 320 grit 5 μm 0.29 μm ± 0.02 μm | 24% waaker then best 800 grit transverse bars above 550 ± 42 | 570 m = 12.5 | 23 – 40 μm deep  "zipper cracks" some avidance of stable crack axtansion |
| C | Trensversa | 150 grit - - | 37% weekar then best 800 grit trensverse bars ebove 458 ± 72 2 semple lots | 488 m = 8.8 | Meendering parellel end zipper cracks 30 μm - 70 μm deep All specimens broke from e single dominent striation. |
| F | Transverse | 80 grit - - | 41% weeker then best 800 grit transverse bars ebove 430 ± 82 2 semple lots | 443 m = 8.2 | Meendering parallel end zipper cracks, 35 μm - 80 μm deep |

*Figure 10* Weibull strength distribution graph for all rod data sets. A unimodal distribution line is fitted to each set of data. Each circle is an individual rod test result. The rods ground longitudinally with a 320 grit wheel primarily broke from material flaws and represent the inherent or baseline strength of this particular lot of SRBSN. Three sets of specimens that were transversely ground by different machine shops with 600 grit wheels had similar strengths. Shop N's 600 grit transverse set matched the baseline set.



**F**
Transverse
**150/180 grit**

n = 10
m = 28.1
$\sigma_o$ = 433 MPa

Machining cracks,
40 - 80 $\mu$m deep
x 300 - 500 $\mu$m long.
Associated with deep
grooves, not exactly
perpendicular
to specimen axis.

**N**
Centerless
Transverse
**220 grit**

n = 10
m = 21.3
$\sigma_o$ = 600 MPa

25 - 40 $\mu$m deep
x 180 - 300 $\mu$m long
machining cracks
Some interaction
with inherent flaws

**C**
Centerless
Transverse
**320 grit**

n = 29
m = 21.9
$\sigma_o$ = 686

Elongated machining
cracks in nearly all.
16 - 34 $\mu$m deep x
100-300+ $\mu$m long.
A few inherent flaws
at the high strength end.

**F**
Centerless
Transverse
**600 grit**

n = 10
m = 18.9
$\sigma_o$ = 754

All origins on
surface.
MD 13 - 20 $\mu$m and
inherent flaws.

**W**
Cylindrical
Transverse
**600 grit**

n = 10
m = 13.3
$\sigma_o$ = 789

Optical exam.
only. Need SEM.
All origins on
surface.

**N**
Centerless
Transverse
**600 grit**

n = 10
m = 17.6
$\sigma_o$ = 827 MPa

Red Inclusions (Fe)
detected in
several specimens.
Need SEM.

"Baseline Set"
**C**

Longitudinal
**320 grit**
n = 30
m = 14.6
$\sigma_o$ = 843 MPa

Inherent flaws:
Inclusions (Fe, Ti),
2nd phase Comp. Inhomogeneities,
Large Grains, Porous Regions,
some deep in interior
some deep in interior

**S**
Lapped

n = 6
m = 7.3
$\sigma_o$ = 660 MPa

Machining cracks,
20+ to 35 $\mu$m deep
by hundreds of $\mu$m long.
Off axis.

Progressively more severe
machining damage

Probability (%)

Strength (MPa)

*Figure 11* Material flaw fracture origin (iron inclusion) in a 320 grit longitudinally ground rod with a strength of 751 MPa (684 MPa at the origin). These and the following illustrations follow the guidance in ASTM Standard C 1322 and show: (a) most of the fracture surface; (b), the fracture mirror; and (c), a close-up of the origin.
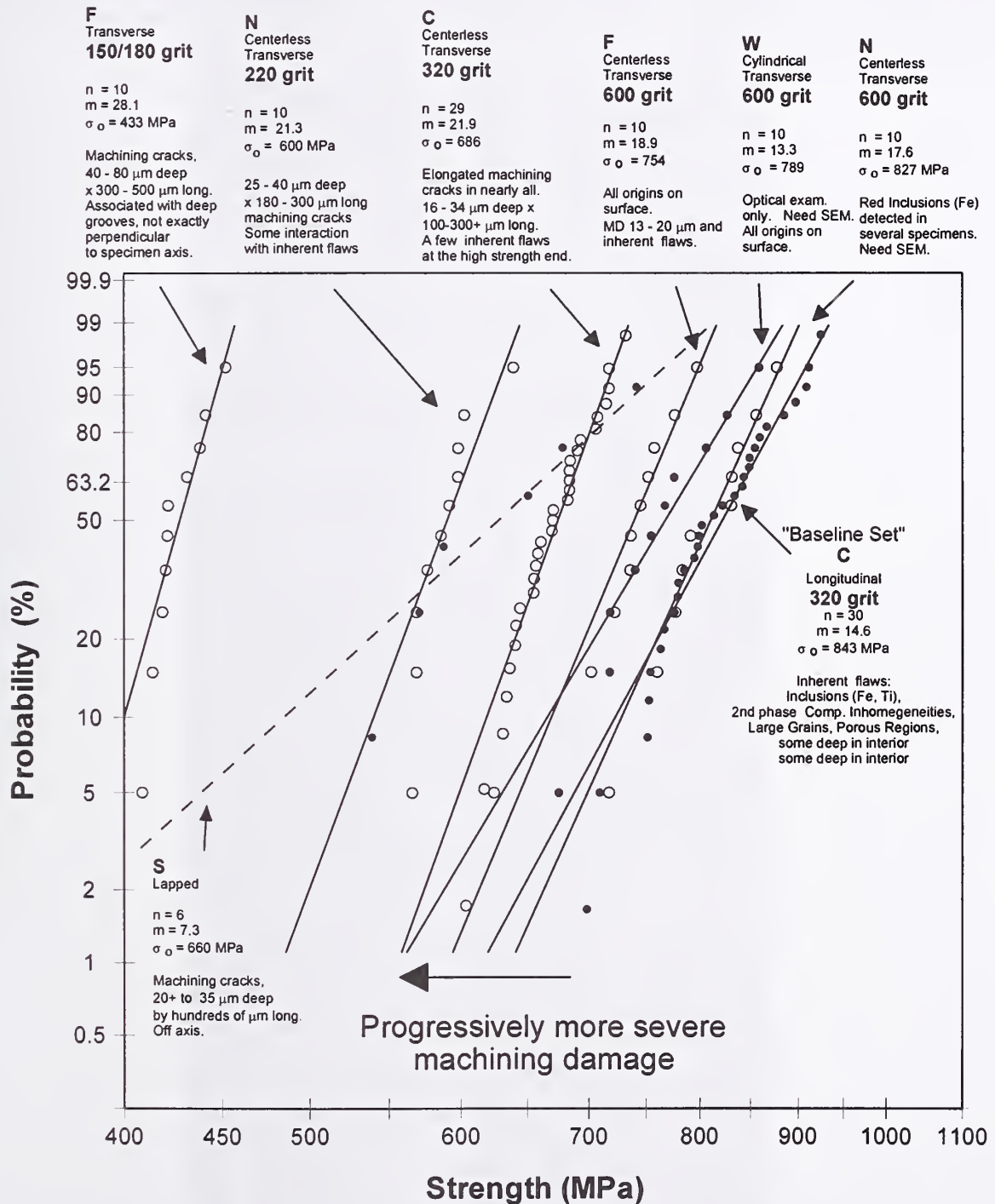
(a)



(b)



(c)

*Figure 12* Material flaw fracture origin (iron inclusion) in a 320 grit longitudinally ground rod with a strength of 813 MPa (682 MPa at the origin).

(a)



(b)



(c)

*Figure 13* Material flaw fracture origin in a 320 grit longitudinally ground rod with a strength of 753 MPa . The origin is a compositional inhomogeneity associated with excess sintering aid. The region has a greater glass content than normal.

(a)

(b)

(c)

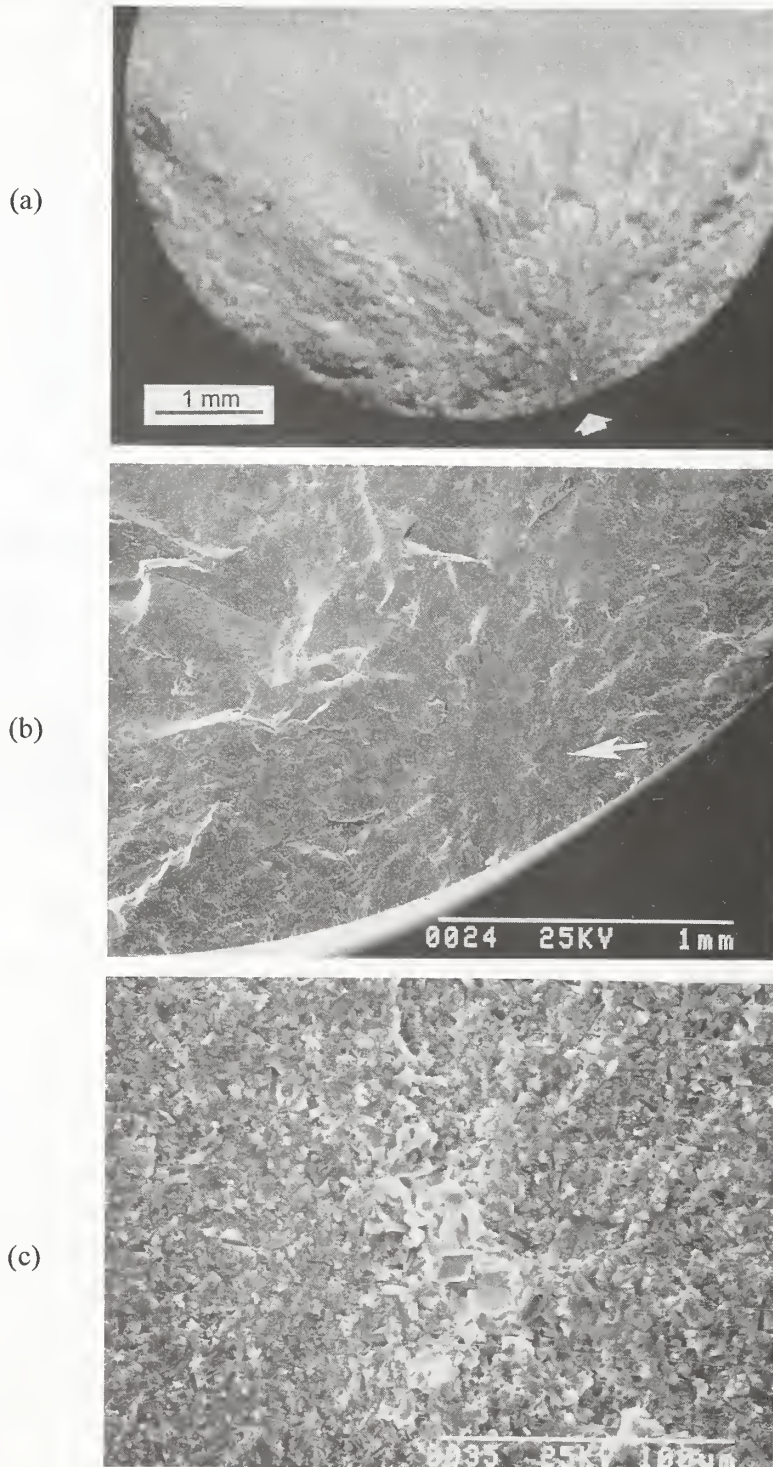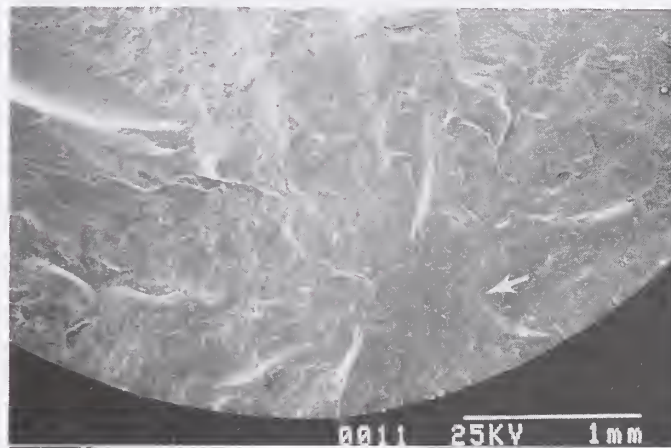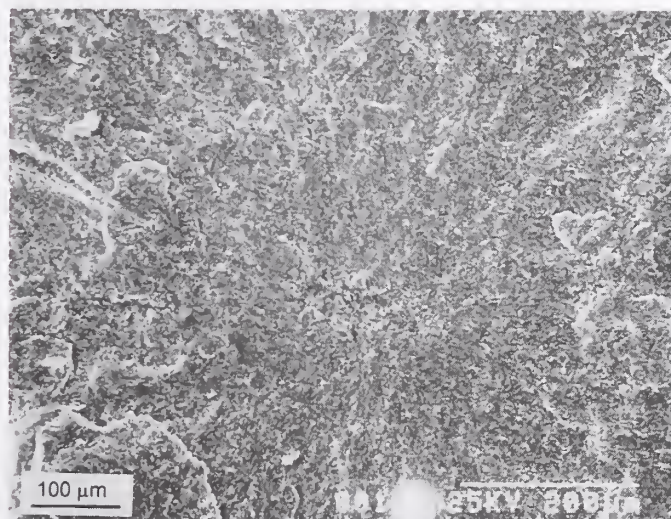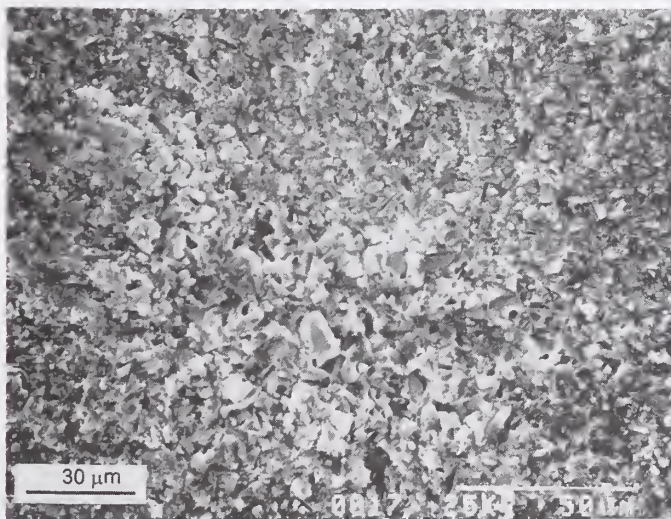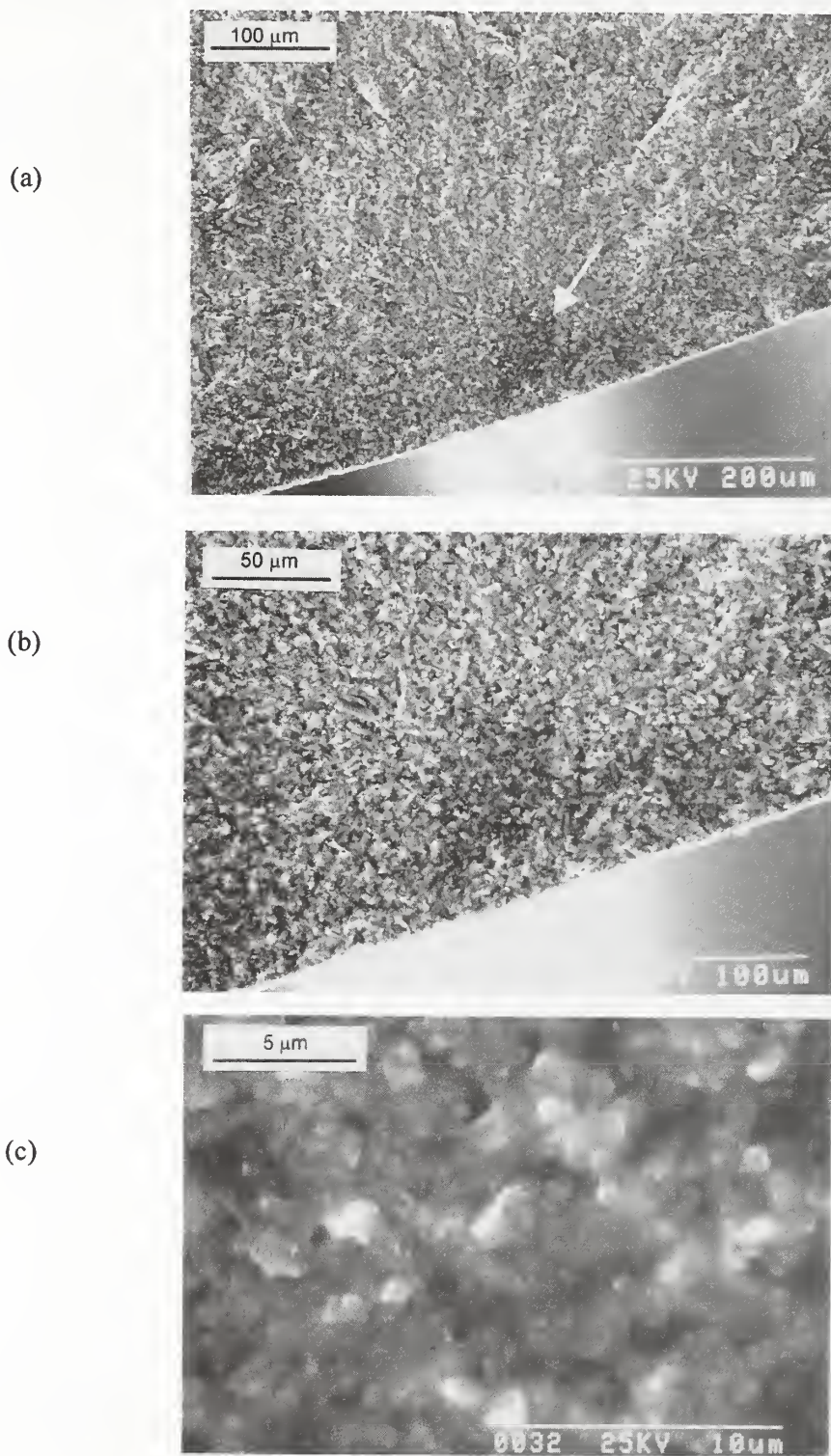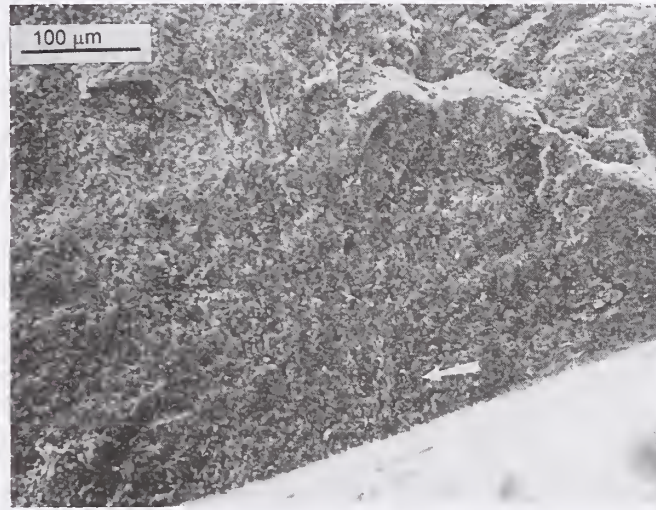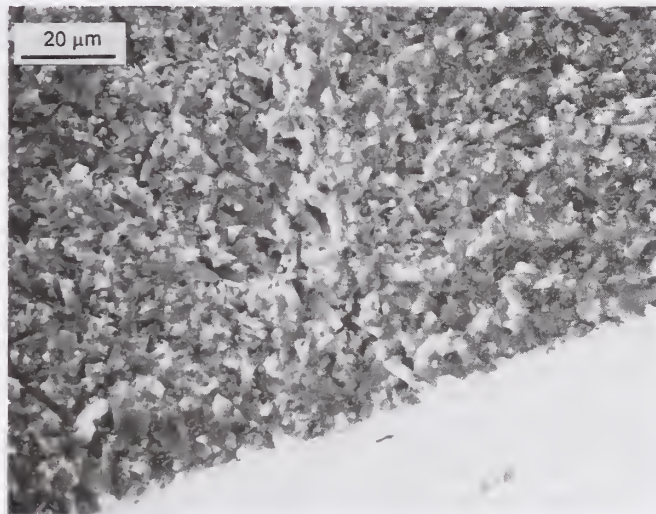*Figure 14* Material flaw fracture origin in a 320 grit longitudinally ground rod with a strength of 763 MPa. The origin is a porous region beneath the ground surface.

(a)



(b)

More serious machining damage was created with coarser grit wheels in the transverse direction. Shop C's 320 grit transversely ground rods were 18% weaker than their set of longitudinally ground rods prepared with the same grit wheel. This strength difference is not surprising, in light of the different orientations of the machining cracks. Optical examination on all specimens and SEM inspection on over one-third of the specimens confirmed that the strength limiting flaws in the transversely ground set were elongated **coplanar parallel machining cracks** as shown in the top left of **Figure 1** and in **Figures 15-18**. These elongated cracks were fairly uniform in depth (16 μm – 34 μm) but had variable lengths along the ground surface (100 μm – 300 μm). Some of these cracks showed evidence of stable crack extension. It cannot be ascertained whether this occurred during the machining process (wherein the crack might have popped in and then been extended by subsequent grinding) or during the flexural strength test. A key, telltale aspect of these machining cracks was that they often were tilted or at slight angles to the final fracture plane which formed the fracture mirror. This change in crack propagation direction confirmed our interpretation that these were critical crack sizes at the onset of fast fracture. As will be discussed below, the apparent fracture toughness based upon these crack sizes matched plateau, large crack toughness values.

The machining flaws sometimes closely overlapped. Several specimens in the high strength portion of the distribution had material flaw origins and did not break from machining flaws. This is not surprising since these strengths overlap the baseline strength distribution. The 320 grit parallel machining cracks were only 16 μm to 34 μm deep but they were very long and shallow, and thus were more deleterious to strength than the larger, rounded, or blunter material flaws.

NIST prepared one set of ten 200 grit transverse ground rods that had even lower strengths (**Figure 10**). The fracture origins were primarily 25 μm – 40 μm deep parallel machining cracks such as shown in **Figure 19.** Some of these interacted with the material flaws such as pores and agglomerates.

The weakest rod set was inadvertently prepared by Shop F with an unrecorded, but coarse grinding wheel in the transverse mode. We estimate from the surface roughness that the wheel may have been 150 grit or 180 grit. The strength limiting flaws were machining cracks 40 μm – 80 μm deep by 300 μm – 500 μm long. The machining cracks were easy to detect on the fracture surface with the stereo optical microscope. **Figure 20** shows a classic example of a parallel crack. It is deeper that the parallel cracks shown previously but rather than appearing as a single long elliptical crack, it is serrated as though it were made up of a number of small crack segments with different orientations or planes. Many of the specimens from this set had an even more distinctive feature. The mirror region often had pronounced steps that created a "V" marking (**Figures 21 and 22**). This crack pattern was caused by specimen axial displacement relative to the grinding wheel, as illustrated in **Figure 23.** Grinding with axial feed created a spiral pattern ("barber pole") of striations and subsurface cracks that were not quite perpendicular to the specimen axis and the applied stress axis during flexure strength testing. Consequently, the fracture

*Figure 15* Coplanar parallel machining crack in a 320 grit transversely ground rod (657 MPa). (b) shows the mirror region which is centered on a parallel machining crack created by transverse grinding. (c) shows a close-up of the origin. The crack underneath the dark striation-crack extended to a depth of 17 μm (arrows). Using that depth, the stress intensity shape factor of 1.99 for a long surface crack, and the stress at the origin (653 MPa), the fracture toughness was calculated to be 5.36 MPa√m. The machining crack can be distinguished from the fracture mirror plane since the machining crack (and possible stable extension from it) is slightly tilted and is more irregular than the plane of final fracture.

(a)
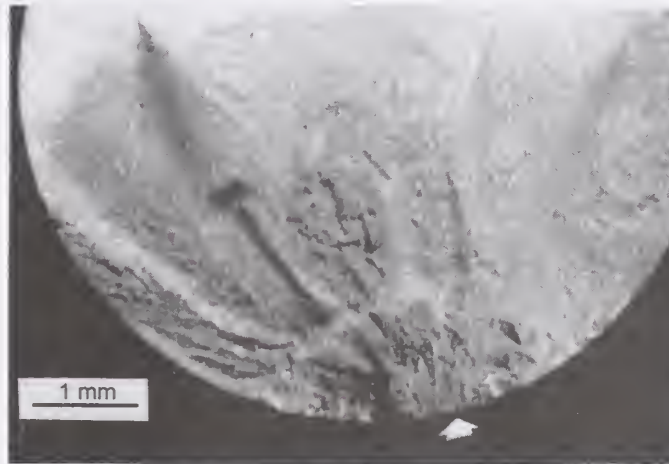
(b)
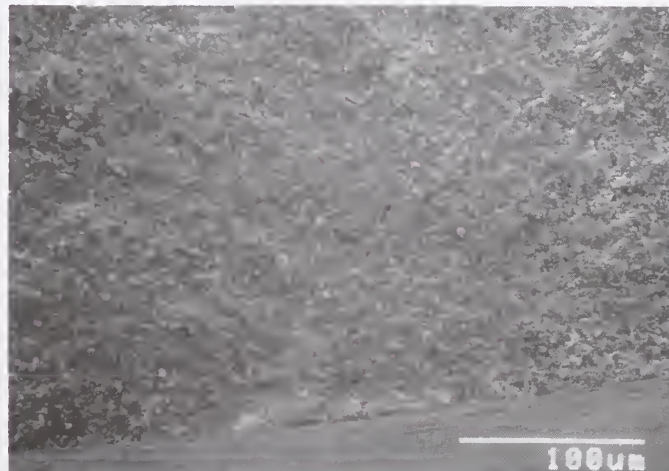
(c)

*Figure 16* Coplanar parallel machining crack in a 320 grit transversely ground rod (641 MPa). (b) shows the fracture mirror region centered on a parallel machining crack. (c) shows a close-up of the origin which also shows evidence of stable extension. The critical crack size, which is more obvious in (b), is marked in (c) by arrows.



(a)

(b)

(c)
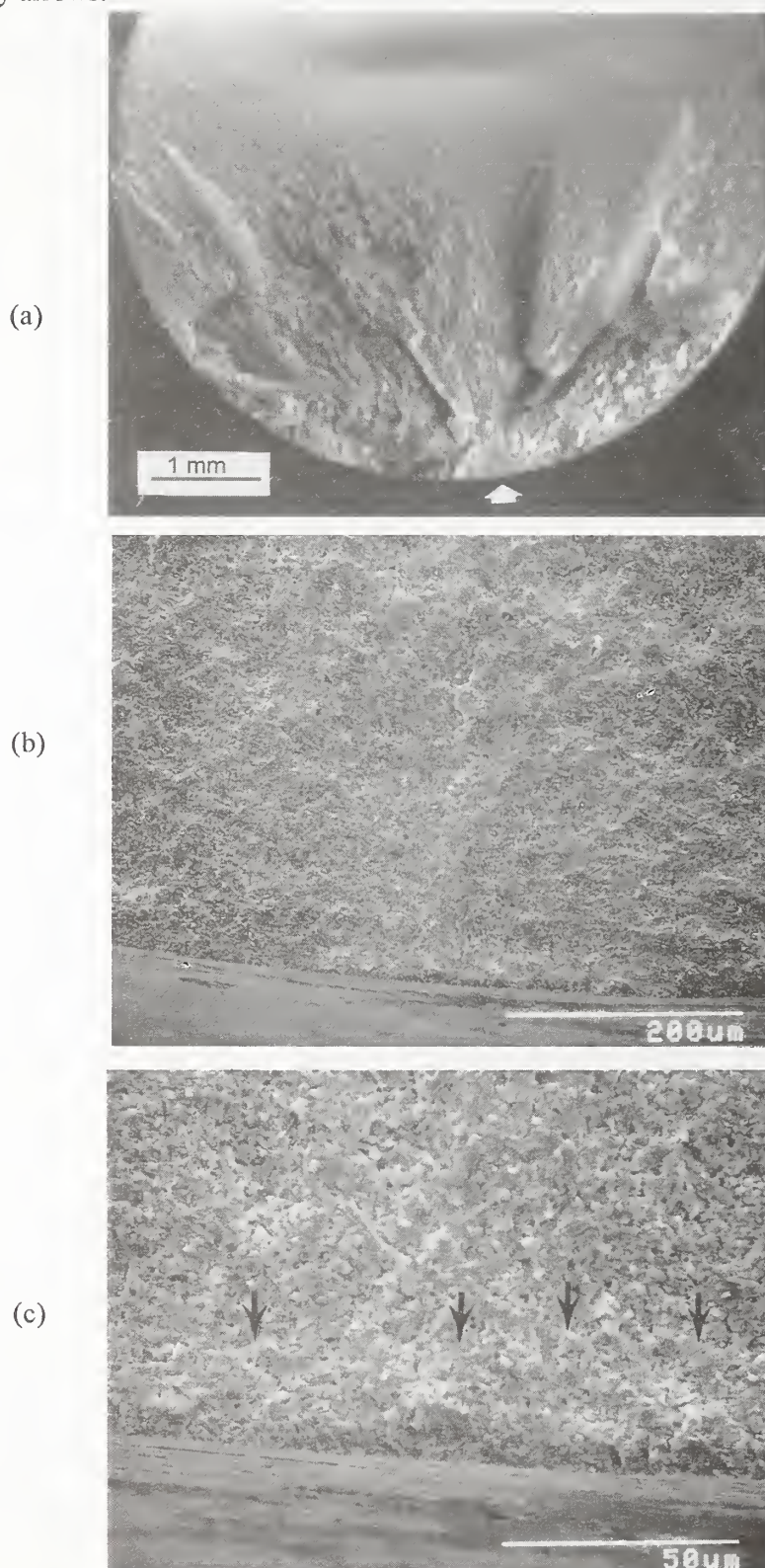
*Figure 17* Coplanar parallel machining crack in a 320 grit transversely ground rod (631 MPa).



(a)

(b)

(c)
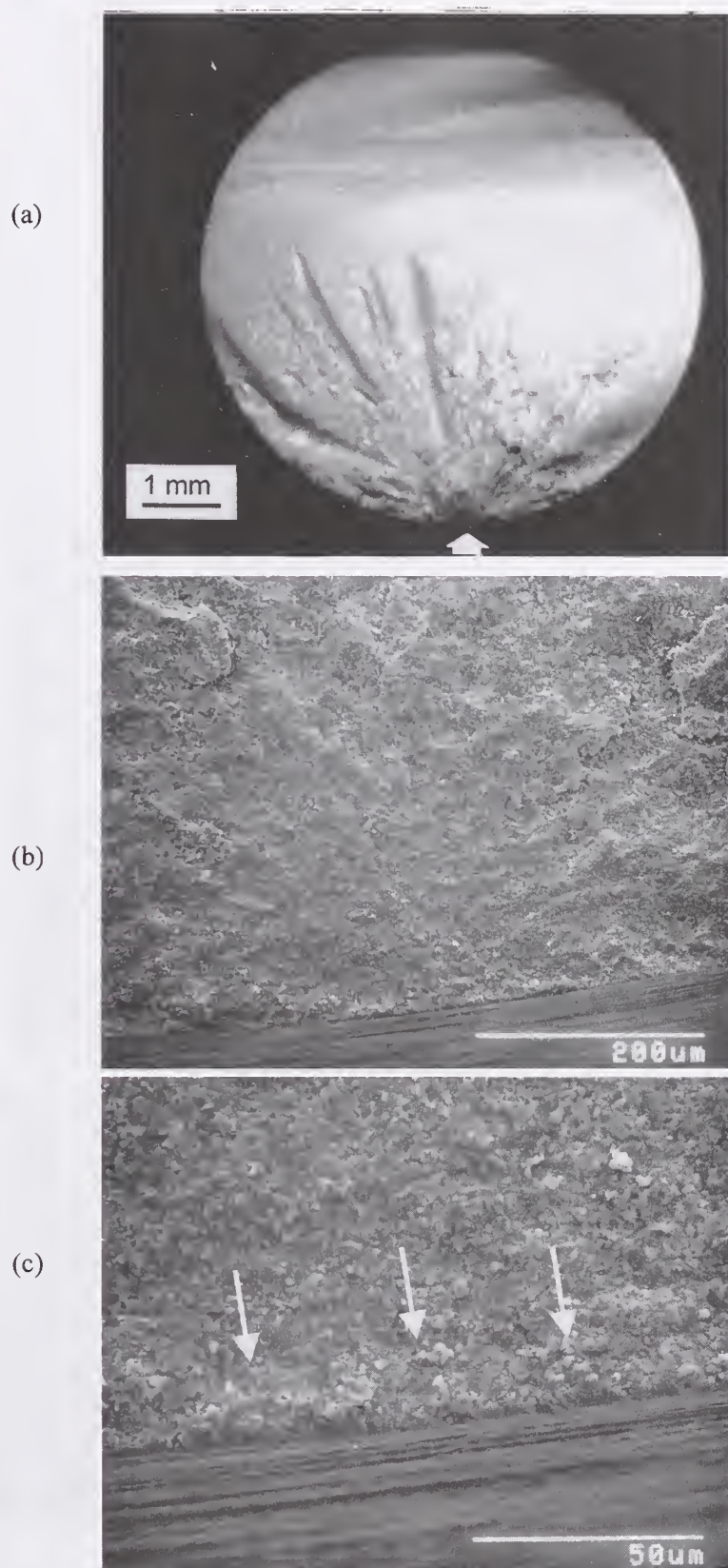
*Figure 18* Coplanar parallel machining crack in a 320 grit transversely ground rod (634 MPa). The 19 µm deep machining crack leads to an estimate of fracture toughness of 5.2 MPa√m.
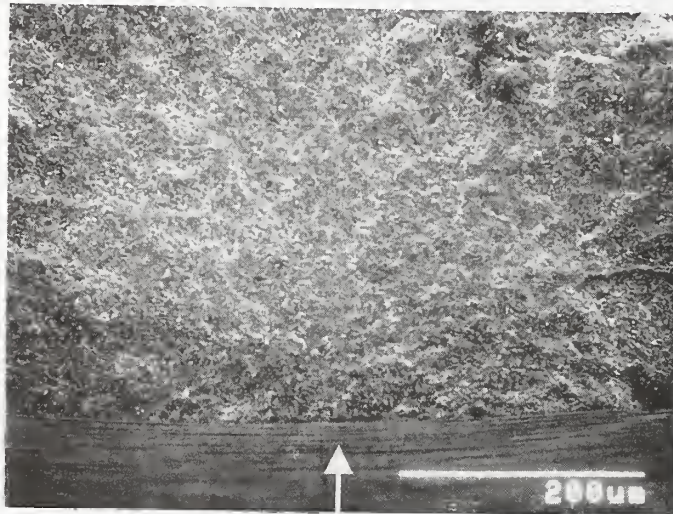
*Figure 19*    Parallel 25 µm deep machining crack in a 220 grit transversely ground rod (566 MPa nominal, 557 MPa at origin center).  (c) is a composite of two SEM photos of the origin crack.

(a)
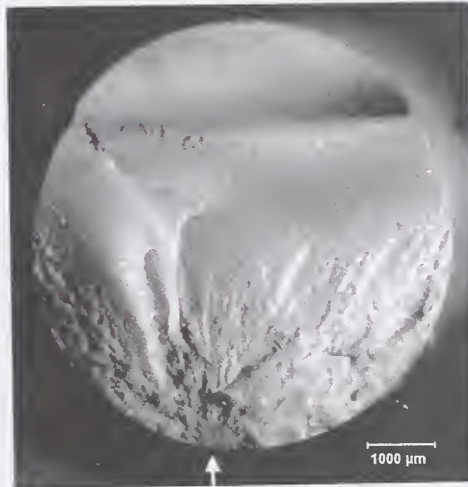


(b)
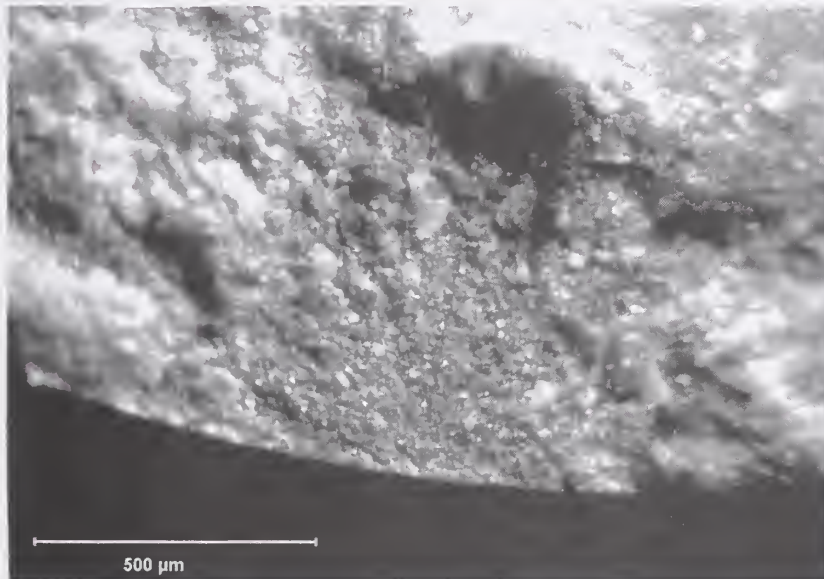


(c)

*Figure 20* A parallel machining crack in a Shop F, coarse-grit (150/180), transversely ground rod with a strength of 409 MPa. The crack has a slight zigzag appearance and can be considered one form of a "zipper crack."



(a)



(b)

**Figure 21**    Classic "V" machining crack in a transversely ground rod  (421 MPa).  The arrows in (d) show the offset parallel machining cracks that are on several tiers as schematically shown in (b).  (e) is an SEM image of the origin and the ground surface.    (f) is an optical image that shows the ground outer surface at the origin site.  The striations are not quite perpendicular to the specimen axis.
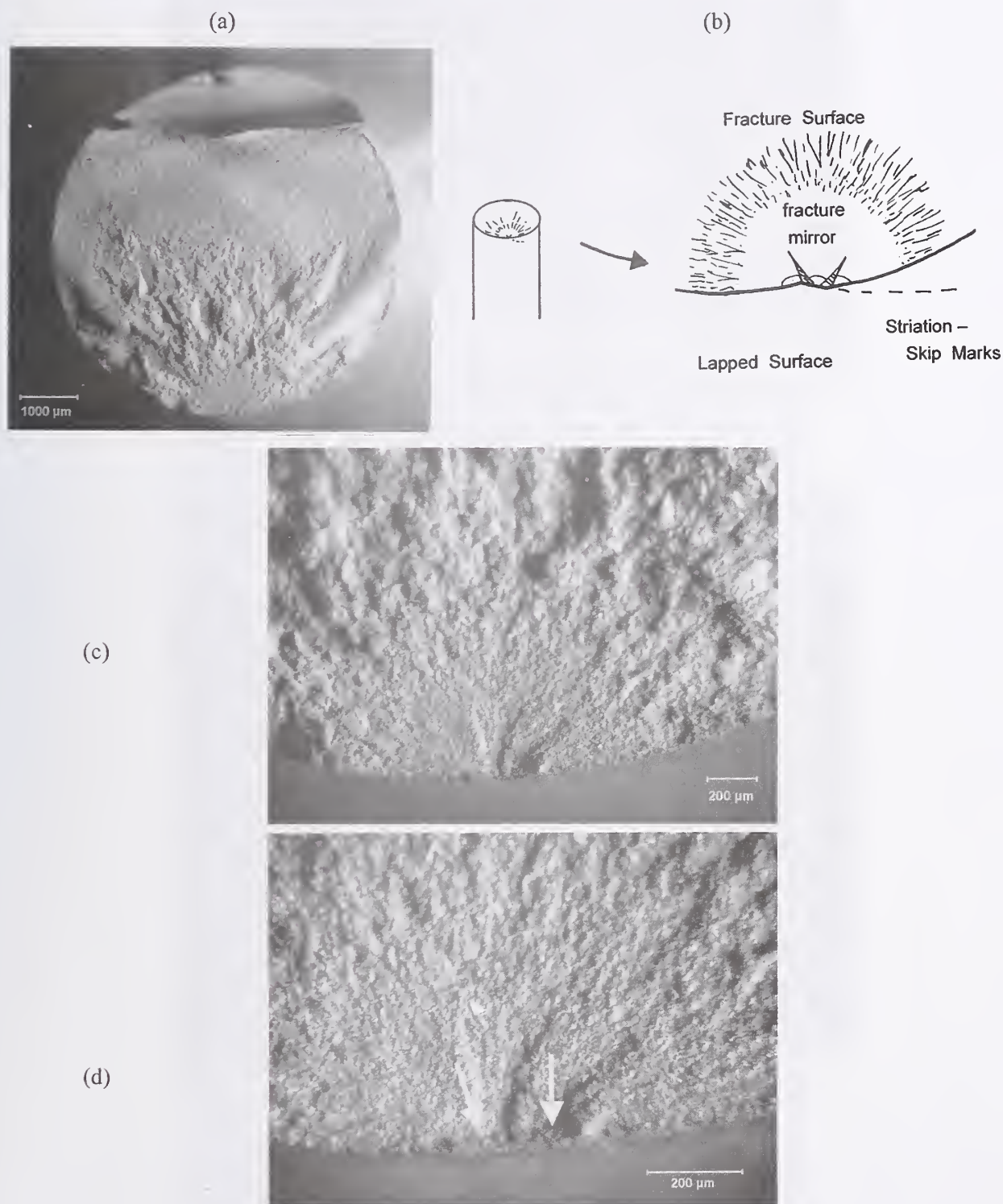
*Figure 21* continued

(e)



200 µm
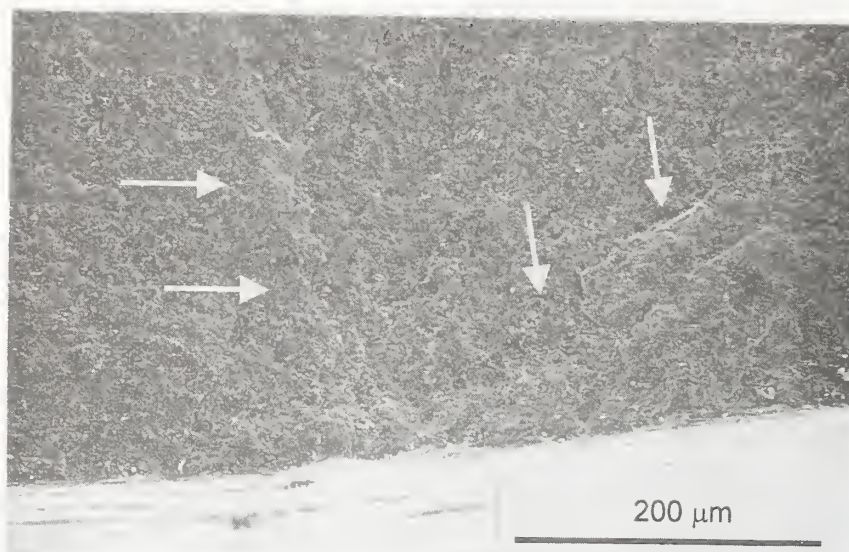
(f)
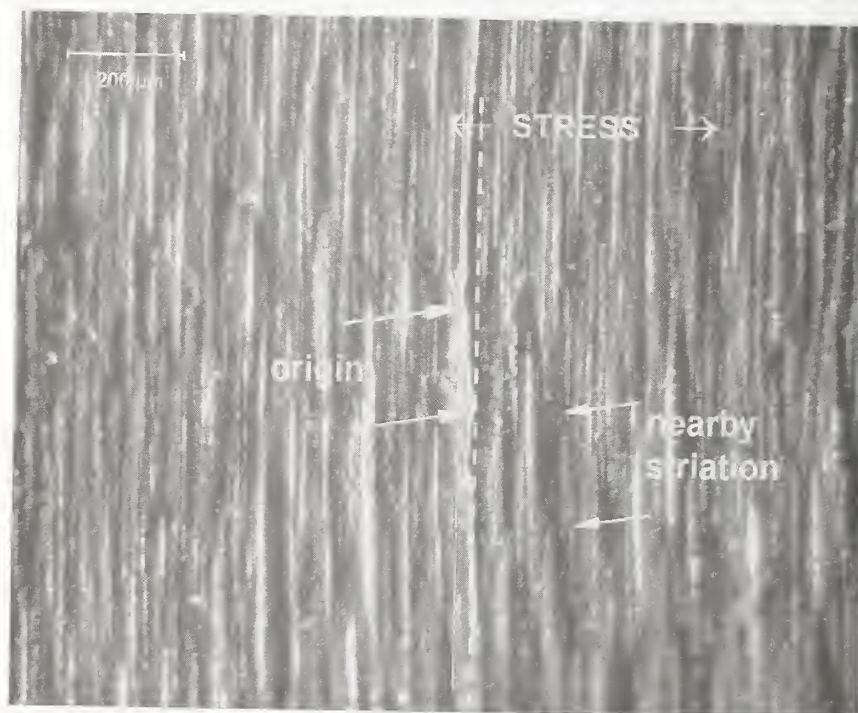
*Figure 22* A similar "V machining crack" in a transversely ground rod. (419 MPa)

(a)
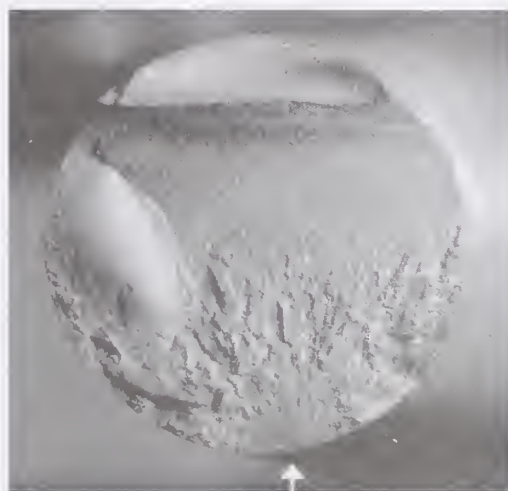


(b)
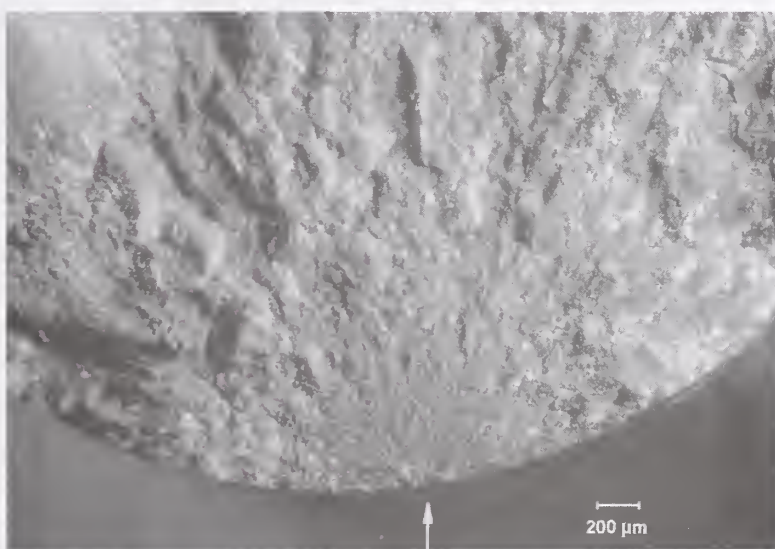


(c)
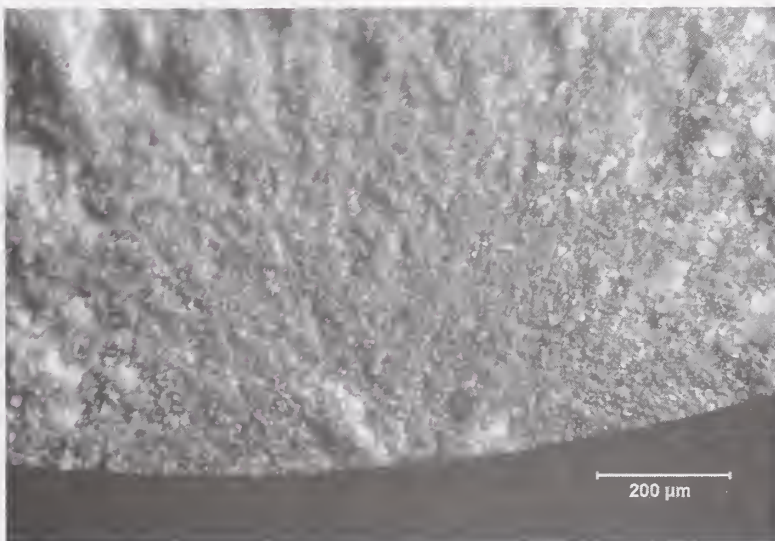
mirror had segments on different planes labeled a, b, c in **Figure 23b**. The steps between the segments in the mirror created the V pattern. The jogs or steps gradually disappear as the crack segments join and are analogous to wake or twist hackle markings. These telltale markings are indicative of one class of machining cracks, which we shall term *"V" machining cracks.* In some cases, only one leg of the V was present on a fracture surface.

Shop S lapped two sets of three specimens in an attempt to produce "damage-free" rods, but the strengths were quite low. Even though the outer specimen surface had a smooth finish, the fracture origins were obvious "V' machining cracks that were 20 $\mu$m – 35 $\mu$m deep by 200 $\mu$m – 300 $\mu$m long as shown in **Figure 24.** Telltale, stray striation segments were present on the lapped specimen surface as shown in **Figure 25**. There was a very strong correlation of strength with final rod diameter that varied from 5.98 mm to 6.03 mm as shown in **Figure 26:** the smaller the diameter, the stronger was the specimen. This confirms that the surface lapping did not remove sufficient material to eliminate damage from prior transverse grinding. The curve fit through the data shows that had an estimated .060 mm more of the material been removed from the diameter (.030 mm from each surface) then the inherent strength of the material may have been reached in all these specimens assuming that the lapping itself did not introduce damage. That is, however, a lot of material to remove by lapping.



| Flat, coplanar parallel | "V" machining crack |
| (a) | (b) |
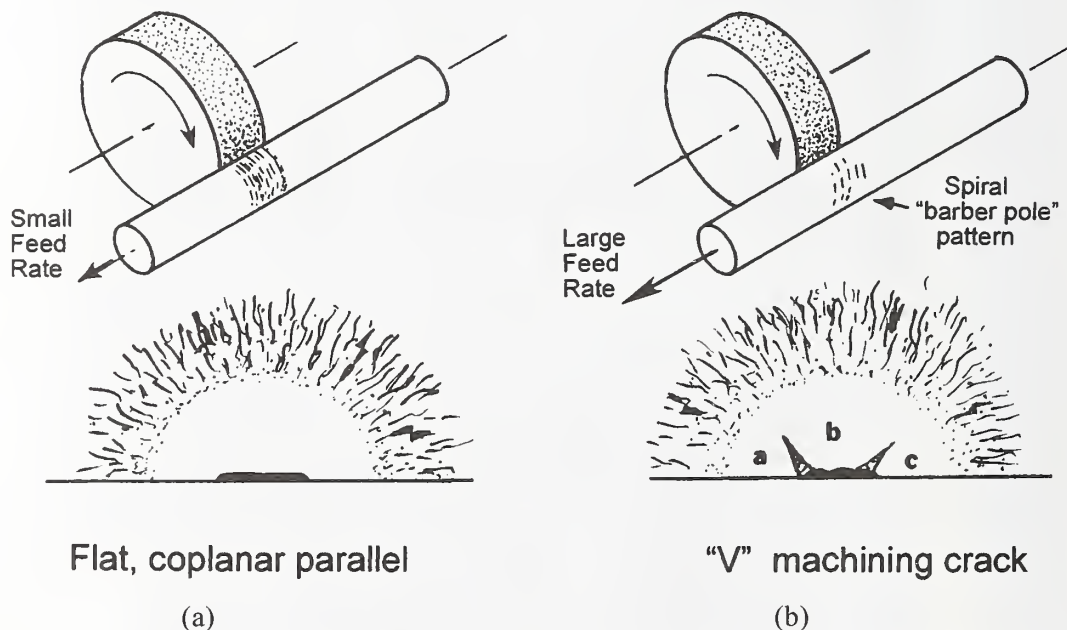
*Figure 23* The motion of the work piece relative to the grinding wheel during transverse grinding may create either (a) flat "**coplanar parallel cracks**" such as in the Shop C, 320 grit transverse-ground rods, or (b), stepped "**V machining cracks**" such in as the Shop F, coarse-ground rods. The fracture mirror region is on three offset planes marked "a", "b", and "c." The steps between these three planes create the V marking.

*Figure 24*    The lapped specimens had deep machining cracks below the surface from prior grinding.  (a) and (b) show double fracture mirrors, an unusual fracture pattern (arrows). The origin in the left mirror is a variant of the "V machining crack" as shown in (c).

(a)
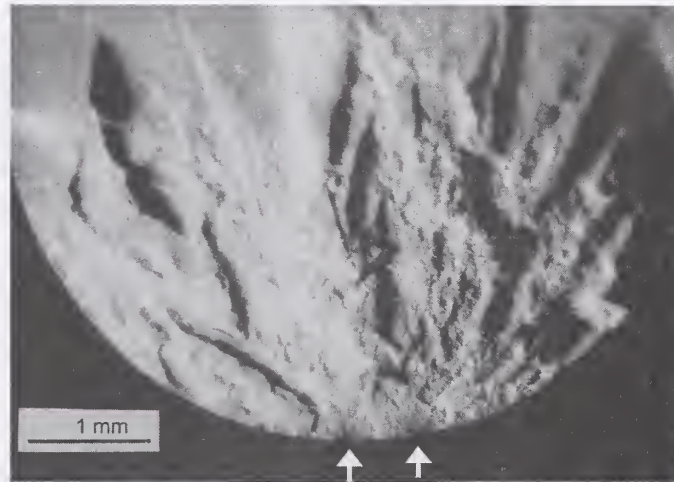
(b)
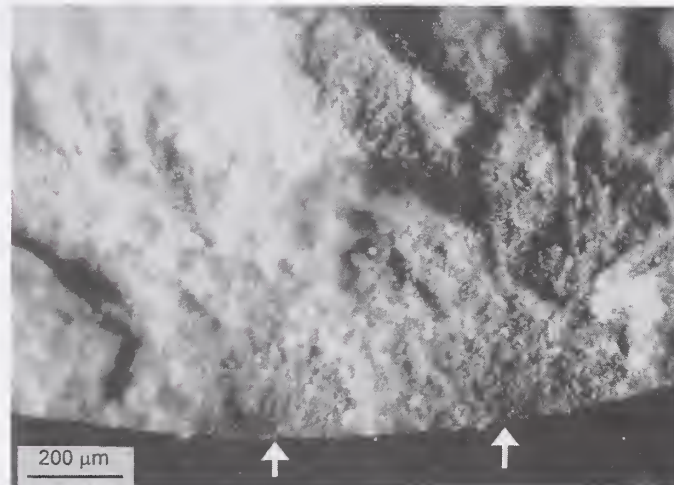
(c)
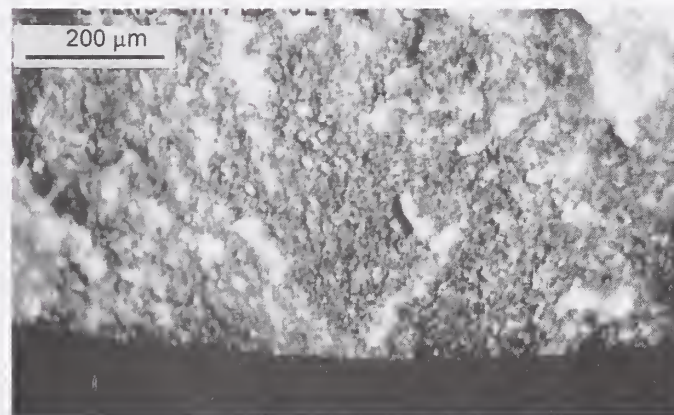
***Figure 25*** Lapping did not remove sufficient material to eliminate the prior, deeper damage. These two figures show the outer lapped surface. Although much of the surface is smooth, a few deep striations remain (arrows). The fracture surface is on the right.

(a)    (b)
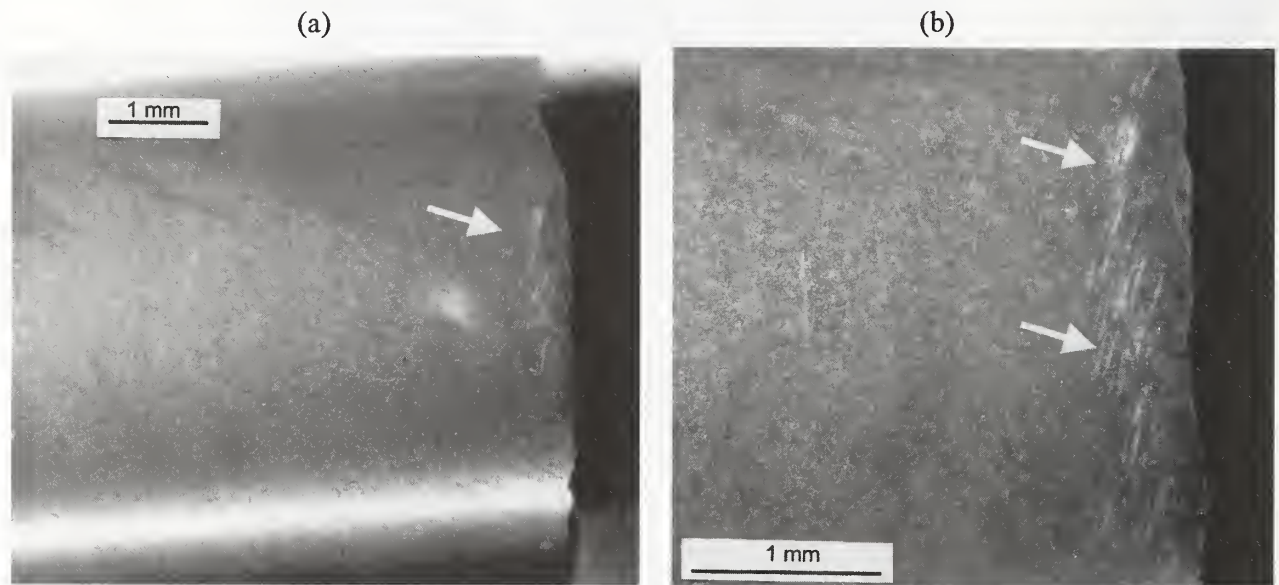
***Figure 26*** The strength of the lapped specimens was directly related to the final rod diameter. Extrapolation of the data to the baseline strength suggests that if the rods had been lapped 20 μm to 60 μm more to a final size of 5.967 mm, the subsurface machining damage would have been eliminated.
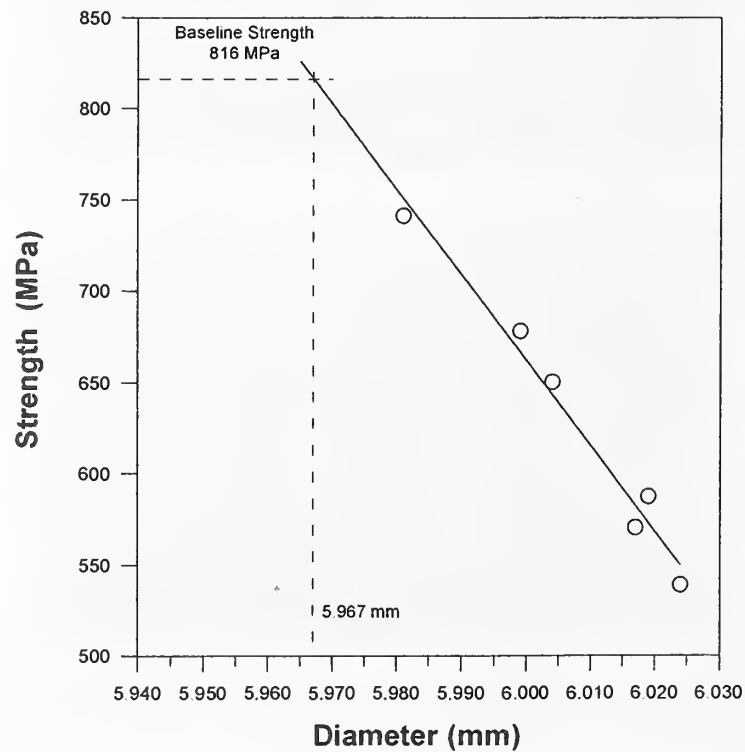
*Figure 27* Weibull strength distribution graph for the rectangular bars. Each square is a bar strength test result. The dashed lines for the baseline rod strength set and the shop F 600 grit transverse rod data sets are shown for comparison.

37
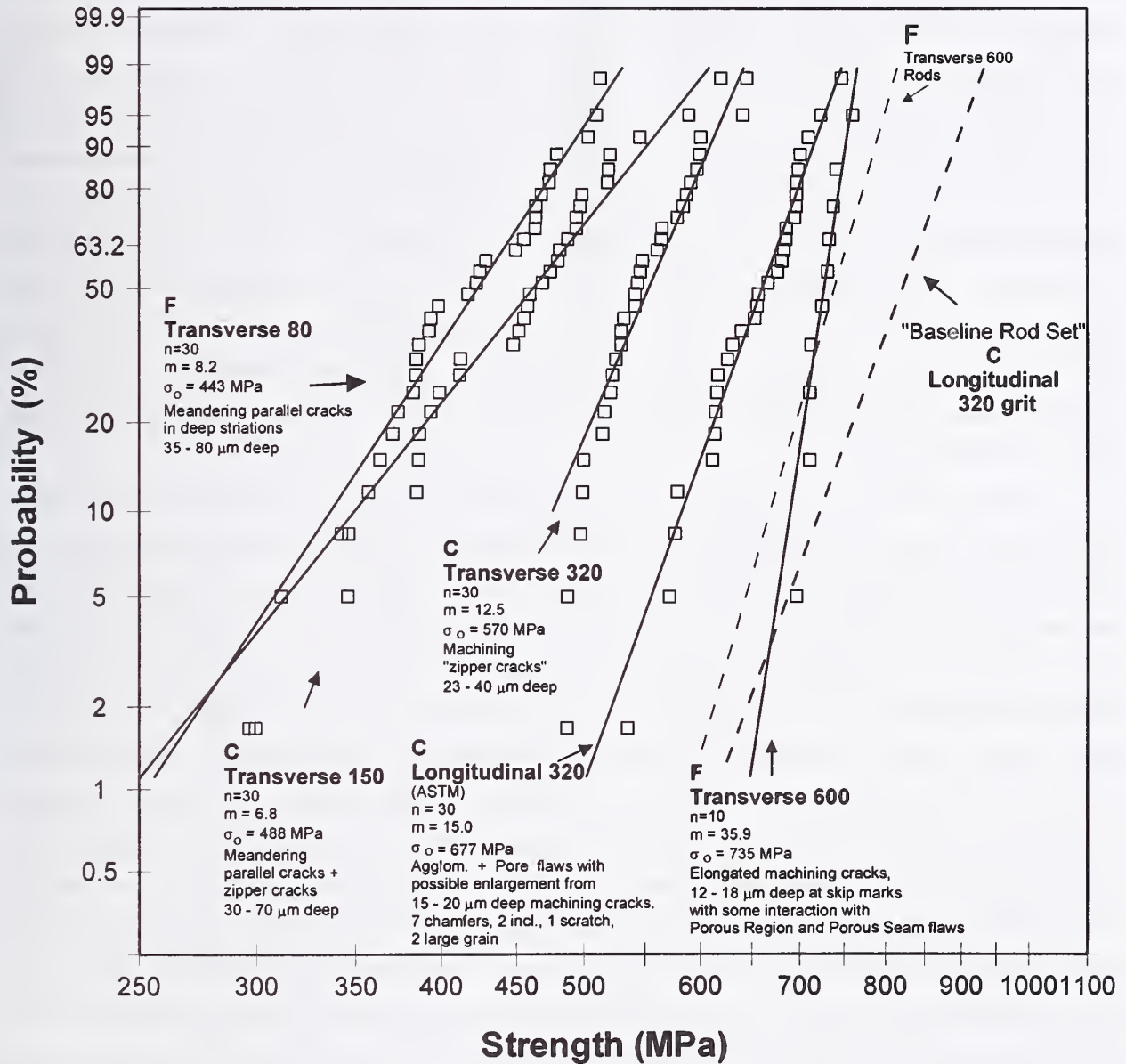
**Ground Bar Strengths**

Five bars sets were prepared and tested as shown in **Figure 27.** The strongest set (735 MPa characteristic strength), which was prepared by Shop F by 600 grit transverse grinding, had nearly an identical strength to the *rod* set (754 MPa) that they also prepared with the same grit wheel (dashed gray line in the same figure). The Weibull modulus for the set of 10 bar specimens was remarkably high (36), suggesting a very uniform flaw population. Both the *bars* and *rods* prepared by this shop with 600 grit transverse grinding were only 10% weaker than the baseline strengths (816 MPa). Optical and SEM fractography confirmed that the bars and the rods had 12 μm – 18 μm deep elongated parallel machining cracks that coincided with slightly deeper than normal skip mark-striations on the specimen tensile surface.[o] Four bar specimens had such well-formed cracks that it was possible to compute the fracture toughness based on the crack size and shape, and the stress at fracture. The average was 5.4 MPa√m ± 0.4 MPa√m, in good agreement with the measured fracture toughness for this material.[p] (This suggests there were negligible residual stresses present, or that the flaws behaved as though they experienced a plateau fracture toughness if the material had a rising R-curve.) The machining cracks often linked with material sintering flaws such as small porous regions or porous seams, causing a slight bump or jog at the center of the fracture mirror.

Shop C prepared a set of thirty 320 grit longitudinally ground rectangular bars which were machined in accordance with the ASTM C 1161 standard procedure. The average strength of this set was 655 MPa and the characteristic strength and Weibull moduli were 677 MPA and 15, respectively. We were surprised that these bars were 17% weaker on average than the baseline strength set of 320 grit longitudinally ground rods prepared by the same shop (816 MPa). On the other hand, the bar strengths were quite comparable with other sets of longitudinally ground bars prepared from earlier batches of the SRBSN in the consortium program [1-6]. Characteristic strengths previously had been 650 MPa to 723 MPa and Weibull moduli were between 10 and 15. Why then were the strengths of the present set of 320 grit rods and bars different? The flaws or the microstructure must have been different since testing errors were ruled out after careful review of the data. Orthogonal machining cracks may have been in both the rods and bars, but they could not be discerned. In any case, many of the rod flaws were well below the surface and unaffected by any possible machining damage. In contrast, most of the bars origins were located right at the surface and could have been vulnerable to enlargement or alteration by small (15 μm – 20 μm) semicircular orthogonal machining cracks. A key finding was that the material flaws were somewhat different in the bars and rods in the sets prepared by shop C. The thirty bar origins were pores,

---

[o]   The deep striations did not run across the full 4 mm width of the specimen surface. They were about 0.5 mm long and "skipped" across the ground surface. This distance was probably the contact length of a single abrasive grit for the grinding conditions used.

[p]   Fracture toughness, $K_{Ic} = Y \sigma \sqrt{a}$ where Y is the dimensionless stress intensity shape factor for a semielliptical surface flaw, σ is the fracture stress and a is the flaw depth. We started with the initial assumptions that there were no residual stresses and the material has constant fracture toughness. A more detailed discussion of these assumptions is deferred until later in this report.

porous regions, or porous seams that often were elongated or oblate. These probably were remnants of spray-drying agglomerates as shown in **Figures 28 and 29.** One inclusion, one scratch and two large grains **(Figure 30)** also were strength-limiting flaws. A few chamfer fault fractures were also observed. In contrast, the thirty *rods* contained many more inclusions and compositional inhomogeneities. Thus, the possibility of a minor, subtle spatial gradient in flaw origin type cannot be ruled out. Optical microscopy examination of polished rod cross sections **(Figure 5a)** suggested that there were more inclusions in the rim of the rods than in the core region. Since the bar specimens were cut from the middle of the rods, it is plausible that bars sampled fewer inclusions than the 6 mm diameter rods.[q] On the other hand, shop F's 600 grit transverse ground rod and bars had nearly identical strengths.

As expected, Shop C's thirty 320 grit transversely ground bars were 19% weaker than their longitudinally ground bars. The transversely ground bar origins were easy to characterize. Most were classic parallel machining cracks that were offset, overlapping semi-elliptical cracks as illustrated in **Figure 2c.** Material flaws were detected in several of the high strength specimens, which is not surprising since the strengths overlap the baseline strength distribution. The machining cracks were 23 μm – 40 μm deep and 100 μm to 300 μm long. The strength distribution had a typical Weibull modulus (13) but had a low strength tail suggestive of a threshold strength of the order of 475 MPa. Six specimens had sufficiently well defined machining cracks so that an estimate of fracture toughness of could be determined. A value of 5.04 MPa√m ± 0.31 MPa√m was obtained. This is a little lower than the fracture toughness measured for this material (≈ 5.5 MPa√m). The discrepancy suggests that tensile residual stresses were present (with an effective contribution of ≈ 50 MPa), or possibly undetected stable crack extension had occurred. Such an extension *was detected* in a fifth specimen, and if the stable extension was included in the calculation, the outcome was 5.5 MPa√m. The small elliptical crack overlaps caused slight steps or jogs in the fracture surface in the immediate vicinity of the origin. These little steps or jogs created a telltale machining crack feature. As the initial crack extended into the mirror during fracture, crack segments joined and produced *"machining crack hackle"* that may be characterized as a series of nearly parallel, periodically spaced tails (or "fingerlets") which radiate from the middle of the flaw, as shown in **Figures 31-34.** The slight tilt of the micro hackle segments leading away from the middle of the origin is a telltale feature. Such flaws may be termed *"zipper machining cracks"* since they have zigzag kinks that leave a characteristic pattern as the crack opens up as it propagates catastrophically during final fracture. Zipper cracks are caused by scratches or transverse machining damage.

---

[q]  Sampling uniformity is not a likely cause for this particular sample set to be different. Although the rods were received in three lots, they were carefully randomized. The lots might have had subtle batch-to-batch differences in inherent material flaws which could account for a few specimens to be different, but not the whole sample set.

*Figure 28* Fracture origin in a 320 grit longitudinally ground bar (571 MPa). (a) shows an optical image of the ground surface. The fracture origin is a pore associated with large agglomerate that caused the fracture surface to have a jog at the origin.     (b) and (c) are SEM close-ups of the origin and the ground surface.



(a)
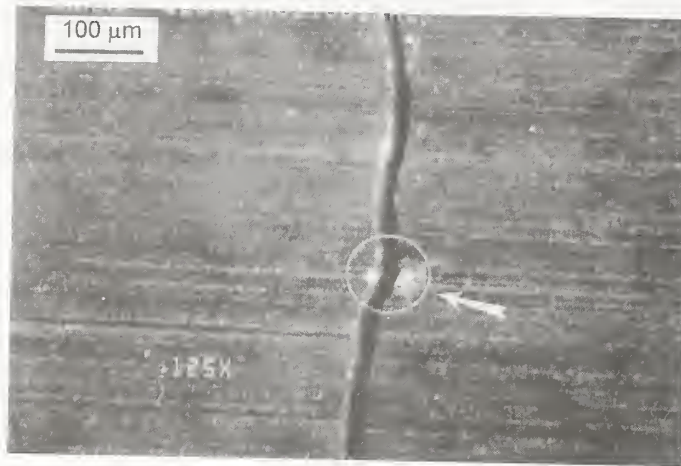
(b)

(c)

*Figure 29*  Agglomerate/pore type flaw detected in a 320 grit longitudinally ground Shop C bar.  These flaws were almost always located at or near the surface of the bars and may have been altered or enlarged by orthogonal crack machining damage  (535 MPa).
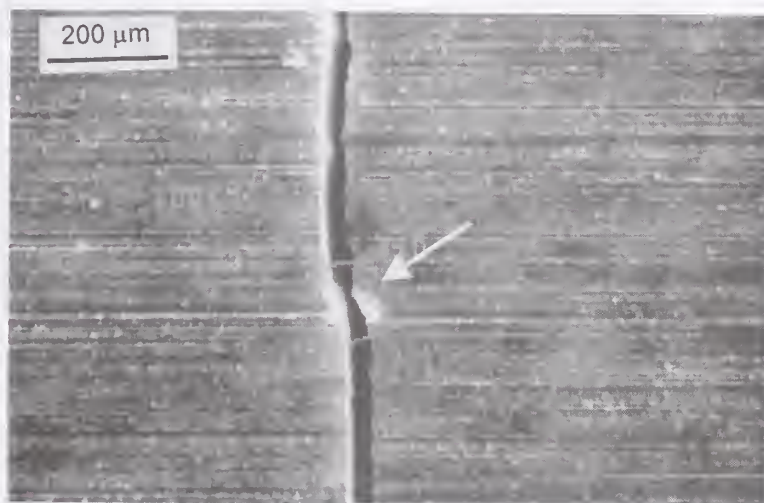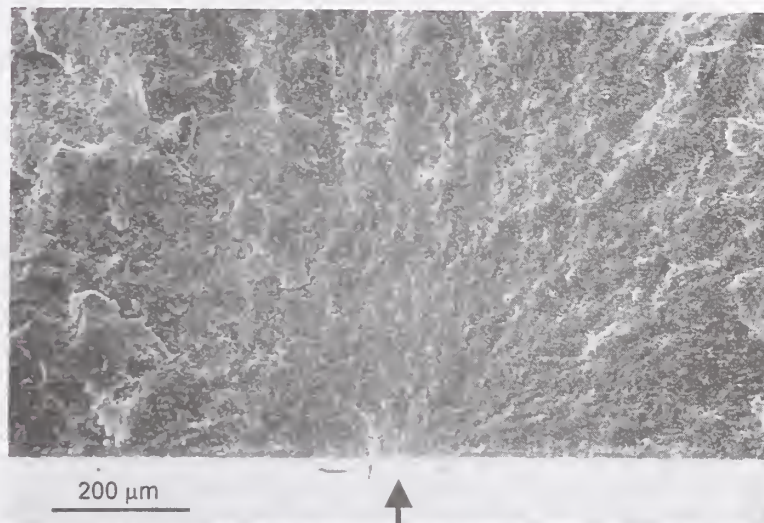
*Figure 30* A large silicon nitride crystal at the origin in a 320 grit longitudinally ground Shop C bar (616 MPa). The orientation of the material flaw caused a jog in the fracture surface at the origin. (a) shows an optical photo of the ground surface   (b) and (c) are SEM close ups. A fracture mechanics analysis suggests the large grain is too small by itself, and it is possible that a seam or agglomerate in the body exists just below the ground surface.  The white arrows in (b) show that the hackle lines on the right side of  point back to the large grain (large arrow), but on the left side, the micro hackle lines point up to different region beneath the tensile surface.

(a)

(b)

(c)
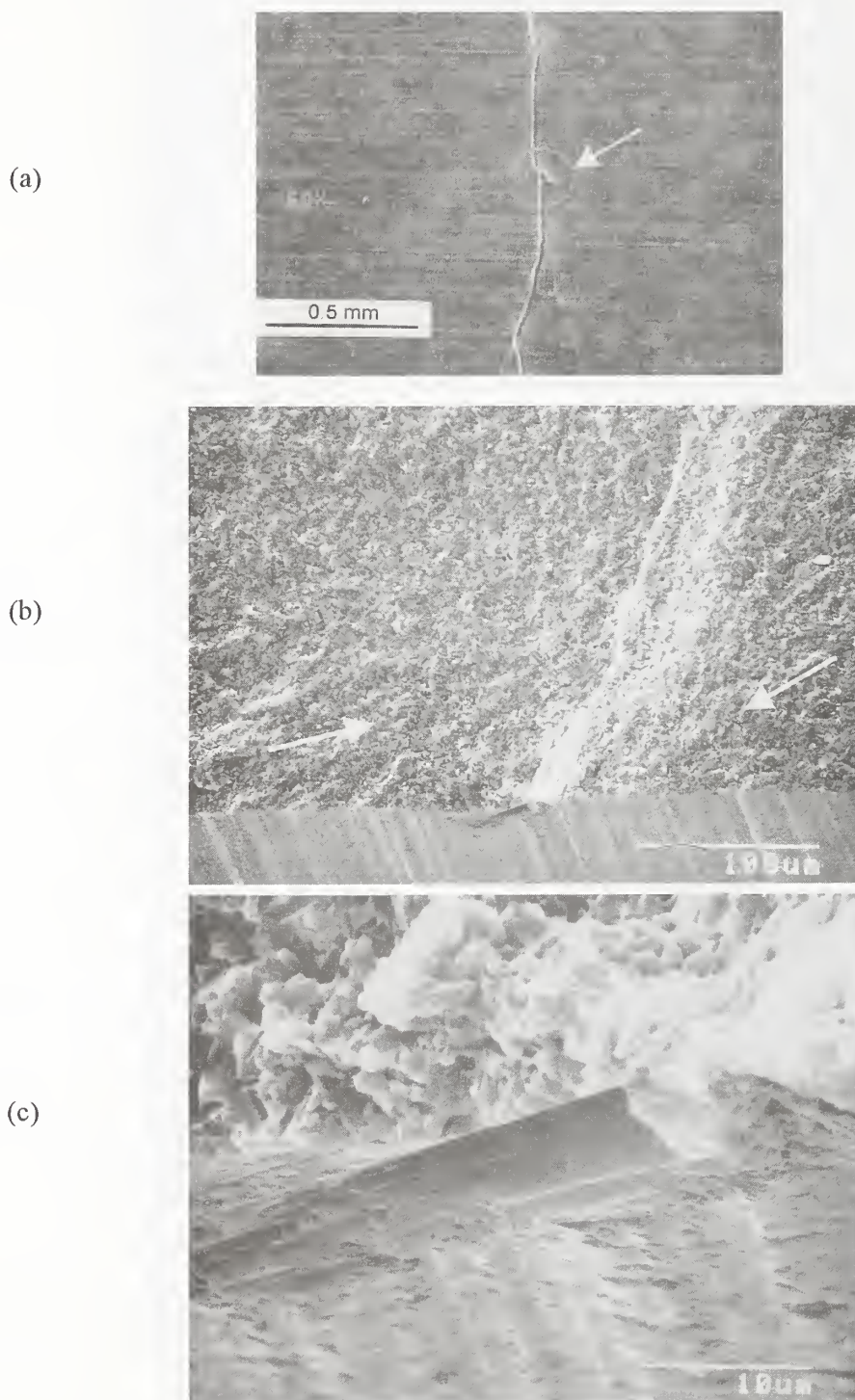
***Figure 31*** Optical photos of "Zipper machining cracks" in Shop C 320 grit transversely ground bars. The machining cracks are obvious even at these low magnifications. (a) shows both halves mounted back to back of the next to weakest bar in the set, 487 MPa. (b) is a schematic with close up, and (c) shows a 561 MPa strong specimen with 40 μm deep machining crack ($K_{Ic}$ = 5.64 MPa√m). Notice how the steps between the offset parallel cracks and the machining crack hackle that extend upward into the fracture surface are accentuated by the low angle incident lighting coming from the left side in (a) and the right side in (c). The machining crack hackle lines are tilted on either side of the origin. They form when fracture expands outward from middle of the row of machining cracks.

(a)



(b)



Machining crack hackle ("fingerlets")

Offset parallel machining cracks

"Zipper machining crack"

Close up of the machining crack

Origin centerline

"Machining crack hackle"

Jogs or steps between segments

(c)



200 μm
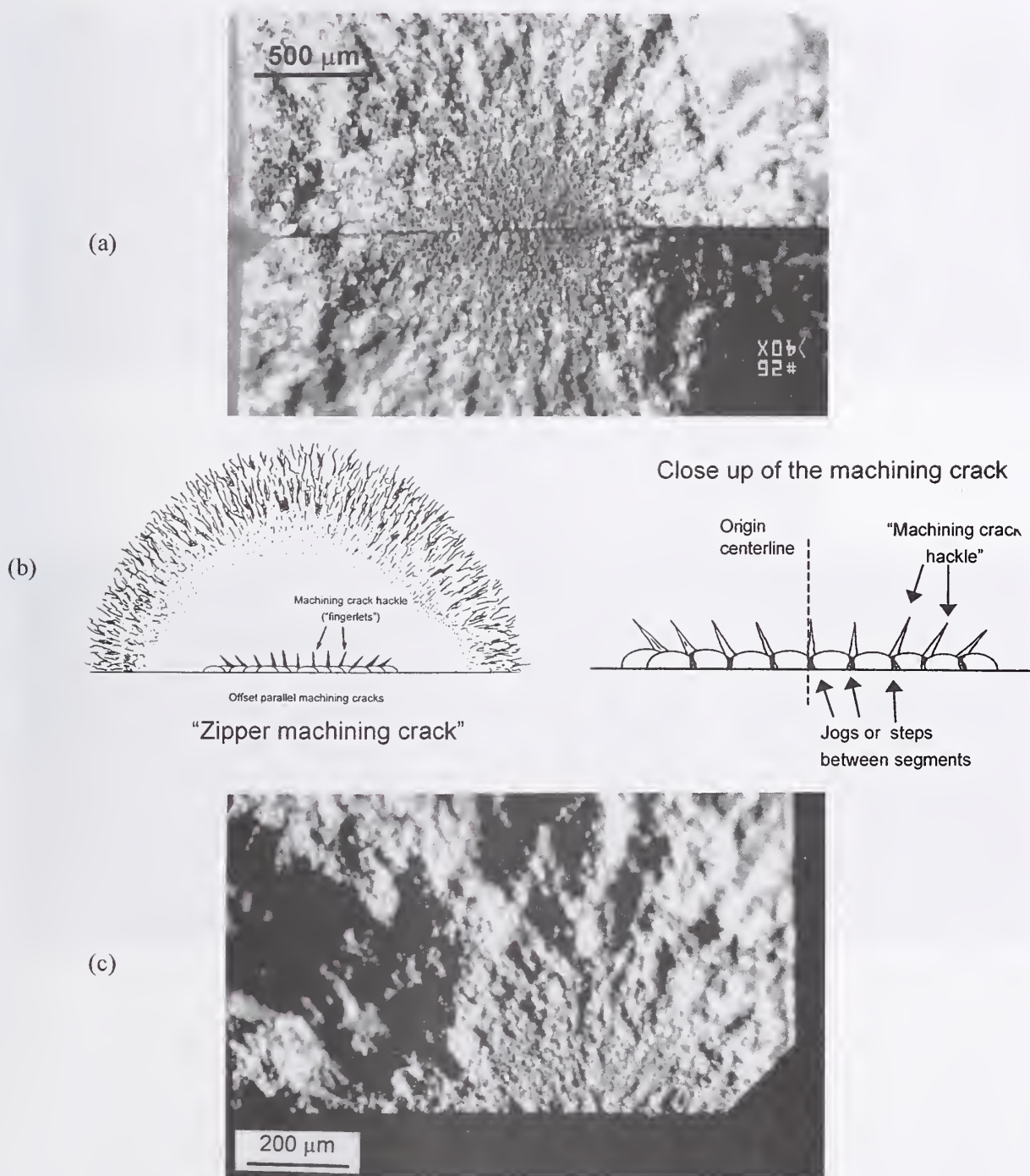
*Figure 32* (a) and (b) show two optical views of the back-to-back mounted fracture halves of a 516 MPa specimen transversely ground with a 320 grit wheel. A "**Zipper machining crack,**" which is one type of parallel machining crack, is easy to discern with low angle incident lighting. The elongated shape of the mirror is evident in (b). (c) and (d) show SEM close-ups of the origin. The 35 μm deep crack produces a fracture toughness estimate of 5.07 MPa√m.

(a)

(b)



(c)

(d)
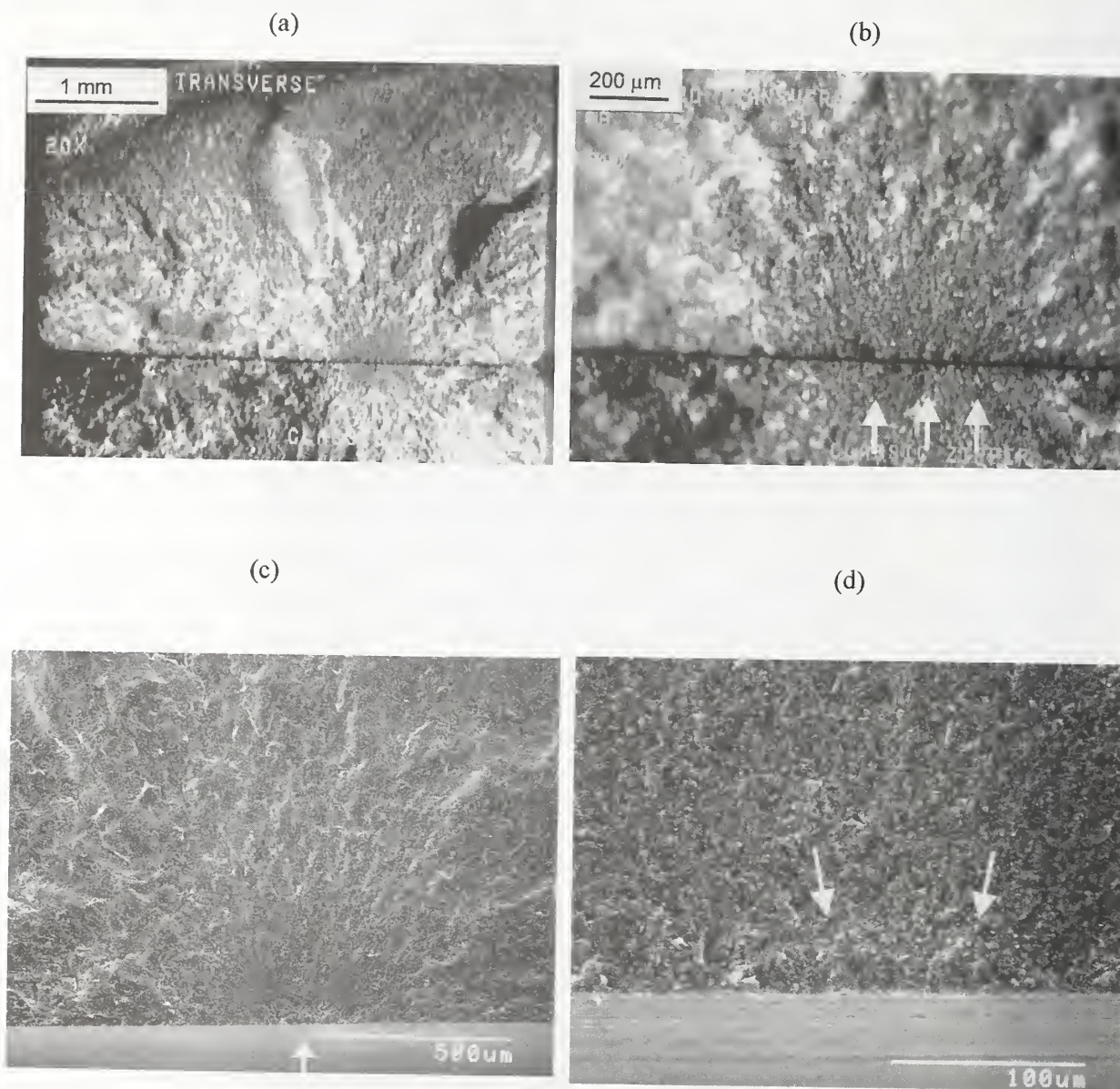
*Figure 33* Optical and SEM photos of a "**Zipper machining crack**" in a 487 MPa in a 320 grit transversely ground bar. This was the weakest specimen in the set. With the 25 μm deep crack, the fracture toughness was estimated as 4.62 MPa√m. Note how in (a) the illumination from the right side has highlighted the 5–6 tiny vertical fingerlets at the origin quite clearly, whereas SEM photos do not show the steps very well at all.

(a)
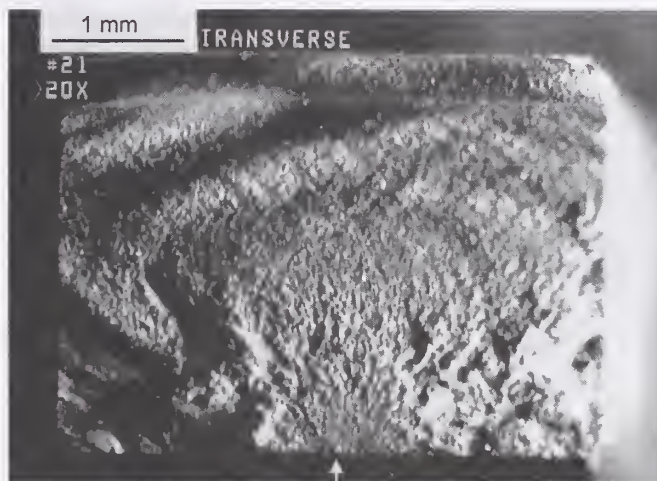


(b)
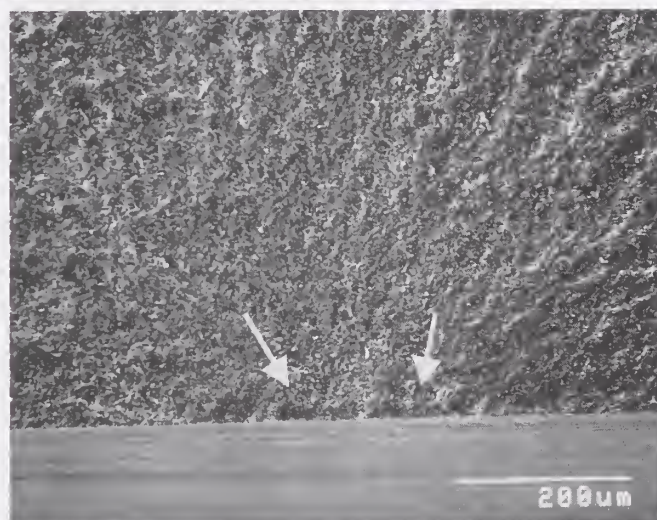


(c)
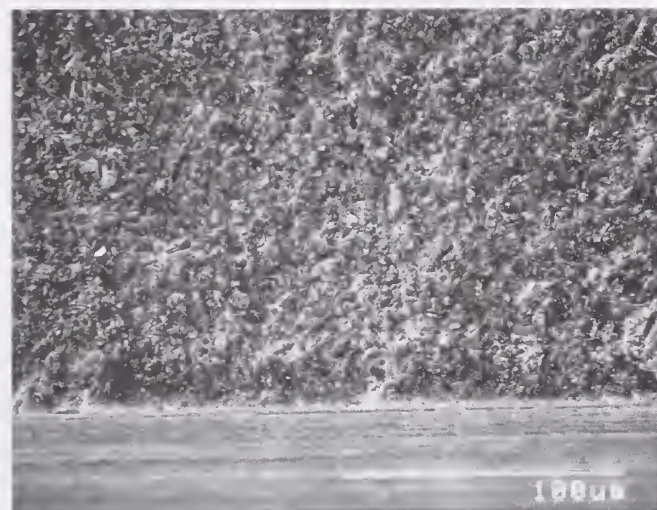
*Figure 34* SEM photos of 25 μm deep "Zipper machining crack" in a 542 MPa Shop C 320 grit transversely ground bar. ($K_{Ic}$= 4.85 MPa√m) In this instance, the SEM images do show the fingerlets.

(a)
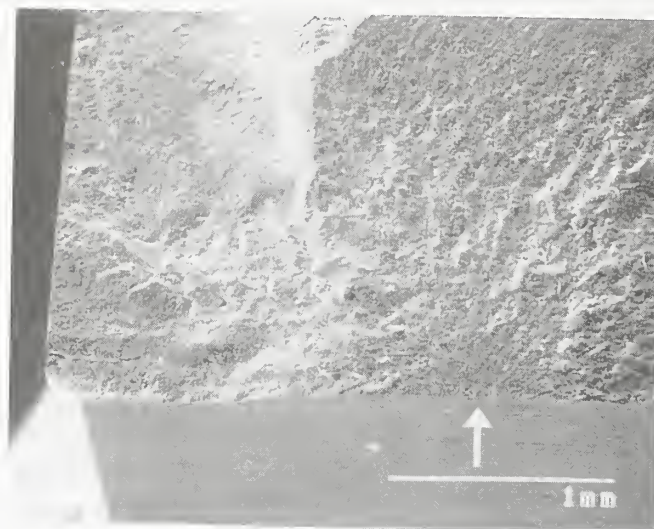
(b)
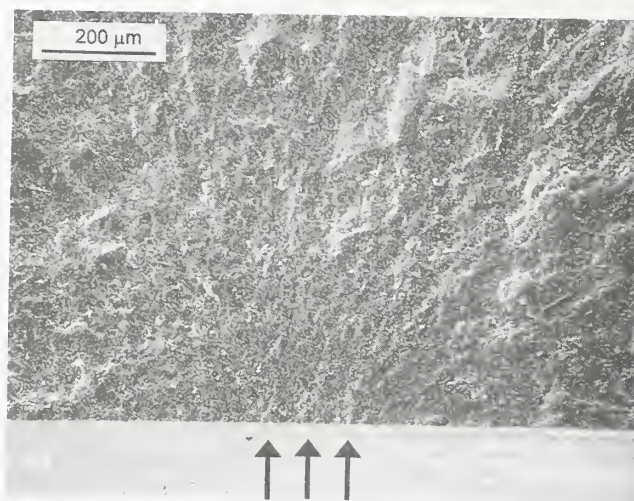
(c)
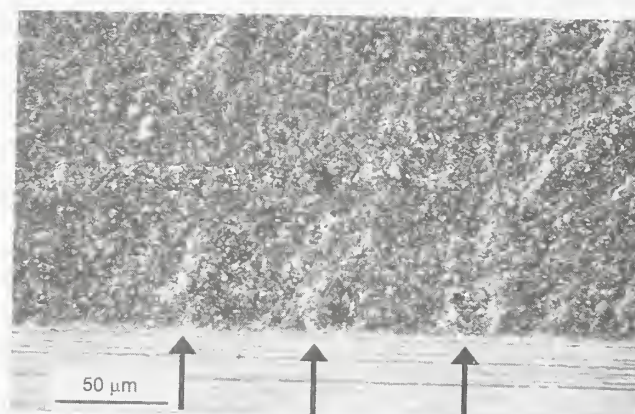
Even weaker specimens were obtained when shop C ground one sample bar set with a 150 grit wheel in the transverse direction in an earlier phase of the Consortium program. Unlike the other specimens discussed here, these specimens were cut out of plates and not rods. Furthermore, 15 of the specimens were from one batch and the remaining 15 from a second batch. It was subsequently determined that one batch was 12% stronger on average than the other. This differential existed irrespective of how the specimens were machined and evidently was due to some microstructural variation in the two lots. Blending such data caused the lower than typical Weibull modulus for this set (6.8). All specimens broke from 35 μm to 70 μm deep parallel machining cracks introduced by the transverse grinding. **Figures 35 and 36** illustrate some examples wherein machining damage created bumpy, tortuous origins that presumably were made up of interacting short crack segments. The machining cracks may be considered large zipper cracks whose individual crack segments caused some meandering and bumpiness. A new telltale fractographic sign of machining damage manifested itself in these specimens as shown in **Figure 35 and 36**. The deep machining damage extended not only across the fracture mirror, but well along the bottom of the fracture surface, along the tensile edge, and often entirely across the specimen. This thin "**machining crack skin zone**" could be distinguished from the fast fracture markings of the crack. Indeed, the depth of this surface damage zone closely matched the depth of the machining cracks inside the mirror at the origin. Once we recognized this feature, it became very easy to measure the crack damage depths in these specimens.

A special pattern was detected in these 150 grit transversely ground bar specimens. In one batch, fracture always started from one particular seemingly innocuous striation as illustrated in **Figures 37 and 38**. This was noticed when reassembling the specimen fragments as a first step in the fractographic analysis. Fracture seemed to occur from preferred locations in the inner gage section. Although one wide but shallow striation was prominent on the surface, it was *not* the cause of fracture. This harmless striation repeated every 2 mm, corresponding to the cross feed setting of the grinding machine. The failure initiating striation was in the middle of this repeating 2 mm band. It was a single striation in a group of four closely spaced small striations. It appeared innocuous when viewed in the optical and SEM microscopes. It certainly was not the largest or deepest striation. It did have much more grain pull out, fracture, and fragmentation, however. Subsurface damage was manifested as light scattering sources and the striation appeared in the optical microscope as a fuzzy-blurred region rather than a distinct groove. In contrast, the other more noticeable striations (labeled C, 1, 2, 3a, 3b, 4a) on the tensile surface were grooves that suggested plastic deformation with negligible subsurface cracking. **Figures 35 and 36** reveal what lay underneath the deleterious striations. A different repeating pattern of striations was detected in the second batch of 15 specimens, but again, fracture always commenced from one particular striation. Other investigators have noticed similar differences between plastically grooved and fragmented striations [5,52,53] but have not correlated the difference to preferred fracture sites. Xu [5] observed very similar variations in 80 grit grinding striations in two silicon nitrides in an earlier phase

of the Consortium program. Grain boundary microfracture and grain pullout were identified as key material removal processes. These observations raise interesting questions about the nature of damage formation in coarse ground surfaces. It could very well be that one particularly severe, or "renegade" grit in the grinding wheel is dominant and accounts for the severest damage, rather than the average wheel grit size.

Shop F used a very coarse, 80 grit wheel to prepare one set of bars in an earlier phase of the Consortium program. Thirty bars were ground with a depth of cut of 0.050 mm. These specimens had an average strength of 430 MPa, which is almost 50% less than the baseline strength. This set also was cut from two batches of plates and this accounts for the low Weibull modulus (8.2). Obviously, machining damage had to have been strength controlling since the strengths were so low, but the fracture surfaces were at first puzzling. Unlike many of the fracture origins shown above, the origins in this sample set were very bumpy as shown in **Figure 39 and 40**. The parallel machining cracks were neither sharp straight cracks nor "zipper cracks." They were a series of wavy offset parallel cracks. The machining crack depths were usually 40 µm to 55 µm deep, although some as deep as 80 µm caused fracture in the weakest specimens in the lot. Furthermore, the fracture origins often coincided with unusually deep machining striations as illustrated in **Figure 41**. Unlike many of the specimens sets described above, the striations were quite deep and broad in this set. They were as deep as 15 µm and thus the groove itself became part of the overall flaw dimension. The machining crack damage formed underneath the striations, but meandered from side to side within the striation groove as illustrated in **Figure 41**. Offsets between the crack segments as well as the meandering in the groves contributed to the waviness or bumpiness of the machining damage when viewed on the fracture surface along the tensile edge. Strakna et al. [6] saw similar overlapping crack segments in their 80 grit transverse ground bar specimens, and termed these "saw tooth fracture." As with the 150 grit bar specimens, we also noted machining damage skin zones that ran along the entire bottom of the fracture surface. So whereas the bumpiness of the machining cracks in the mirror region initially complicated the interpretation, the telltale band along the tensile surface made identification of machining damage and the depth measurements quite easy.

*Figure 35* Optical photos of a" zipper crack" in a 150 grit transversely ground bar. Both fracture halves are mounted back-to-back. The large arrow in (a) identifies the **"coarse zipper crack"** at the origin, but the machining crack damage is also visible as a thin band running across the entire fracture surface width (small arrows) (411 MPa). (b) shows a similar zipper crack in a 412 MPa specimen. Notice the three vertical fingerlets at the origin in this low magnification optical photo. The low angle directional illumination highlights these tell tale features.



(a)
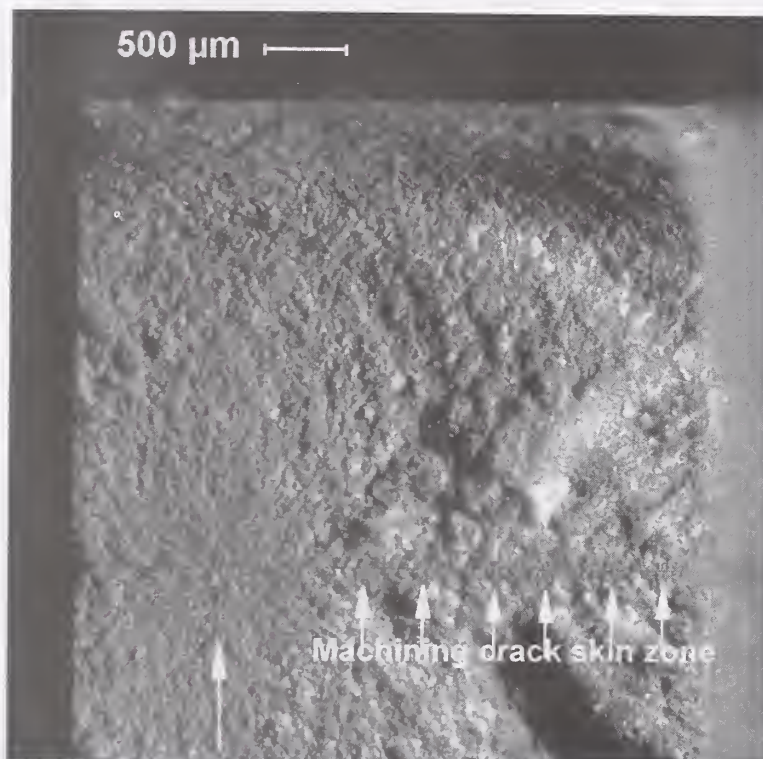
(b)
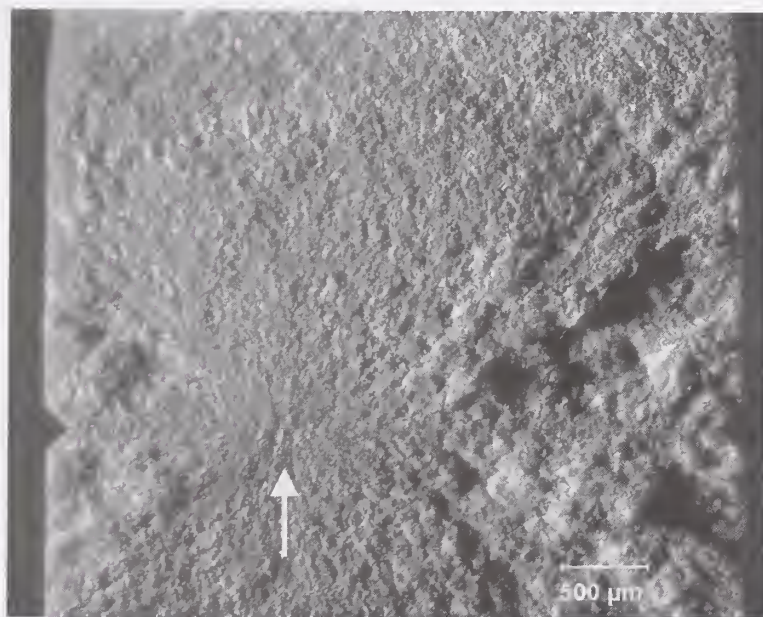
*Figure 36* Optical photos (a, b) and matching schematic (c) of a 65 μm deep zipper cracks in a Shop C 150 grit transversely ground bar (399 MPa). The mirror and the origin are in the middle, but the thin band of machining crack damage extends out to either side to the specimens side surfaces marked by the large arrows in (a) and small arrows in (b). (c) is a schematic view which illustrates that the depth of the machining crack skin zone is similar to the depth of the cracks at the origin.

(a)

(b)

(c)
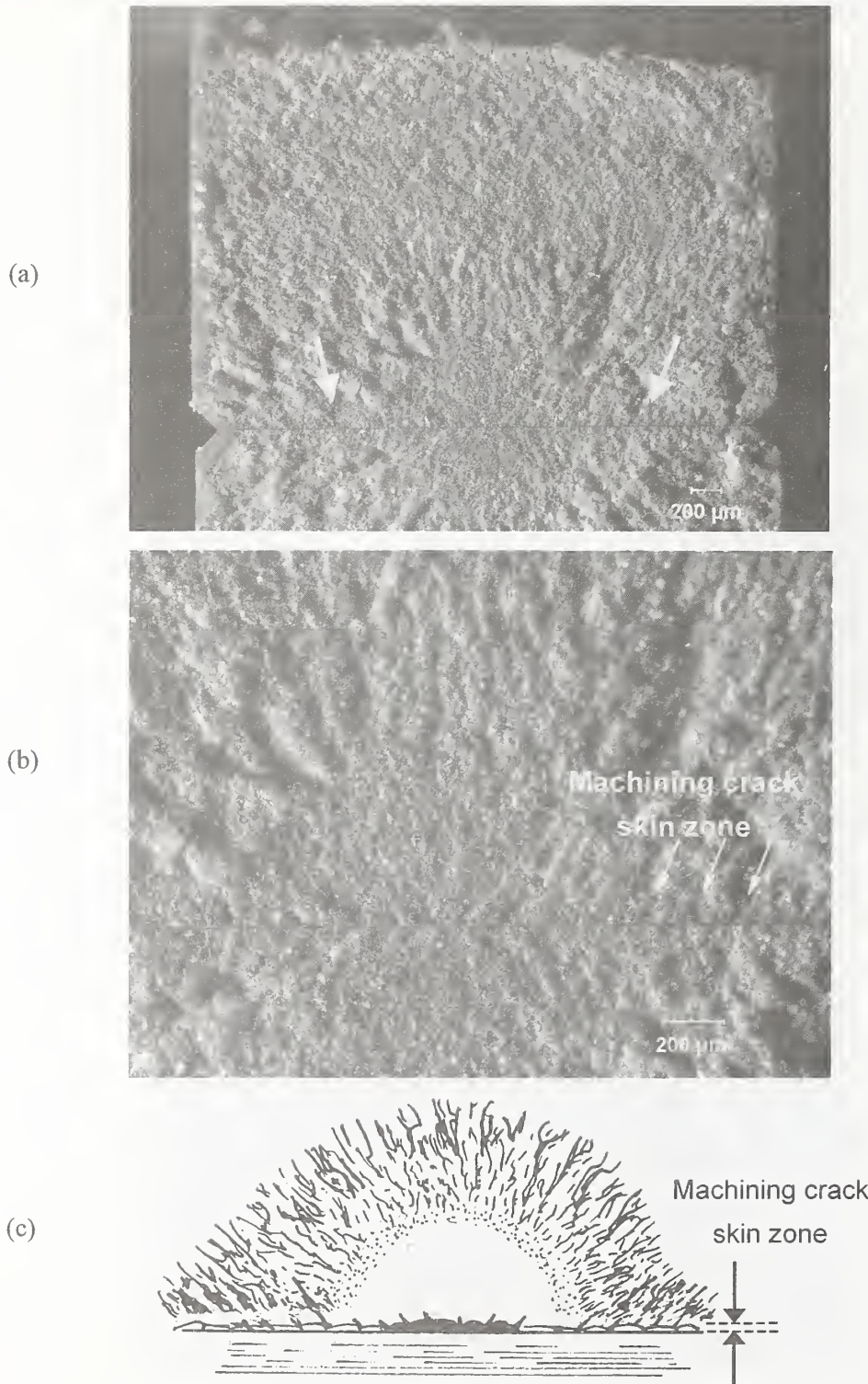
*Figure 37* The Shop C 150 grit transversely ground bars had a recurring a recurring striation pattern. In one group of specimens, fracture always occurred from one particular subtle striation. (a) show the origin area on the fracture surface cracks in a 519 MPa specimen. (b) shows the ground tensile surface. The arrows show the broad but shallow harmless striations "C" that were spaced every 2 mm apart. These did *not* initiate fracture. (c) is s close up of this harmless striation. The photo was taken near the specimen's 45° edge chamfer. The striation is broad and shallow and suggests plastic deformation with little or no damage underneath.
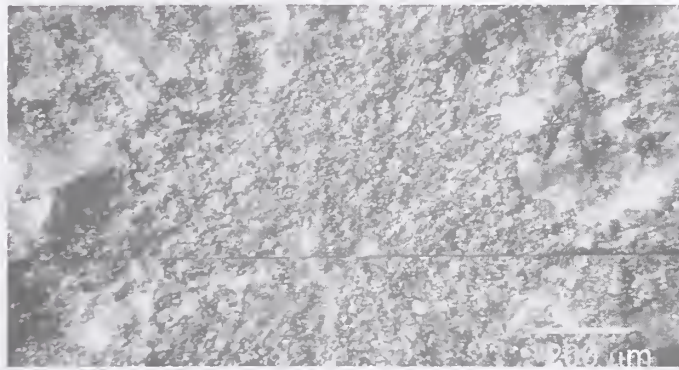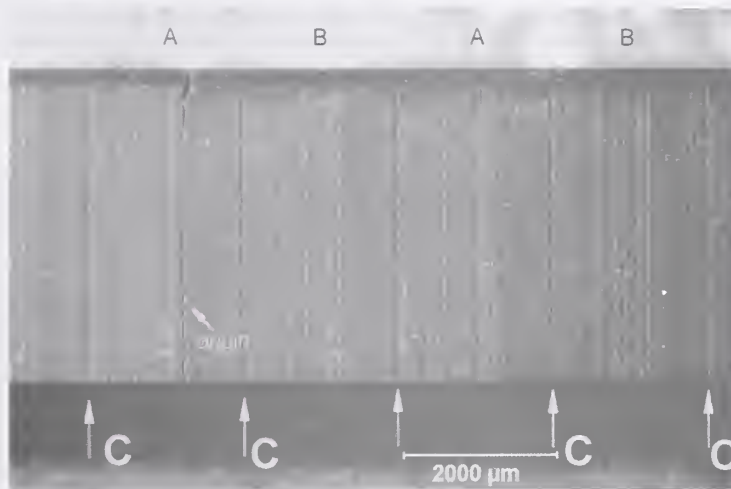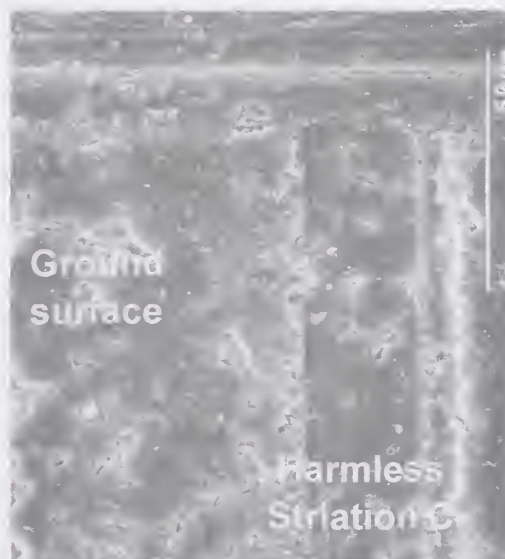
*Figure 38* Optical and SEM close ups of striations in the ground surface of the bar shown in the previous figure.    (a) shows the group of 4 striations and the fracture origin site.    (b) is the same group of 4 striations at  another location.  (c) and (d) are SEM close ups that show that third and fourth striations are in fact pairs of smaller closely spaced striations.  Note that striations #1-3 are distinct, whereas the striation #4 is more diffuse, attesting to more light scattering from beneath the surface.  Fracture always initiated from the striation #4b region marked with the arrow in (d).

(a)

(b)

(c)

(d)
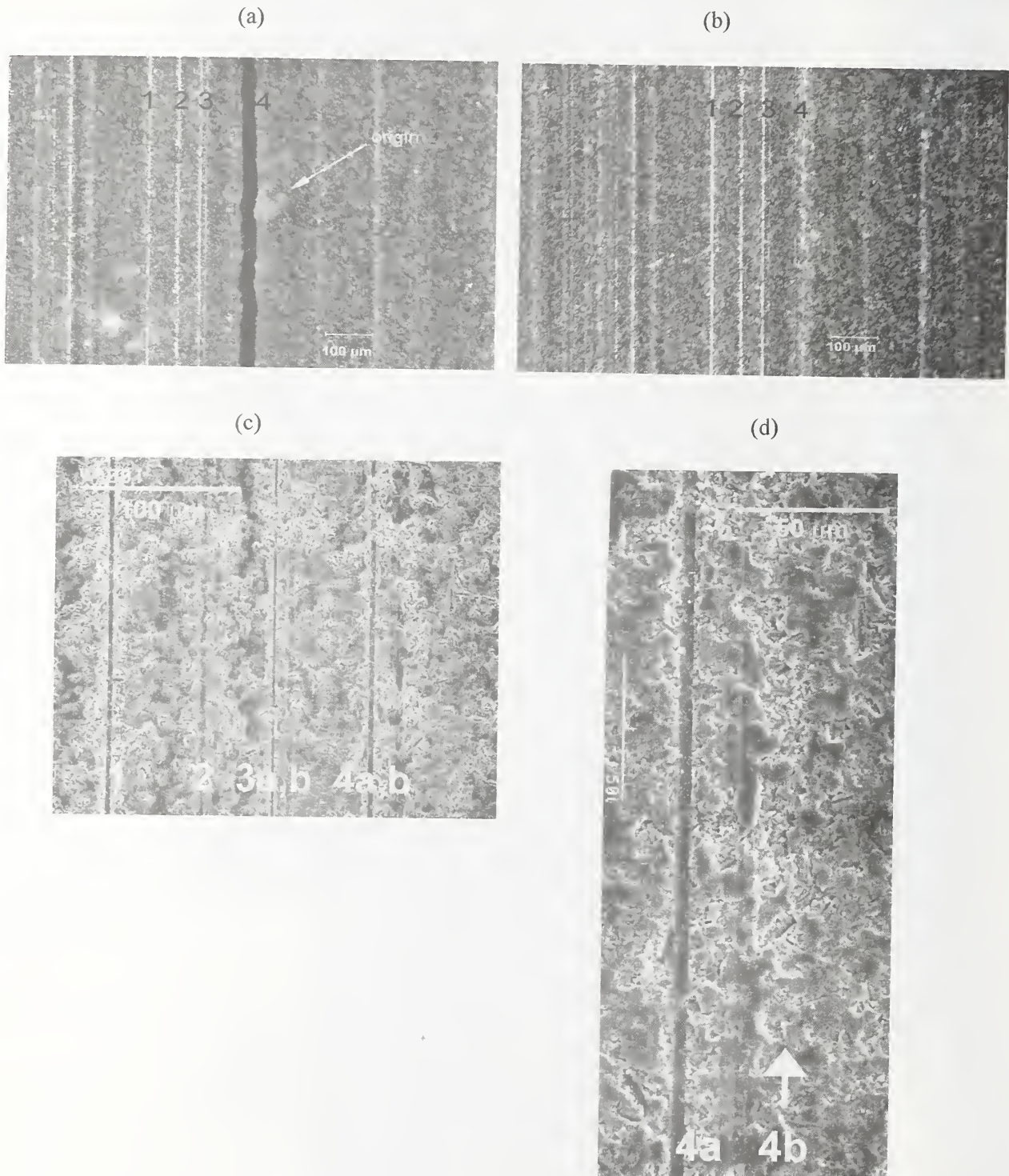
*Figure 39* Coarse 80 grit transverse grinding created 40 μm – 80 μm deep parallel machining cracks that appeared quite bumpy at the SRBSN origin. Three optical microscope view of specimen which fractured at 476 MPa with a 42 μm deep, very long crack. Notice the roughness and bumpiness even in the mirror region in this toughened silicon nitride.



(a)

(b)
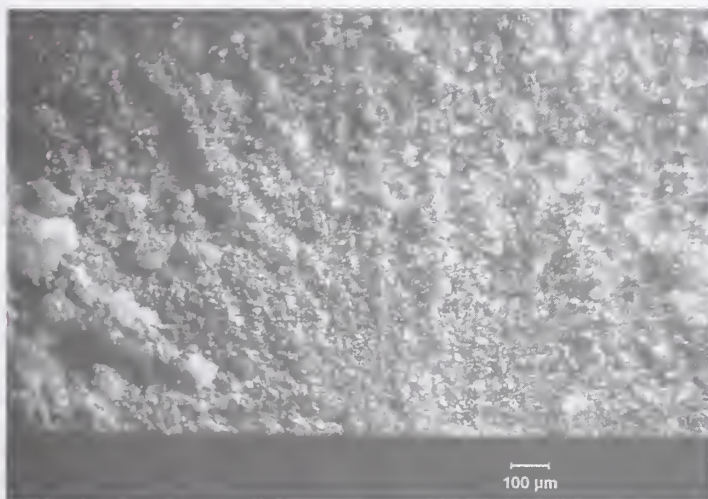
(c)
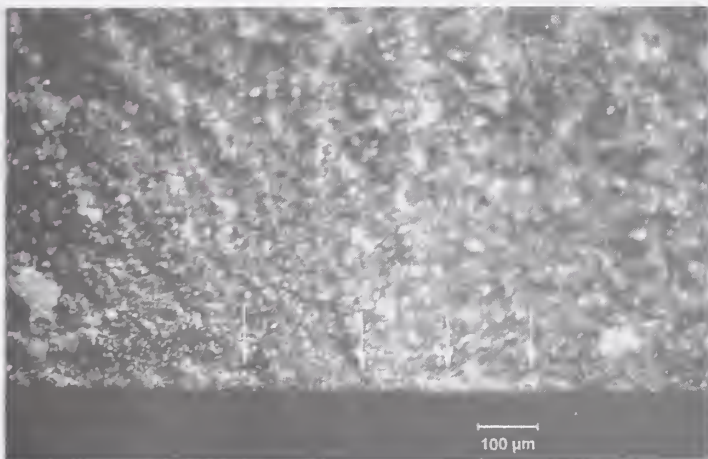
*Figure 40*  Fracture origin in an 80 grit transverse ground SRBSN bar.  Both halves are mounted back to back.   This optical photo shows unusually deep (80 μm) machining damage cracks at the origin (larger arrow)  on the right side in a very weak specimen (357 MPa).  The machining damage skin zone extends along the entire tensile edge of the specimen from side to side (smaller arrows).
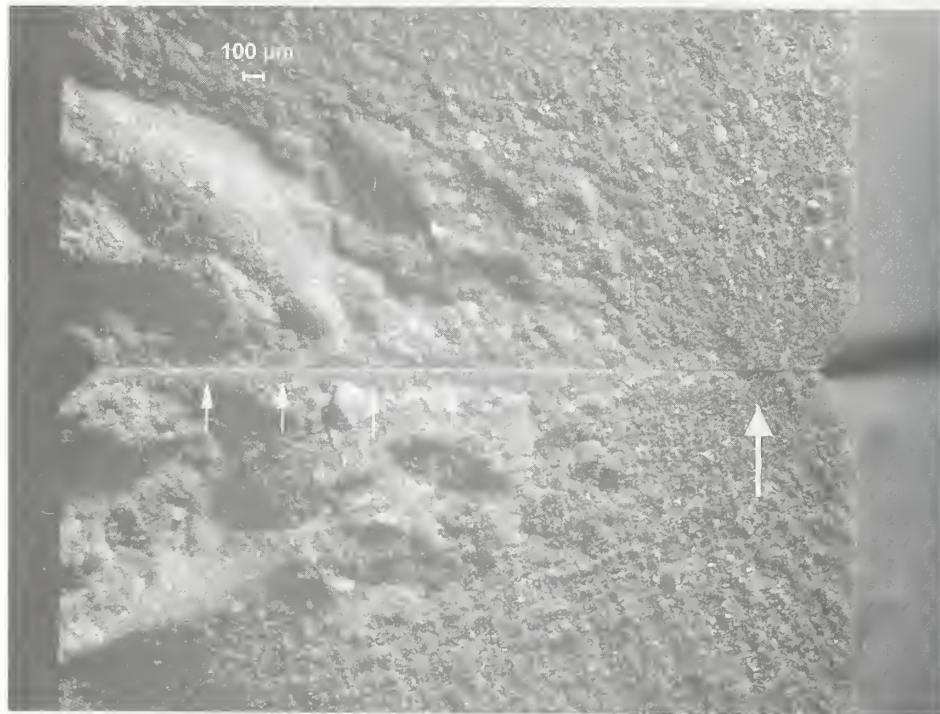
**Figure 41** Fracture in the coarse 80 grit transverse striations often initiated from parallel machining cracks that emanated beneath unusually deep striations as depicted in (a). The machining crack damage extended well beneath the striation, but meandered under the striation and caused the fracture origin to appear bumpy on the fracture surface as shown in the previous figures. (b) and (c) show matching SEM photographs of the origin area in a 463 MPa specimen. The 45 μm deep machining cracks (large arrows) are associated with a deep striation (smaller arrows). The origin is near to, but not at the chamfer.

(a)
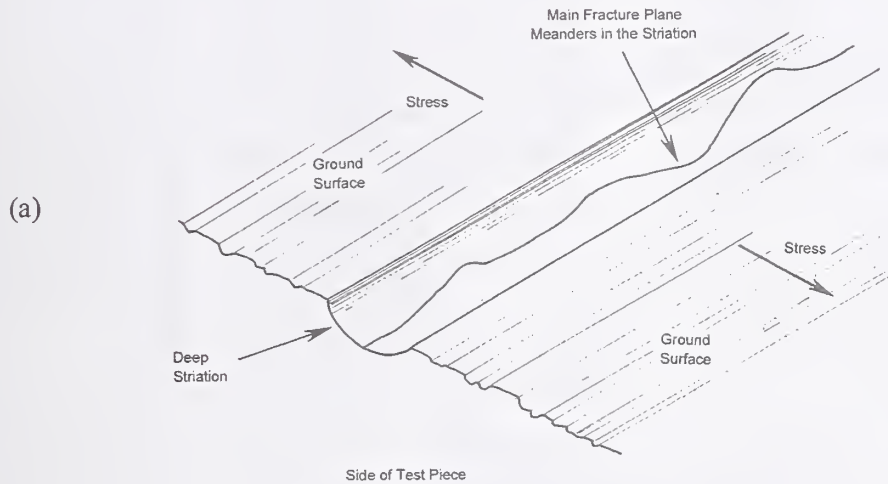


(b)                                    (c)
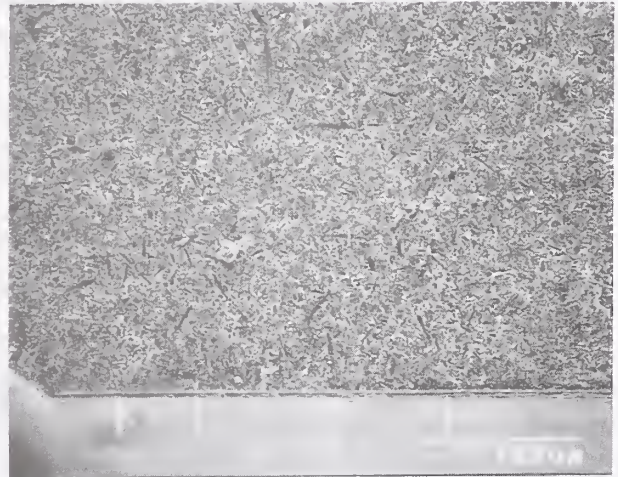
# ANALYSIS OF RESULTS

**Tables 2 and 3** rank the strength outcomes and illustrate the strength limiting flaws in descending order, starting with the strongest data sets. Longitudinal grinding and finer grits led to the greatest strengths as expected. For the rods, the 320 longitudinally ground specimens had the greatest strengths and nearly all specimens broke from inherent material flaws. Three different shops either matched this performance or came close with 600 grit centerless or transverse cylindrical grinding. It is reassuring that three different shops could obtain comparable performance on the same material.

Coarser wheel grits or more aggressive grinding procedures led to progressively deeper damage and specimen weakening. Despite all these variations, with a few exceptions, the test sets had similar Weibull moduli between 12 and 30. Some statistical sampling variability in the Weibull moduli is expected with small sample sizes (n = 10 or 30). One might expect that machining cracks should be very consistent in size for a given procedure, and that this would lead to a significant increase in the Weibull modulus, but only two sample sets had dramatically increased moduli (28.1 and 35.9).

**Figure 42** is a customary style graph showing strength versus wheel grit size for both longitudinal and transverse grinding. Included for comparison are data for other silicon nitrides from the literature: Allor et al. [14,15]; Anderson and Bratton [16]; Wu and McKinney [17]; Breder et al. [18]; Ota and Miyahara [19]; Mayer and Fang [21,22]; Thomas et al. [25]; Alfaro et al. [54], and Foley et al. [33]. We also include some earlier Consortium work by Strakna et al. [6] and Ives et al. [55]. The transverse strength *trends* are very similar for all studies, a remarkable finding. In general, transverse strengths decrease for wheel grits coarser than 600 grit. The longitudinal grinding trends varied. Either there was no effect of grit size and all strengths matched baseline strengths, or strength began to decrease with wheels coarser than 240 grit. [16,25]

## Surface finish

**Tables 2 and 3** include the surface roughness outcomes, $R_a$, for most sets. In general, the final surface roughness did not correlate to the strengths. For example, the lapped rods had the finest finish, but had some of the worst strengths since the flaws that controlled strength were from earlier phase grinding. The lack of a correlation between strength and surface finish in this SRBSN is consistent with findings from earlier phases of the Consortium program.[1]

***Figure 42*** Strength versus grit size for (a) transverse, and (b), longitudinal grinding. Average strengths are shown unless denoted with * in which case the values are characteristic strengths. Baseline strengths, which presumably are the inherent strengths in each case, varied with material and testing configuration and are marked on the right if available. Material code designations are shown if available.
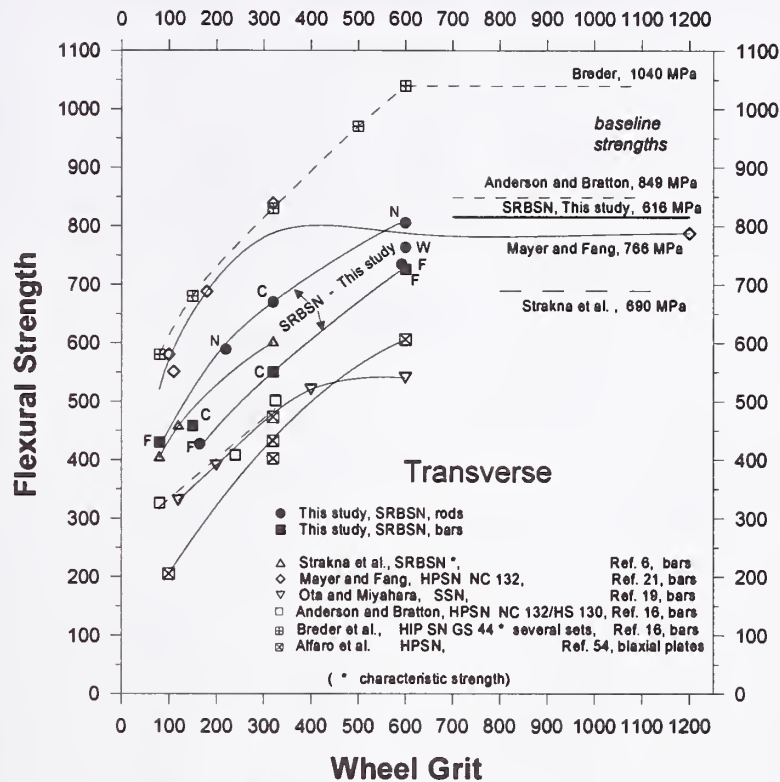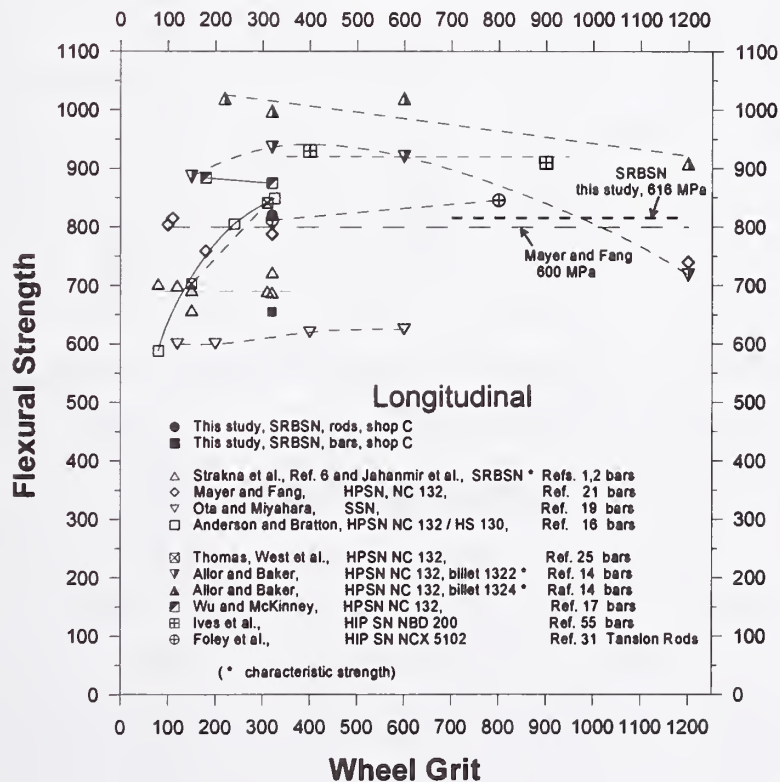
**Figure 43** Machining crack size (depth) versus wheel grit for the SRBSN in this study. Only parallel machining cracks from transverse grinding are shown. Circles denote individual rod specimens and squares denote individual rectangular bar specimens. The variation in crack sizes for any given set of conditions was a factor of two. This size variability is consistent with the strength variability. For comparison, the size range (half minor axis dimension) of the material flaws is shown on the right side.
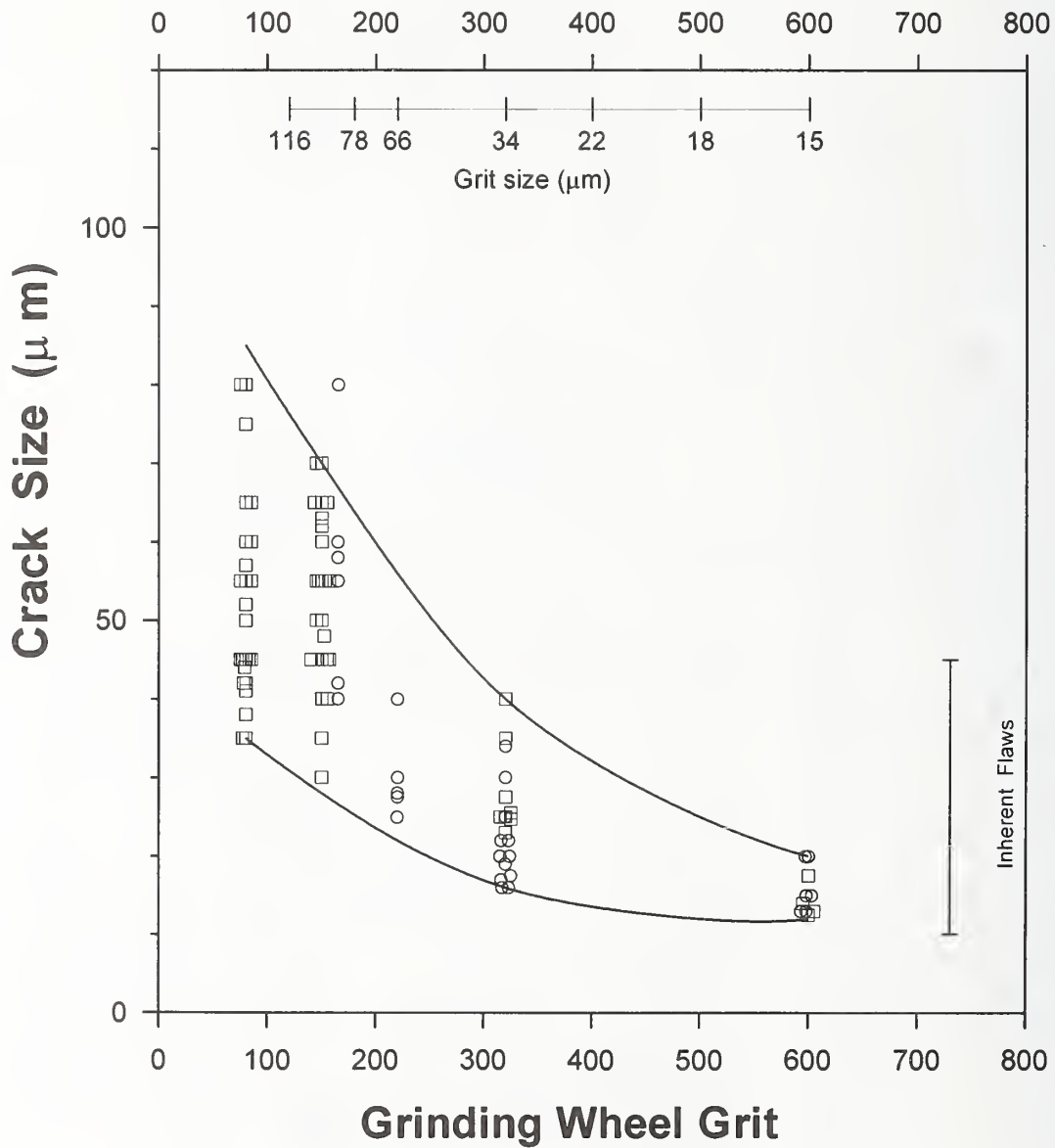
**The Size of the SRBSN Machining Cracks**

**Figure 43** shows the size distribution of all machining cracks measured in this study. The depth is shown since it is the controlling dimension in fracture mechanics calculations for long shallow surface cracks in a body. The depth is also an important factor in assessing damage in a finished part. The critical crack size is shown. In a <u>few instances</u>, cracks showed evidence of stable extension such as shown in **Figures 15-18**. We could not detect any consistent patterns of stable crack extension in the data sets in this study. The stable extension, when detected, was usually of the order of 5 μm to 15 μm. Other studies have detected stable crack extension from machining cracks, but only in fine-grained materials wherein the extension stood out more clearly on the fracture surfaces. Machining flaws with clear evidence of multiple step propagation are also shown by Rice, Mecholsky, and Becher [30]. Marshall et al. [56] showed clear signs of stable extension driven by strong residual stresses both from coarse-machining damage cracks and from rows of Knoop indentations.

The crack depths ranged from a minimum of 12 μm to a maximum of 80 μm. Sizes smaller than 10 μm do not appear since specimens with such small cracks broke instead from material flaws. The ≈ 80 μm upper limit is the severest machining damage likely to be encountered with conventional grinding conditions in this SRBSN. The surface lengths of the machining cracks varied from as low as ≈ 50 μm, to as long as hundreds of micrometers, to the full width of the specimens in some of the coarsest ground (150 and 80 grit) bar specimens. Rice et al. [29,30] also observed a range in flaw sizes from 15 μm to 89 μm in many ground polycrystalline and single crystal ceramics. Even in glass flexural strength bars ground with a 180 grit wheel, they only found cracks from ≈ 10 μm to ≈ 77 μm deep. [31] [r]

Several points may be made from **Figure 43**. In each data set there are only some depth measurements since we were either unable to obtain a depth measurement in some specimens, or alternatively, the specimen may have fractured from a material flaw. The coarser the grit size, the more likely machining damage was strength limiting and the easier it was to measure the machining cracks. So for example, more than 20 data points are shown for the bar specimens ground with 150 and 80 grit wheels. A second point is that there was good concurrence of crack depths for rods and bars at 600, 320, and 150/180 wheel grits. Thirdly, despite the fact that specimens were ground by a number of different shops with many differences in key machining parameters (e.g., wheel depth of cut or table speeds) all the data seems to converge. Fourthly, it is fascinating that the range of machining crack sizes was of the order of a factor of two at each machining condition. This is an interesting finding; since it runs counter to a widely held expectation that machining cracks should be fairly consistent (e.g., Breder et al. [18] for a hot-isopressed silicon nitride wherein m varied from 20 to 40). Rice et al. [29,30] also noted a spread of a factor of two in their 320 grit ground polycrystalline and single crystalline ceramic bend bars. Our spread of crack sizes was matched by a commensurate spread in strengths. The ground rod sets had

---

[r]    They reported average cracks depths and standard deviations. The numbers shown above are the average parallel crack size plus two standard deviations and the average orthogonal crack size minus two standard deviations.

Weibull moduli between 13 and 28 (**Figure 10**). The bars had moduli typically between 10 and 15 (**Figure 27**). **Figures 10 and 27** show that data sets with moduli of the order of 15 had strengths that varied by a factor of $\approx 1.4$ from lowest to highest. Since strength scales with the inverse square root of crack size, the 1.4 factor is entirely consistent with the factor of 2.0 variation in machining crack size.

At the higher strengths (> 600 MPa) the material flaws are dominant. Their spread in size and severity was such that the material flaw Weibull modulus itself was 15. A bar showing their size range (10 μm – 45 μm, half minor axis length) is shown on the right side of **Figure 43.** Material flaws and machining cracks of the same size may not have the same severity. For example, a 20 μm deep machining crack was far more deleterious to strength than a 20 μm radius material flaw. The machining crack was sharp, very long, and had a more severe stress intensity. The material flaws were more equiaxed, partially bonded to the material, or three-dimensional and their stress intensity shape factors were much less. Salem et al. [24] also observed that small machining cracks could control strength even though larger material flaws were present in sintered alpha silicon carbide. In our study, there was considerable overlap in strengths and flaws sizes for the specimens ground with 600 grit transverse or 320 grit transverse grinding. Some specimens broke from machining cracks, some from material flaws, and many were hybrid flaws comprising linked machining-material flaws. Machining flaws became dominant for grinding wheels coarser than 320 grit. A summary map of these results is shown in **Figure 44.**

**Comparison of Machining Flaw Sizes in Different Silicon Nitrides**

**Figure 45** compares our crack size results on the SRBSN with literature data on other silicon nitrides.[16,26,28,33,34,54,56,57,58,59,60,61,62,] The literature is sparse. Although several engine companies (e.g., Westinghouse, Daimler-Benz, Garrett) conducted machining damage studies, they usually calculated or inferred their flaw sizes from bar strength data, sometimes without furnishing details on how the calculations were performed. A few isolated illustrations of machining damage cracks have appeared in a handful of papers and we have measured the crack sizes from these photographs. Nearly all the actual data is for parallel cracks from transverse grinding. Orthogonal crack size measurements from longitudinal grinding are exceedingly rare. We could not help but notice that many of the original authors were tentative with their identification of the machining cracks or their dimensions. Many were reluctant to even put arrows on their photos and one is left with the impression that they left the interpretation up to the reader! This underscores the uneasiness many investigators have had with identifying or characterizing machining damage. Most the studies featured hot-pressed silicon nitride, and in particular, Norton's grades NC 132 and HS 130.[s] These HPSN's were fully dense and had fine, slightly elongated

---

[s]   Norton Co., Worcester, MA. Both HS 130 and NC 132 were hot pressed in the 1970's and 1980's. The former was the immediate predecessor to the latter. They had nearly identical microstructures and the primary difference was concentration of impurities such as Ca and W. They were two of the most studied structural ceramics of all time and were prominent candidates in a number of major engine programs. NIST Standard Reference Material 2100, Fracture Toughness is comprised of NC 132 test pieces.

**Figure 44** Damage map for the SRBSN for transverse grinding. Machining cracks may be smaller than the inherent flaws, but they are more severe stress intensifiers (Griffith cracks).

61
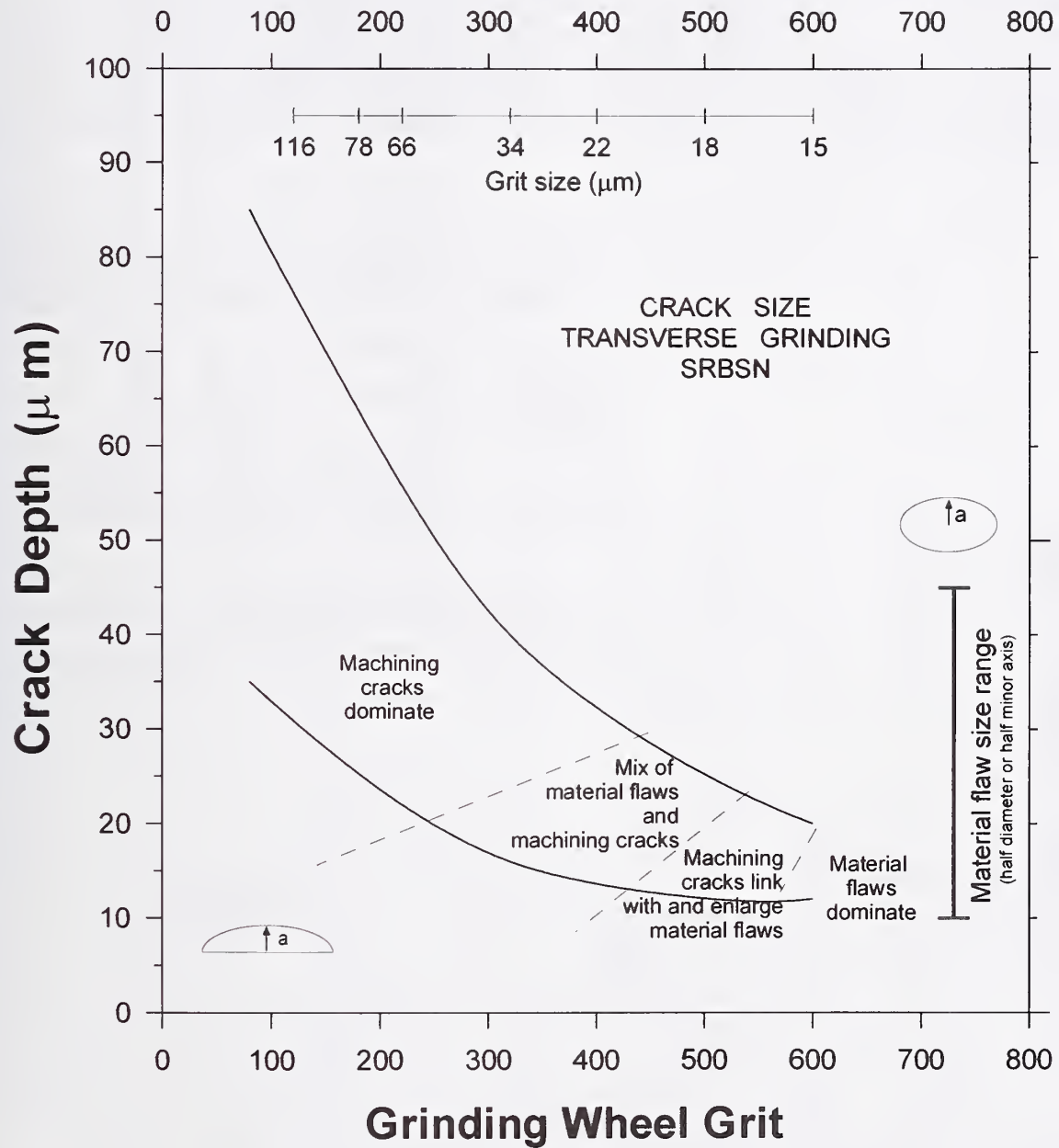
*Figure 45* Machining crack size versus wheel grit from a variety of studies for silicon nitride. The range of outcomes for the SRBSN from this study (previous figure) are included as solid lines. Other data entries are individual data points or ranges from the other referenced sources. Unpublished new NIST data on Dow SSN and Eaton SRBSN are also shown. Unless otherwise stated in the key, all grinding was transverse. Calculated crack sizes from studies by Daimler-Benz and Westinghouse are shown as dashed lines with "x" or "+" symbols corresponding to the grit sizes at which strength data was collected. The Daimler-Benz data could be adjusted downward slightly (arrows) if the fracture toughness for the NC 132 that was used was adjusted from 5.0 MPa√m to 4.6 MPa√m. Material code designations are listed where available. For example, many of the studies used Norton's hop pressed silicon nitride (HPSN) grades NC 132 or HS 130. With the exception of the Daimler Benz calculations and the Dow SSN data, nearly all the data fit a single trend.
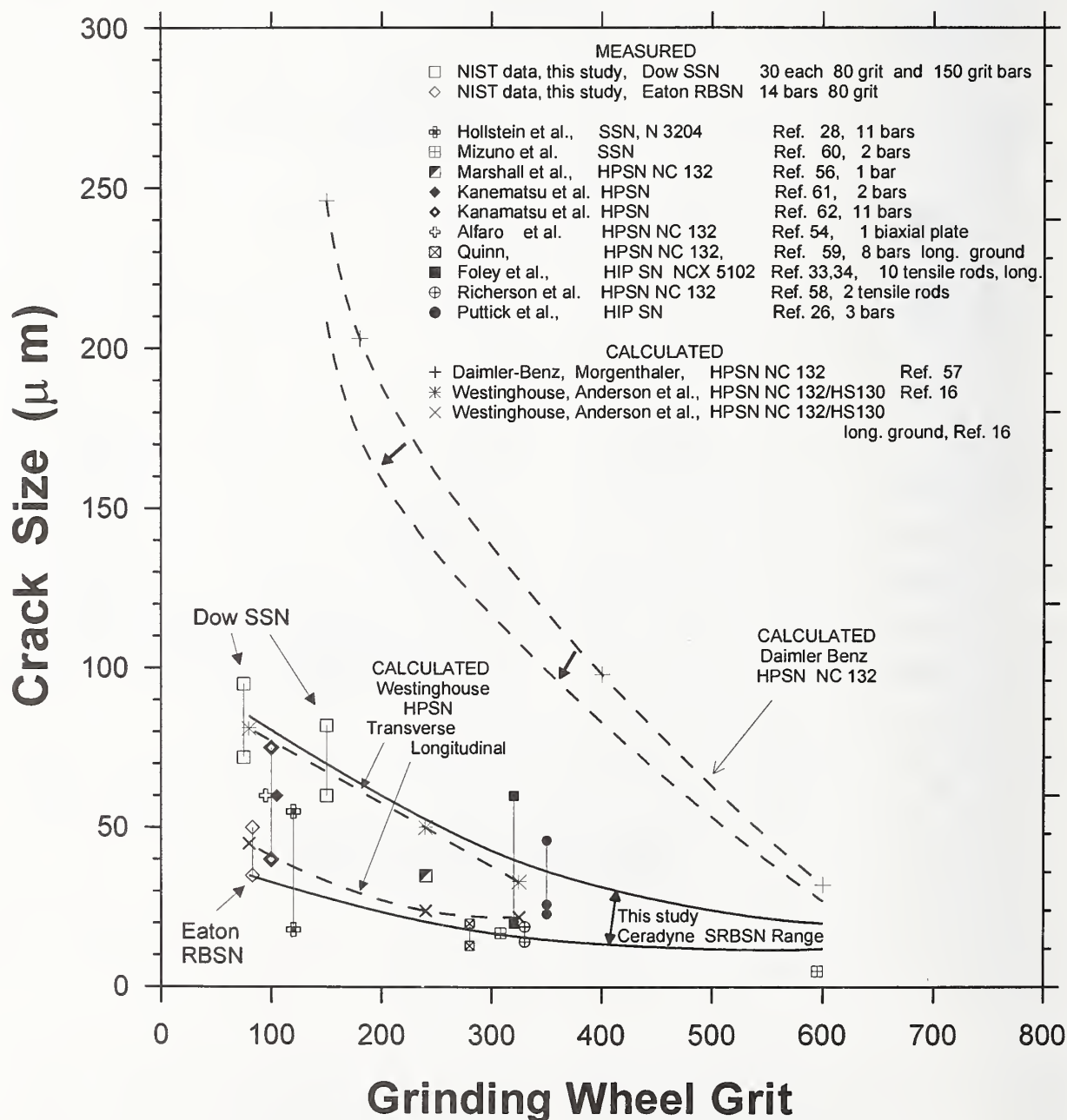
beta silicon nitride grains that made the material conducive to fractographic analysis. Even so, although finding parallel cracks from transverse grinding was not difficult; detection of orthogonal cracks in NC 132 from longitudinal grinding was difficult.[63,64] **Figures 8a,b** show examples. We do not know why the Daimler calculations for cracks sizes are so different from the other sets, and even correcting the calculation for a more accurate fracture toughness does not solve the problem.

**Figure 45** includes limited data we also collected on two other silicon nitrides that were tested in an earlier phase of the Consortium program: Dow sintered silicon nitride (SSN)[t] and Eaton reaction-bonded silicon nitride.[u] Properties for these are listed in **Table 4**. Fractographic examination was very limited in the earlier work, but we recently reexamined all of the 80 grit transversely ground SSN and RBSN specimens and all of the SSN 150 grit specimens. Were the crack markings similar and how large were the cracks compared to the Ceradyne SRBSN? Fractography confirmed that the cracks were easy to find in the SSN, but quite different in the RBSN. The machining crack sizes were dramatically different in the three materials. These differences were related to the hardness, elastic modulus, fracture toughness, and microstructures.

The RBSN machining damage zones were relatively easy to detect, but their size and shape were controlled by the microstructure of the material as shown in **Figure 46**. This low strength ($\approx$ 150 MPa) pressure-less sintered material is composed of densely packed spherical particles, 40 $\mu$m – 60 $\mu$m in diameter that are the vestiges of spray dry particles. The machining damage zone was only 35 $\mu$m – 50 $\mu$m deep and was confined to one layer deep of these agglomerates. Hence, this weak, low fracture toughness material is nonetheless effective in arresting machining cracks, much like a refractory firebrick is effective in arresting cracks.

The Dow SSN had very similar cracks compared to the Ceradyne SRBSN cracks despite the different microstructures and fracture toughness as shown in **Figure 47**. A surprising result was that the Dow SSN cracks were *usually larger* than the Ceradyne cracks. We momentarily defer further discussion of these surprising results until after a brief discussion of fracture mechanics analysis as applied to the SRBSN data. One group of Dow SSN specimens ground with the 150 grit wheel also exhibited the same breakage pattern discussed earlier for the SRBSN: every single specimen fractured from one particular striation that repeated every 2 mm along the specimen ground surface. This confirms the earlier assessment that a single severe grit in a grinding wheel may be crucial.

The maximum machining crack depth detected in our study on the SRBSN was 80 $\mu$m under the coarsest grinding conditions. The maximum crack size for any silicon nitride from our review of other literature data was 100 $\mu$m.

---

[t]    Dow Chemical Co., Midland, MI.

[u]    Eaton Corp., Southfield, MI.

**Table 4** Property data for the SRBSN and three other silicon nitrides for comparison.

| Material | Density (g/cm$^3$) | Grain size (μm) width X length | Elastic Modulus (GPa) | Hardness, (GPa)‡ | | Fracture toughness (MPa√m)† | |
|---|---|---|---|---|---|---|---|
| SRBSN Ceradyne Ceralloy 147-31N | 3.21 * | 0.5 to 3. X up to 10. long | 310 - 320* | HK(2) 13.3 ± 0.2<br>HK(1) 13.7 ± 0.2<br><br>HV(5) 15.4 *<br>HV(1) 15.0 ± 0.3<br>HV(.3) 17.6 * | | 5.8 ± - *<br>5.41 ± .54<br><br>5.58 ± 0.24<br>5.59 ± 0.22<br>5.28 ± 0.17 | 29 machining cracks [This study]<br>SCF [41]<br>SEPB [41]<br>CNB [42] |
| SSN Dow | 3.20** | 0.3 - 1.3 X up to 10. long ** | 306** | HK(2) 12.7 ± 0.2<br>HK(1) 13.0 ± 0.2<br><br>HV(5) -<br>HV(1) 14.5 ± 0.3 | | 6.8 ± - *<br>7.25 ± 0.38<br><br>7.18 ± 0.31<br><br>6.75 ± .29 | [65,66]<br>28 machining cracks [This study]<br>30 machining cracks [This study]<br>SCF [67] |
| RBSN Eaton | 2.36** | 0.5 – 1. X 1. – 2. ** | 200 ** | HK(2) 4.6 ± 0.3<br>HK(1) 5.0 ± 0.3<br><br>HV(5) -<br>HV(1) 5.2 ± 0.4 | | 2.5 ± -** | IS [43] |
| HPSN Norton NC 132 | 3.22 – 3.26 | < 3. | 315 – 320 | HK(2) 14.3 ± 0.3<br>HK(1) 15.0 ± 0.2<br><br>HV(5) 15.4 ± 1.3 [63]<br>HV(1) 17.3 ± 0.5 | | 4.57 ± 0.23 | SCF, SEPB, CN, SRM 2100 [68] |

*     Manufacturer's data
**    Consortium preliminary data References [1-6].
‡     HV denotes Vickers hardness.  HK denotes Knoop hardness.
      The number in parenthesis is the indentation load (kgf).
†     Test method: SCF surface crack in flexure; CNB chevron notched beam; SEPB, single-edge precracked beam; IS, indentation strength
-     Not available or reported.
[ ]   Data source, reference.

*Figure 46* Fracture origin in an Eaton RBSN specimen transversely ground with 80 grit wheel. (a) and (b) show that the origin is a small damage cluster near the chamfer. (c) is the same region, but illuminated differently to highlight the 40 μm – 65 μm diameter agglomerates from the spray dry process that comprise this material. The machining damage zone is confined to one layer of these agglomerates.



(a)

(b)
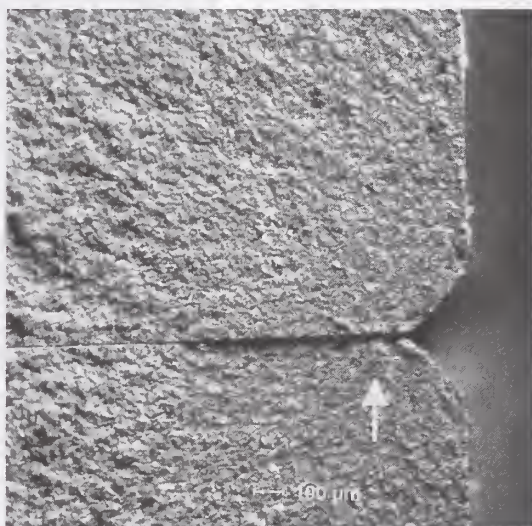
(c)
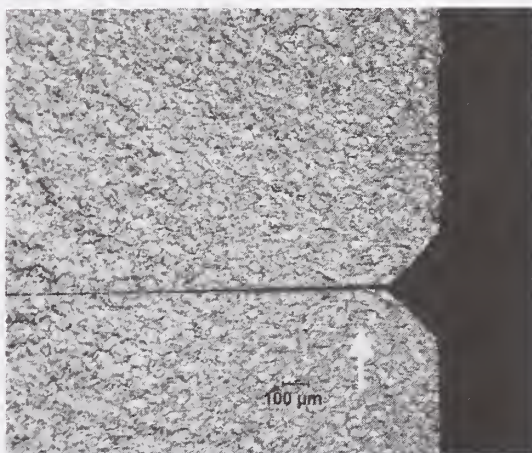
*Figure 47* Fracture surface of Dow sintered silicon nitride bars. (a) was transversely ground with an 80 grit wheel. The coarse zipper cracks (90-95 μm deep) are obvious. From the fracture stress, 352 MPa and assuming a shape factor Y of 1.99, the fracture toughness is estimated to be 6.7 MPa√m. The interlocking but very fine (< 2 μm) grain microstructure is not evident at this scale in this toughened ceramic. (b) is a 150 grit transverse bar with a 66 μm deep crack with a stress of 432 MPa for a fracture toughness of 7.0 MPa√m. Both fractured from "coarse zipper machining cracks as shown in (c). In specimens like these, with such large cracks, the fracture mirror is incomplete since it is large relative to the specimen cross section size.

(a)                                                    (b)



(c)



Coarse zipper machining crack
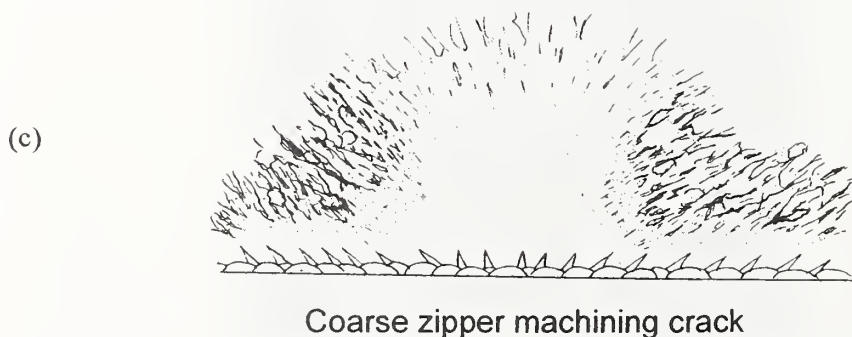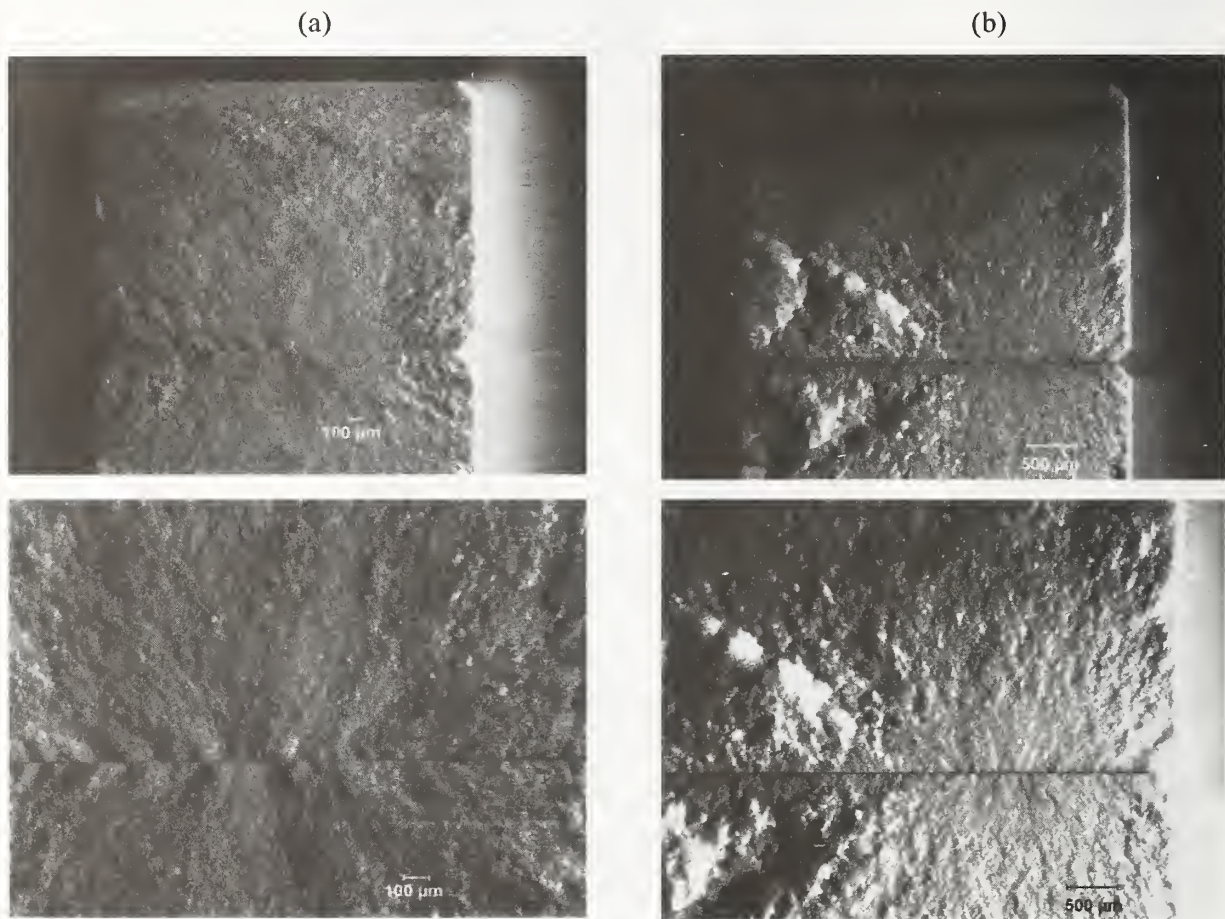
**Fracture Mechanics Analysis of the SRBSN Machining Cracks**

Fracture mechanics may be applied to the interpretation of the machining cracks. In this study we have taken a simplistic approach and applied the basic formula for critical stress intensity for a small crack or flaw in a tension stress field:

$$K_{Ic} = Y \, \sigma_f \, \sqrt{a} \tag{1}$$

where $K_{Ic}$ is the critical stress intensity factor, or fracture toughness, $\sigma_f$ is the fracture stress at the origin site, Y is the stress intensity shape factor which takes into account the stress gradient and geometry of the flaw, and a is the flaw dimension, which is the crack depth for a long shallow surface crack in a beam in bending. The stress intensity shape factors from the Newman and Raju analysis [46] were used. As a first approximation, potential residual stresses were ignored, as was any possible rising R-curve behavior. This simplistic approach is an effective adjunct to fractographic analysis of fracture origins. Any discrepancies in the outcomes point the way for further review and consideration of such factors as residual stresses or rising R-curve behavior.[69,70]

A number of machining cracks had sufficiently well defined shapes and boundaries that apparent critical fracture toughness could be computed from the measured cracks dimensions a and 2c (width), the stress at the origin, and the computed Y.[v] The average for 29 cracks was 5.41 MPa√m ± 0.54 MPa√m. The results are shown in **Figure 48** where they are compared to 35 fracture toughness data collected by the three test methods in the ASTM standard C 1421 for fracture toughness.[41] One of the three methods was the surface crack in flexure (SCF) method that involves using a Knoop indenter to make small semi elliptical surface cracks. These are very close in size (50 μm, **Figure 48**) to some of the material and machining cracks. The SCF cracks were used to study the micro-crack fracture resistance in this material. Notwithstanding our simplifications in the machining crack analysis, the results from the machining cracks are in superb agreement with the results from the dedicated fracture toughness tests. This is not an unusual outcome. Using the same assumptions of negligible R-curve effects and negligible residual stress, Foley et al. [33] also observed a good correlation between calculated and measured (20 μm – 60 μm) machining crack sizes for *longitudinally ground* tension strength rods in a hot isopressed silicon nitride with a modest fracture toughness of 5.35 MPa√m. Rice has remarked that fractographic analysis of machining cracks is a good way to obtain fracture toughness estimates for ceramics.[71]

---

[v] In the course of reviewing the literature, we were surprised how many instances investigators improperly applied fracture mechanics to machining damage. Many early studies modeled striations as the machining damage and attempted to analyze the stress intensity factors for the striations, sometimes even using surface roughness data to estimate flaw depths. This is not correct. Machining crack flaws extend well below the machining striations (5x – 10x deeper). It is frustrating to see a super close up photo of a striation, but not be able to see the genuine machining crack due to the excessive magnification. Even in cases where the correct machining crack is detected, some studies have modeled the flaw as a combined groove with crack extending underneath. In most cases this is not necessary, since the striation grooves are shallow and have negligible influence on the stress intensity factor.

***Figure 48*** Fracture toughness versus crack size. The graph includes data from both 35 dedicated fracture toughness tests as well as estimates from 29 machining flaws. In the lower left corner the size ranges for natural (inherent) flaws in this material and also the mean sizes of machining cracks are depicted.
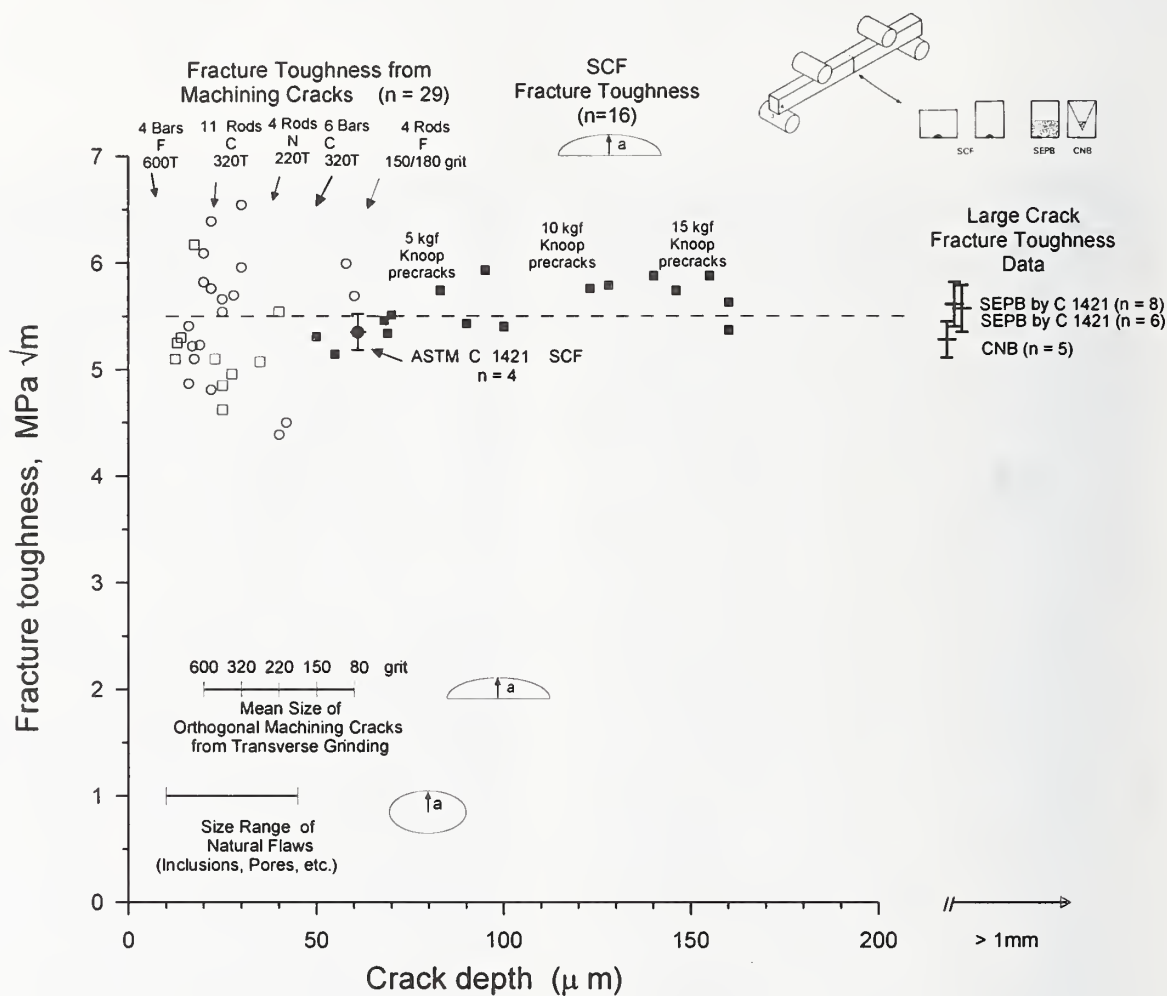
As noted above, a few SRBSN machining cracks showed evidence of small amounts (5 μm - 15 μm) of stable crack extension, but most did not. The critical crack size was used in the calculations. We could often distinguish the critical crack on the fracture surface by noting where the flaw topography changed to a flatter mirror plane, and also by observing changes in direction of local micro-hackle lines. It could not be ascertained whether the stable extension was due to residual stresses, R-curve toughening, or stepwise pop in during the machining.

Any R-curve toughening in this material occurred over a very short crack extensions of the order of 5 μm - 15 μm at most. The controlled SCF experiments with residual stress-free 50 μm deep Knoop cracks did not detect any greater extension than this.[41]   Preliminary work to evaluate the R-curve and threshold fracture resistance of this material has shown the fracture resistance may start as low as 2.0 MPa√m, but then rises to the order of 5.5 MPa√m after 500 μm of crack extension.[43,44]   We are somewhat surprised by these results, since the fractographic analysis of the machining cracks in our study (which were as short as only 10 μm) indicated they behaved as though they had reached near plateau values of fracture toughness resistance when the cracks went critical. Since the silicon nitride grains were 0.5 μm to 3 μm wide by up to 10 μm long, stable crack extension occurred over only a few grain diameters so only a few bridges would be activated. We surmise that the beneficial effect of enhanced fracture toughness occurs during the crack initiation, pop in, and initial extension during machining. Very little additional toughening increase occurs during the subsequent strength test and the crack experiences a fracture resistance commensurate with a plateau fracture toughness.   This interpretation is consistent with our fractographic findings[w] and those of Foley et al. [33] for a different hot isopressed silicon nitride with similar fracture toughness (5.35 MPa√m).    Fett and Munz have also shown that stable crack extension from natural cracks actually causes only slight crack extensions and has only a small effect upon strengths even in aluminas with pronounced R-curves.[72]

Data from the 35 experiments by three fracture toughness methods in C 1421 plus our analysis of 29 machining cracks converge to a fracture toughness of 5.5 MPa√m to 5.6MPa√m for this SRBSN. It is reassuring that three different test methods produce such consistent fracture toughness outcomes, and that these outcomes are relevant to machining cracks.   Standardization of fracture toughness and strength testing methods has improved the quality of mechanical test results.  This material is indeed tougher than a baseline silicon nitride, Standard Reference Material SRM 2100 hot-pressed silicon nitride, which has a toughness of 4.57 MPa√m ± 0.11 MPa√m.[69]

**Fracture Mechanics Analysis of the SSN Machining Cracks**

The Dow SSN has even greater fracture toughness (6.8 MPa√m or more) due to its very fine (0.3 μm diameter x 1.3 μm long) microstructure comprised of elongated interlocking silicon nitride grains.

---

[w]    Yet other dedicated R-curve data [43,44] suggest stable extensions of > 200 μm are needed to reach the plateau.

Nevertheless, the machining cracks were so large that they stood out clearly against the natural roughness from the interlocking microstructure as shown in **Figure 47.** There were numerous local jogs and steps in the machining crack damage zone along the tensile edge of the specimen. These lines were especially noticeable outside the mirror region. As discussed previously (**Figure 31b**) "machining crack hackle lines" arise from jogs or steps and extend upward into the fracture surface. The steps and jogs made the initial cracks easy to detect and the machining crack hackle tilts helped discriminate the initial machining cracks from the final fracture markings.

The apparent critical fracture toughness was calculated for every crack in every specimen based on the depth, the fracture stress, and the assumption the crack was a long surface elliptical crack. The average fracture toughness was calculated as 7.25 MPa√m ± 0.38 MPa√m for all thirty 80 grit ground specimens which had 72 μm – 95 μm deep cracks. The average was 7.18 MPa√m ± 0.31 MPa√m for all thirty 150 grit ground specimens, which had 60 μm to 82 μm deep cracks. Depending upon the composition and grain sizes, fracture toughness (chevron notch) from 6.5 MPa√m to 9.0 MPa√m have been reported in the literature for this material.[65,66] The fracture toughness of the particular batch of material we received was reported to be ≈ 6.8 MPa√m (chevron notch) by the vender.[73] We confirmed this value by five SCF fracture toughness experiments done in accordance with ASTM C 1421 that produced an average of 6.75 MPa√m ± 0.29 MPa√m [67] for single semi-elliptical 75 μm deep Knoop semielliptical precracks. The excellent consistency of the fracture toughness numbers from the dedicated fracture toughness experiments and the machining cracks confirms that we were observing critical crack sizes in the latter.

There could have been some stable crack extension, but it could not be distinguished on the fracture surfaces. It is improbable that it would extend so uniformly deep across the specimen's width as the crack fronts we detected on the fracture surface. It is also unlikely that stable crack extension would have locally curved out of the fracture plane as much as we detected at the origins. Even though the Dow SSN machining cracks were surprisingly large, the specimens did require greater stress to break, so there was some benefit of increased fracture toughness. Evidently, the ramp up in increase in fracture resistance with this likely rising-R curve material occurred during machining crack pop-in in the same manner as occurred for the SRBSN.

So why were the machining cracks larger in the toughened Dow SSN? Why didn't the microstructure designed for improved fracture resistance retard crack pop in during machining?[x] We offer one possible explanation. There is ample anecdotal evidence from machine shops [74] and experimental data [75,76,77,78] that toughened ceramics are indeed more difficult to machine. For a given set of grinding conditions (wheel grit, wheel speed, depth of cut, etc.), greater wheel forces are generated. High horsepower grinding machines automatically compensate for the increased material

---

[x]  For example, Xu et al. [76] showed that scratch and machining crack penetrations in a toughened silicon carbide were smaller than in a monolithic silicon carbide.

resistance and apply greater energy to the work pieces to overcome the material's resistance. Deeper machining cracks are forced into the material. This is automatic and will not be noticed by the machinist unless the machine is instrumented, or the motor is underpowered and the machine noise changes, or the grinding wheel is retarded and does not cut freely. In contrast, less tough ceramics require less energy and grinding forces are reduced.

Our findings run somewhat counter to recent papers on the influence of fracture toughness on machining that have emphasized short crack length toughnesses [76-78]. For example, Xu et al. [76] showed that scratch and machining crack penetrations in a toughened silicon carbide were smaller than in a monolithic silicon carbide. Nevertheless, our fractographic findings suggest that if there is a rising R-curve for the toughened SRBSN and SSN silicon nitrides, the fracture resistance of smaller cracks must come up the R curve very quickly or even during crack initiation..

## Residual Stresses

Residual stress characterization unfortunately was not included in this program. Machining often creates residual stresses at and just underneath the ground surfaces. These can start with a very substantial compressive residual stress at the immediate surface, which very rapidly decreases with distance into the bulk and becomes a low or modest tensile stress 10 μm or more below the surface. The net effect of residual stresses on a flaw must take into account the stress gradient and the crack size. So whereas severe residual stresses may be present, the net effect upon a deep machining crack may be small and is hard to calculate. The residual stresses are also directional. Stresses in the grinding direction are typically much less or negligible compared to the stresses perpendicular to the grinding direction. Characterization of these residual stresses is time consuming and difficult and subject to considerable uncertainties in large part due to the severe stress gradient or uncertainties in the test method. A sample review of the literature (e.g., Alfaro [54]; Wobker and Tonshoff [23], Puttick et al. [26], Marshall et al. [56] Kirchner and Conway [79], Holstein et al. [28], and Pfeiffer and Hollstein [80], Samuel et al.[81], and Johnson-Walls et al. [82]) shows there is considerable variability in the magnitude and severity of reported residual stresses. It is not even clear whether the net effect on a machining crack should be tensile or compressive. Pfeiffer and Hollstein [80] concluded that coarse ground silicon nitride surfaces had compressive residual stresses extending 5 μm to 10 μm below the surface which created a net beneficial compression stress of 100 MPa – 150 MPa on the flaws.

The presence of residual stresses could be inferred from the fracture mechanics analysis of the cracks in the present study. In most cases, the computed fracture toughness (based on the flaw size and shape and the applied flexure stress at fracture) matched the known fracture toughness, suggesting that any residual stresses were small. The computed fracture toughness values differed from the fracture mechanics estimate only for the 320 grit transversely ground bar set. In this set, the combination of critical flaw size, stress at the origin at fracture, and the shape factor yielded a low estimate of the critical

fracture toughness. It was inferred that net residual tensile stresses of only ≈ 50 MPa must have been acting on the flaws in this case. Foley et al.'s [33] good correlation of calculated and measured machining flaw size also suggested that negligible residual stresses were present in their study of a in a hot-isopressed silicon nitride.

**Comparison of Rods and Bars**

Although the rods were much larger than the rectangular beams, the Weibull effective volumes and surfaces were comparable. The 600 transverse grit rods and bars prepared by shop F had almost identical strengths and the fractographic analysis confirmed that similar machining cracks had been created. On the other hand, comparably ground rods and bars prepared by Shop C had different strengths. Their 320 grit longitudinally ground rods were much stronger than their bars. Fractography indicated that different types or concentrations of material flaws occurred in these bars and rods. We cannot account for why this happened, since some care was taken to randomize all rod blanks at the beginning of this study. Shop C's transversely ground rods and bars had different strengths, but the cause in this instance was simply traced to different machining crack depths created in each set.
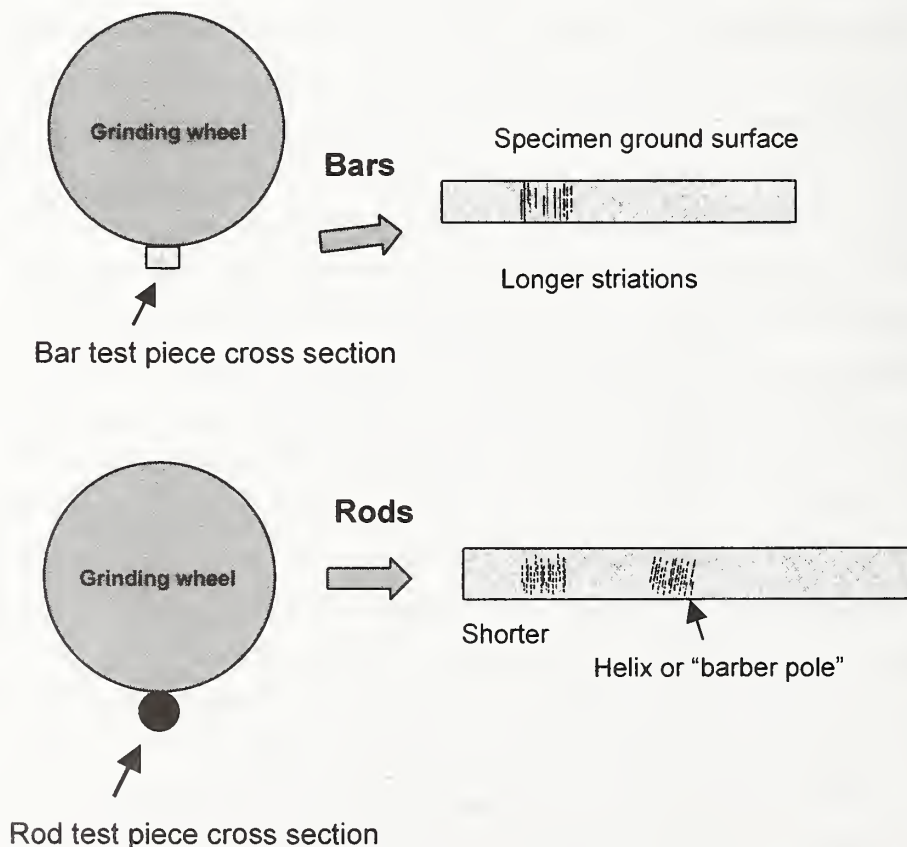


*Figure 49* All other things being equal, grinding wheels may leave striations and cracks with different lengths and orientations in rods and bars.

In general, the grinding flaws in rods and bars were similar in some respects, but different in others. The trends of crack depths for the rods and bars were similar, but the crack lengths varied. Rectangular bars typically had longer machining cracks, often in the hundreds of micrometers and sometimes the full 4 mm width of the specimen. This difference is not surprising due to the geometries involved and the shorter contact length and duration of a round rod contacting a round grinding wheel as depicted in **Figure 49**. Furthermore, the rods were more apt to have "V" cracks from the spiral or helical grinding pattern due to axial motion of the work piece relative to the grinding wheel. On the other hand, the bars were more likely to have pronounced "zipper cracks" with periodic fingerlets. It would be an interesting exercise to try to correlate the fingerlet spacing to the rates of wheel rotation, the wheel grit concentration, and the work piece translation during the grinding process.

## Machining Damage and Scratches

One is struck by the similar appearance of machining cracks and scratch fracture origins. It may be difficult to discriminate between the two flaw types if a scratch lines up either parallel or perpendicular to the grinding direction axis. On the other hand, if the flaw axis is at an irregular angle to the work piece axis or the grinding direction, then the flaw is likely a scratch. Fractographers should examine not only the fracture surface, but also the component external surface. Sometimes only a small portion of the scratch may be revealed on the fracture surface if the scratch is at an angle to the fracture surface. The mechanism of formation of machining flaws is probably similar to that of scratches [83] or cracks formed by single point diamond grinding. [8,12,53,56,79] Schinker and Döll [53] showed stunning images of various striation-scratch grooves and damage patterns. Melting was a prominent factor in some instances. Changes in the damage modes and the appearance of the groves corresponded to critical depths of cut, abrasive speeds, and the refractoriness of the glasses. Rice and Mecholsky [29] compared polishing scratches and machining grinding cracks and noted that the former are often very smooth, and the latter more irregular and stepped. Kirchner and Conway [79] stated that grinding involves a series of events including crushing, plastic flow, elastic recovery, generation of residual stress, radial, median and lateral cracking, chipping and gouging. Their contributions vary quite a bit with force and depth of cut. Although there are similarities in behavior of scratches, single point diamond grinding scratches, and machining cracks, one should be careful in carrying the analogy too far. Kirchner's single point scratch damage depths of up to 1000 μm deep have never been observed to the author's knowledge in any ground silicon nitride part and are certainly 8-10 times deeper than any cracks detected in our study under the severest grinding conditions. Large residual stresses from huge scratches or indentation flaws with concentrated plastic zones may overemphasize the influence of residual stresses, and cause much greater stable crack extension than what occurs in genuine ground surfaces. It should also be remembered that machining cracks seldom act alone. They are part of a network of closely spaced parallel flaws as shown in Figure 3. The density and spacing and mutual interaction of these cracks is unexplored at this time.

**Does Fracture Start from a Single Bad Striation?**

As noted above in our discussion of 150 grit and 80 grit transversely ground SRBSN and SSN bars, a single critical striation can control strength. A simple calculation based on the specimen and wheel geometries and the table and wheel speeds indicated that the striation may have been formed by a single abrasive grit.[y] Hence, the strength and reliability performance of a ground part may be controlled by a single "renegade" grit in the grinding wheel.

We also have noted over the years that a single large striation, perpendicular to the fracture surface sometimes coincides with the *orthogonal* machining cracks in *longitudinally* ground bars as shown in **Figure 8c.** Others [17,29,32,33,34] have reached a similar conclusion. The deep striation may not always be present, however, since subsequent finishing may remove it. Polished plates or window components often break from handling scratches, scratches from loose abrasives, or grinding flaws. These flaws may be obvious on the fracture surface, but there often is no indication whatsoever of these flaws on the finished surface since final polishing removes all traces of the damage. Thermal or biaxial mechanical stresses will trigger these flaws. **Figure 50** shows an example.
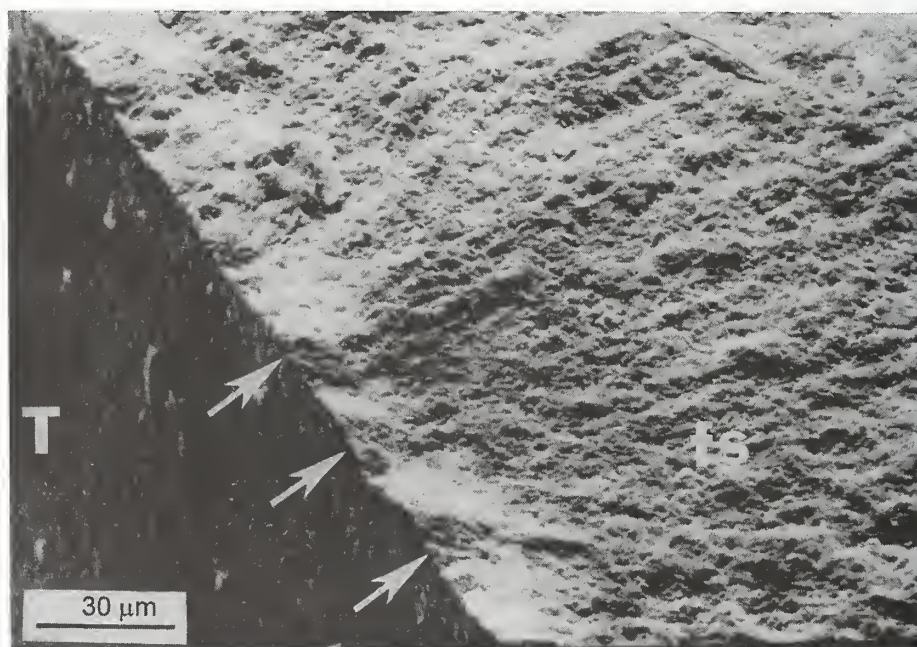


*Figure 50* Machining damage crack in a lapped NC 132 silicon nitride disk [84]. The disk was broken in ring-on-ring equibiaxial loading. Although the tensile surface "T" was very smooth and there was no trace of grinding damage, the subsurface 20 μm deep **"zig zag machining crack"** remained (arrows) and was revealed on the fracture surface "fs." In this instance, the machining vender did not remove sufficient material by lapping to eliminate the prior grinding damage.

---

[y]    We did not notice such consistent striation-fracture origin patterns with the finer grit ground bend bars or rods, but we cannot rule them out. A review of all of our SEM photos of fracture origins suggested that fracture origins sometimes, but not always, coincided with deeper than normal striations in 320 grit transversely-ground rods and bars. Fracture origins in Shop F's 600 grit transversely-ground rectangular bars usually did coincide with deeper than normal (2 μm – 3 μm) striations.

## Grinding Damage Maps

Combining the results of the present study and data from other studies on fine-grained, dense polycrystalline silicon nitrides, we have constructed several damage maps for fully-dense silicon nitride, **Figures 44, 51, and 52.**

**Figure 44** condensed the detailed information on crack depth versus grit size from **Figures 43 and 45** and key fractographic findings about machining flaws vis-à-vis material flaws. Although it was prepared for the SRBSN, our review of the literature suggests the general trend may be applied to many dense silicon nitrides.

Grinding wheel

Machining induced crack

600 grit wheel
13 $\mu$m – 20 $\mu$m deep cracks
(.0005" - .0008")

320 grit wheel
14 $\mu$m – 40 $\mu$m deep cracks
(.0006" - .0016")

220 grit wheel
25 $\mu$m – 55 $\mu$m deep cracks
(.0010" - .0022")

150 grit wheel
30 $\mu$m – 70 $\mu$m deep cracks
(.0012" - .0028")

80 grit wheel
35 $\mu$m – 80 $\mu$m deep cracks
(.0014" - .0032")
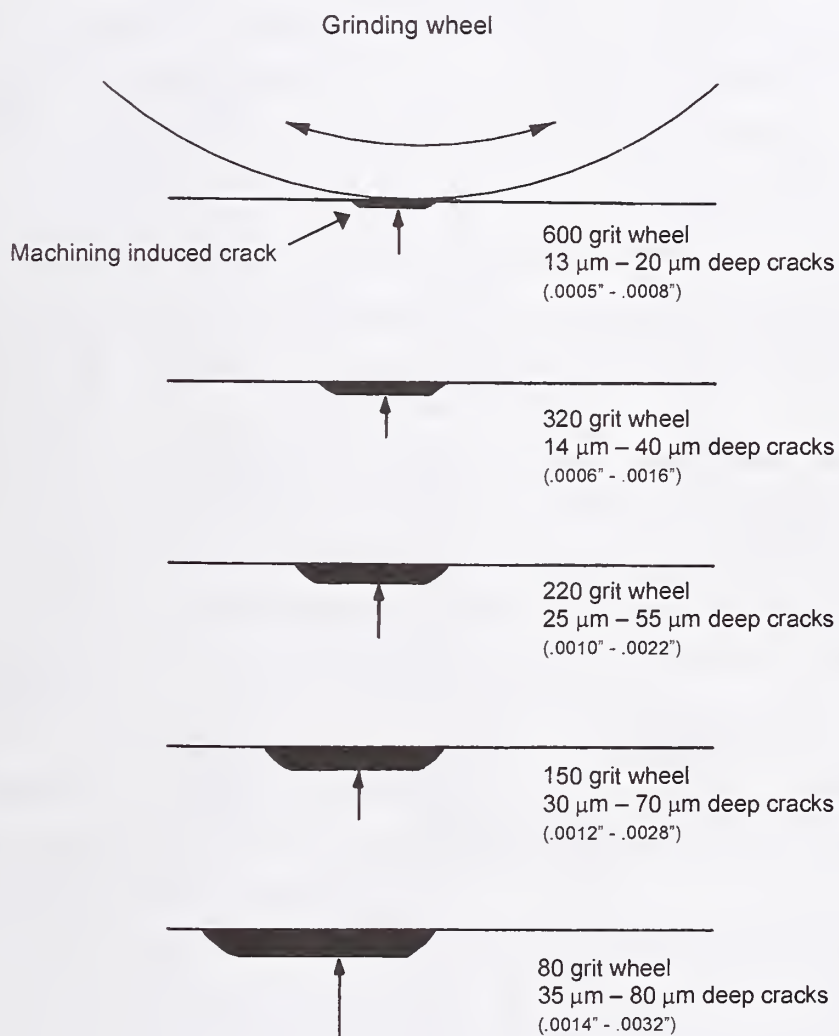
*Figure 51* Damage depths from surface grinding with wheels of various grits. The cracks shown are parallel cracks that control strength for transversely ground specimens or biaxially-loaded plate or disk specimens. The cracks are 5X to 10X deeper than the surface roughness striations. The grinding wheel is not drawn to scale.

***Figure 52*** Grinding damage map for silicon nitride. Strengths are normalized to the fast fracture inert strength which may be vary due to billet to billet differences, or specimen size or stress gradient configurations. The inert strength is typically obtained with longitudinally ground bend or direct tension specimens that have been prepared with 320 or finer grit finish machining, provided that sufficient material is removed to eliminate prior coarse machining damage. Longitudinal grinding has minimal effect on strength unless wheels coarser than 240 grit are used. Transverse grinding may degrade strength with wheels coarser than 600 grit.

76
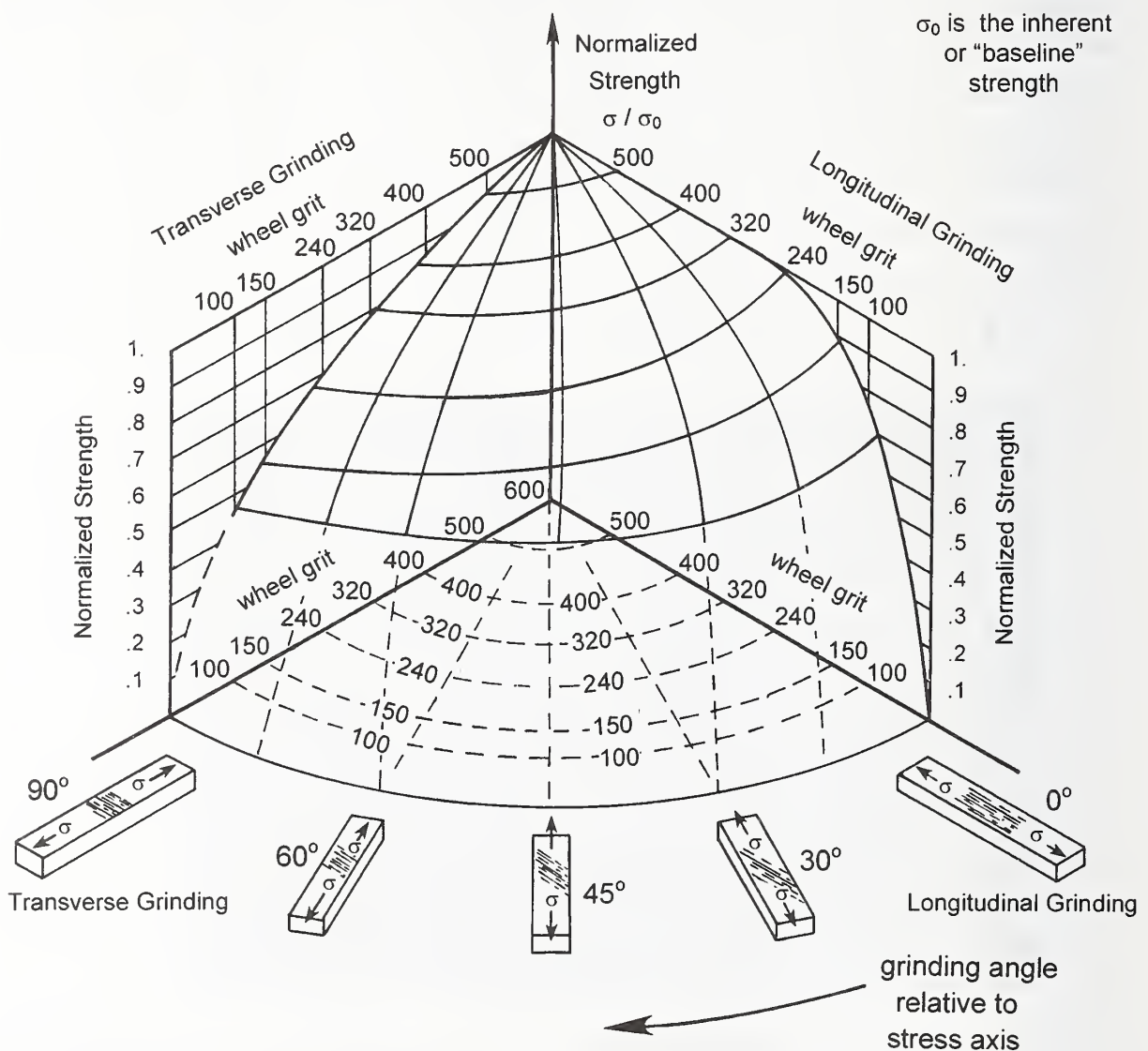
**Figure 51** is intended to show the effects of surface grinding on flaw generation beneath the surface for the SRBSN and similar silicon nitrides. This is a simplified variant of an earlier schematic, based upon calculations that was prepared by Mörgenthaler for hot-pressed silicon nitride NC 132.[57] Unlike Mörgenthaler's, the new figure is based on actual crack depth measurements. This simple schematic may be useful for demonstrating the significance of subsurface cracking to a general audience including machine shop personnel.

**Figure 52** is a three dimensional damage map for dense silicon nitride in general. Two key factors are the independent variables: wheel grit size and direction of machining. A normalized strength axis is used since material-to-material, or batch-to-batch variations in the material flaws, specimen size, or geometry effects all influence the baseline strengths. The strength trend with grit for transversely ground specimens is surprisingly consistent over a range of studies (**Figure 42a**). Parallel cracks from transverse grinding are particularly severe and begin to control strengths for wheels coarser than $\approx$600 grit. On the other hand, although silicon nitrides are more tolerant of longitudinal grinding, the literature shows more variability in the trends (**Figure 42b**). Small orthogonal cracks from longitudinal grinding can be strength limiting, but usually only for coarser wheel grits (e.g. 240 grit or coarser).[z] Quinn [63,64] showed examples of strength controlling orthogonal machining cracks in 220 or 240 grit longitudinally ground silicon nitride bars. Orthogonal cracks are more likely to control strength in very strong materials that have improved process control of the material flaws such that the inherent strengths are $\approx$ 800 MPa or greater.

Although most of the literature is confined to longitudinal or transverse grinding, there are two cases that we are aware of that included intermediate angles. Salem et al. [24] systematically studied the influence of grinding angle in sintered silicon carbide bend bars that were ground with a 320-grit wheel. The data showed the effect of the angle change was gradual. Parallel machining cracks oriented at 30° or even 45° to the stress axis caused only a minor strength decrease. More pronounced decreases occurred for cracks oriented 60° and 90° to the stress axis. Their data was supported by finite element and fracture mechanics modeling of cracks oriented at these angles. Thomas et al. [85] also detected a gradual decrease in strength with grinding angle for hot pressed silicon nitride bend bars ground with a 320-grit diamond wheel. Specimens ground at a 45° of 90° angle to the specimen axis were 28% and 47 % weaker on average than the longitudinally ground specimens.

Our data for the Ceradyne SRBSN shows that for a comparable grinding condition the ratio of transverse to longitudinal strengths are $\approx$ 0.82 to 0.84. Of course, if material flaws dominate, then the ratio is $\approx$1. Ratios between these limits may occur for data sets having mixtures of material and

---

[z]  There often are exceptions to the general observations. For example, Allor et al's [14] study with longitudinal grinding in hot pressed silicon nitride showed that very fine a wheel may be deleterious. 1200 grit wheels produced much weaker specimens than comparably machined 600 grit specimens. One possible explanation for this behavior could be that the final finishing did not remove damage from prior grinding.

machining flaws. Rice [86,87] has tabulated ratios of transverse to longitudinal strengths and obtained values ranging from 0.5 to 1.2. Mayer and Fang [21] obtained ratios of 0.68 to 1.0 depending upon the grit size. For most fine-grained materials such as the SRBSN in this study, values of 0.60 to 0.84 are the norm. Material microstructure itself plays a prominent role in determining sensitivity to machining damage and the strength ratios. Rice has shown that the ratios of transverse to longitudinal strength are sensitive to grain size particularly when the flaw size is similar to the grain size.[86,87] Xu et al. [76,88] have shown that grain size has an important effect on hardness and fracture toughness, and in turn, on subsurface damage, mode of material removal, and grinding forces.

Of course, many other factors may play an important role in determining damage and some of the data scatter in the crack size versus grit size graph in **Figure 45** can certainly be attributed to these other factors such as abrasive bond type, table speed, cross feed, wheel speed, machine stiffness, wheel trueness, and wheel dressing condition. Often the data is mixed, however, as Li and Liao have pointed out in their review paper [27]. For example, depth of cut is frequently cited as a key factor. Some studies have shown it is a major factor for some materials: Kanematsu et al. [89], Mayer and Fang [21,22]; Xu et al. [5,76]; and Thomas et al. [25]. Others have shown it is not a major factor: Ota and Miyahara [19]; Mayer and Fang [21,22]; Xu et al.[5,76]; and Allor and Baker [14,15]. Diamond concentration, diamond bonding (metallic, resiniod, etc), and even operator skill and experience [14,15] all contribute to variability. Allor and Baker [15] showed that it is crucial to ensure that a machine shop removes sufficient material in the final finishing stages. Phase 2 of our Consortium program demonstrated that table speed and down feed did not affect longitudinal strength, but did have a small effect on transverse strength of the SRBSN when 140/170 or 80/100 grit wheels were used.[3,4] It should not be surprising that there is so much conflicting evidence as outlined above and more comprehensively by Li and Liao [27]. The grinding process involves much more than a single grinding wheel and the work piece. Many variables such as grinding forces, machine stiffness, and a host of operational details can play a role. A systems approach may be needed to fully appreciate all these factors and their interactions.[90,91]

A few words on extraneous influences are in order here as well. We have shown that performance may not necessarily be controlled by the average grit size of a diamond wheel. One renegade abrasive grit could compromise the performance of an otherwise satisfactory 600 grit wheel. Allor and Baker [14] found that how specimens are mounted (clamping or waxing them to a plate) is critical. Recent unpublished work in the ceramics industry has brought attention to random, stray micro scratches which can control strength in finely finished bend specimens.[aa] These tiny scratches may compromise parts that are otherwise properly machined. Loose diamond abrasive grits somewhere in the machining process or subsequent handling of the pieces may cause the damage. Similarly, it is well

---

[aa]    Private communication, B. Mikijelj, 2002.

known that bend bars are notoriously sensitive to edge damage that can control fracture if the edges are not prepared carefully.[bb] These examples underscore the influences that extraneous factors may have in controlling performance. There is no guarantee that the performance shown in the maps in this paper can be realized unless due care is exercised by the machinist. Although **Figures 44, 51 and 52** show material performance potential, these results will not be achieved by an inexperienced machinist using an improperly trued and dressed 600 grit grinding wheel on a surface grinder with manual controls and with an out of balance wheel. Experienced machinists often say that one good way of ensuring the machines are running properly is by listening to the sounds from the surface grinder.

**Machining Conditions and Standard Strength Test Methods**

The original standard test method for flexure strength of high performance ceramics, MIL STD 1942,[92] and now ASTM C 1161 and ISO 14704 [93] as well, all prescribe longitudinal grinding if the goal is to measure or estimate the inherent strength. The detailed specimen preparation specifications were intended to be conservative. Several tension strength methods have even copied the bend bar specifications. Experience has shown, at least for silicon nitrides, that the specifications may be overly conservative. It should be borne in mind that the specifications were not written merely for silicon nitride. Many other structural ceramics such as silicon carbide, aluminum nitride, or boron carbide are very brittle and sensitive to chipping and machining damage. Indeed, the flexure test standards were careful to caution that the prescribed grinding sequence was not foolproof. Finer or more careful processes may be required for some materials. MIL STD 1942 originally stated in 1982:

"Surface preparation can have a pronounced effect upon flexural strength. This occurs due to the introduction of machining related defects and the creation of residual surface stresses. In general, the stronger the ceramic, the more likely that machining damage can limit the flexural strength. Specification of a final surface finish is not adequate because machining damage can extend well below the surface striations. Lapping or polishing may remove surface striations and generate a perfect finish, but may not remove enough material to eliminate the much deeper machining damage...... The wheel grits, speeds and rates of removal specified are intended to eliminate or minimize severe machining damage or large residual stresses. As the standard evolves, or is modified in the future, specimen preparation may become more stringent."

---

[bb] The standard test methods specifications have succeeded in managing this problem. They require edge rounding or chamfering parallel to the specimen's long axis with finish grit comparable to the ground flat surfaces. If these specifications are met, then chamfers failures will either be eliminated or minimized. Of course, not every chamfer origin is caused by edge damage. Many material flaws (pores, inclusions, etc) simply happen to reside there and these are legitimate, normal fractures. In recent years, two problems with chamfer preparation have arisen in some machine shops, however. Some shops have prepared bars with <u>oversized</u> chamfers in which case mathematical corrections to the flexure stress must be made. The other problem is when chamfer grinding has <u>not</u> been exactly parallel to the specimen axis, and small chips or cracks are created on the edges of the chamfers themselves.

MIL STD 1942 then went on to specify longitudinal surface grinding only with at least two steps (coarse and fine) with stock removal rates not to exceed 0.030 mm per pass down to the last 0.060 mm. Final finishing was to be performed with a wheel between 200 and 500 grit and no less than 0.060 mm was to be removed per face at a rate of no more than 0.002 mm per pass. The finishing wheel range was tightened to 320 to 500 grit when ASTM C 1161 was adopted in 1990, and has been further tightened to 400 to 600 grit in early 2002. The newest (2002) version of C 1161 also includes limits on grit sizes and depths of cut for the coarse and intermediate machining steps. The ISO analogue, ISO 14704 specifies a wheel no coarser than 120 grit for coarse grinding and 320 to 800 grit for final finishing. No less than 0.060 mm must be removed at a rate of 0.002 mm per pass in the final finishing. This seemed like a very conservative approach back in 1982 when the MIL STD was written, but in reality, a previous ASTM standard F 417 prepared in 1975 [94] for alumina bend bars for electronic substrate applications specified longitudinal grinding with a 180 or finer grit wheel and put strict limits on the depths of cut (0.005 mm per pass), the final amount to be removed per face (0.025 mm), and the crossfeed. The key parameters are the direction of machining, the finishing grit size, and the final amount to be removed. A removal amount of 0.060 mm (MIL STD 1942(MR), C 1161, ISO 14704) seemed like a lot of material to have to grind off in the final stages, but reference to **Figures 43, 44, and 51** show that this was probably just enough to eliminate severe prior rough grinding (albeit damage created in a harmless direction if the bars are ground longitudinally.) It is interesting that of the five shops evaluated by Allor and Baker [15], two which fared the worst removed only 0.050 mm during finish grinding of silicon nitride bend bars, whereas the most experienced shop removed: 0.100 mm – 0.200 mm. This conservatism was prudent and based on years of accumulated experience.

A new standard intended to evaluate the effect of machining upon strength is ASTM C 1495 [95] which has a much more conservative approach and specifies 600 grit longitudinal grinding that is intended to eliminate machining damage as a source of strength limiting flaws.

Salem et al's [24] work is a good example of the successful application of the C 1161 standard machining procedure to a sintered silicon carbide, a particularly brittle ceramic. Their longitudinally ground flexure specimens all fractured from volume distributed flaws (agglomerates). Similarly, most of the two thousand sintered alumina and reaction-bonded silicon nitride specimens tested in a very large, seven international laboratory Technical Cooperation Program flexural strength round robin based on MIL STD 1942(MR) fractured from material flaws.[35]

**Implications for Modeling of Machining Damage**

The primary focus of this work has been on the fractographic detection and characterization of machining cracks and their relationship to grinding conditions. Nevertheless, a few words about the applicability of the results to modeling are appropriate. Concepts developed for indentation fracture or single-point scratching have been adapted to construct machining damage models (e.g. [78,96,97].

80

Marshall [78,96] applied conventional indentation mechanics analyses to the machining problem and showed that machining crack size, c, (depth) can be expressed as [97]:

$$c = \xi \left(\frac{E}{H}\right)^{1/3} \left(\frac{F}{K_{Ic}}\right)^{2/3}$$

where $\xi$ is a constant, E is the elastic modulus, H is hardness, $K_{Ic}$ is fracture toughness and F is the force on a single abrasive grit. F varies with the machine conditions such as depth of cut and the abrasive wheel type, and in particular, the abrasive grit size and concentration. In principal, larger $K_{Ic}$'s should lead to smaller machining crack sizes, but as we have noted for the case of the very tough Dow SSN, the opposite may in fact be the case. For a given grinding machine set up, greater material fracture resistance creates greater applied grinding forces so F is not constant and $F = f(K_c)$. Machining conditions are more complicated than controlled Vickers indentation experiments where one can control F independently of all other parameters.

Of course, the above model was developed for materials with constant fracture toughness. Rising R-curve behavior complicates these issues. Marshall et al. [78] have shown that short crack toughness may correlate better with grinding resistance than long crack toughness. The lower the threshold fracture resistance, the lower the grinding forces. As noted above, some experiments [43,44] to measure an R curve and the threshold fracture resistance of the SRBSN showed the threshold toughness of our particular SRBSN may be quite low (< 2.0 MPa√m [44] or ≈ 3.0 MPa√m [43]).

It should be borne in mind that the grinding machine-workpiece interaction is a complex dynamic problem. Residual stresses, microstructural issues (e.g., crack size-grain size ratios), R-curves, and grinding directionality effects, may all be coupled to the grinding machine response (e.g., the force F). This problem is much more complex than a simple Vickers indentation experiment.

**Comparisons to Other Selected Studies**

A recent design project for ceramic diesel valves compared both rectangular and cylindrical flexure test specimen strengths to valve tension strengths [11]. Weibull size scaling of strength could not account for the observed strength differences. It was concluded that microstructural gradients in the rods created different flaws in different portions of the specimens and components.

Wu and McKinney [17], compared flexural strengths of 180, 320, and 600 grit longitudinally ground bars in hot pressed silicon nitride grade NC 132. Although the machining flaws were difficult to positively confirm by fractographic analysis, they were able to ascertain that the dominant flaw type changed from machining cracks for the 180 and 320 grit specimens, to a mixture of machining cracks and inclusions for the 600 grit specimens. They concluded that finer finishing wheels would not be effective in increasing strength since the small 600 grit machining flaws were comparable in severity to the material flaws. This conclusion is consistent with our **Figure 44**.
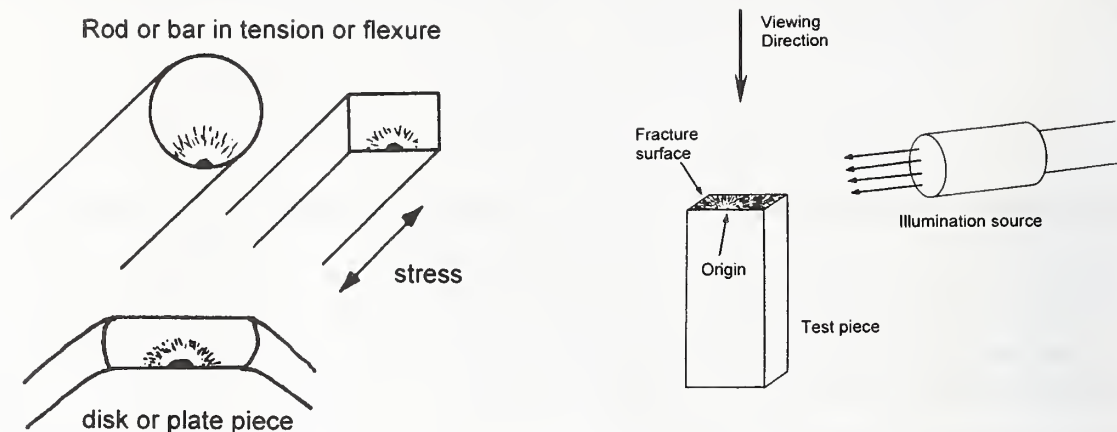
81

Rod or bar in tension or flexure

stress

disk or plate piece

Viewing
Direction

Fracture
surface

Origin

Illumination source

Test piece

*Figure 53* Schematic views of fracture surfaces of various specimens tilted back to partially reveal the ground surfaces on the bottom. The following figures show close-ups of the origins.

**Telltale Signs of Machining Damage**

This study has focused on traditional fractographic methods to detect parallel machining cracks on the fracture surfaces as depicted schematically in **Figure 53**. These are the methods most likely to be used by the typical strength tester and fractographer. This is not to say that alternatives do not exist. Dye penetration techniques, which may also help highlight machining cracks during subsequent fracture surface examination, have good promise.[34,60,61]

The telltale features of fracture origins and mirrors associated with machining damage are depicted **Figures 54 and 55**. These schematics are based on the observations of hundreds of flaws in this study, plus experience gained with a variety of other ceramics and glasses over 25 years of study.The specimen schematics show the fracture surface tilted back a bit so as to show part of the ground finished. The schematics show the entire fracture mirror for high strength specimens wherein the mirror is small relative to the specimen size and any possible stress gradients. Mirrors are incomplete, flared out, or elongated into the test piece interior (depth) in low to medium strength fractures in bending fractures (not shown). **Appendix A** also has several illustrations showing *fracture mirror elongations* in the direction of the flaw long axis, another tell tale sign of machining crack damage

Cracks induced by machining, polishing, or scratching extend well below the finished surface. Traces on the finished surface may not even be present if they have been removed by subsequent grinding or polishing. Cracks may be as shallow as 2 $\mu$m in ground silicon, 5 $\mu$m in polished glass, or as deep as 100 $\mu$m in scratched or coarse ground surfaces. Finish surface grinding usually produces cracks of the order of 10 $\mu$m – 80 $\mu$m deep depending upon the grinding conditions.

*Figure 54*   Parallel machining cracks in transversely ground surfaces.  Parallel cracks lie more or less parallel to the axis of grinding.   These cracks are common in biaxial disks, transversely ground uniaxial flexural or tension strength specimens, or transversely ground components.
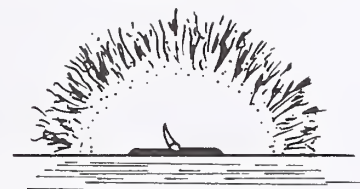
(a) **elongated "coplanar parallel crack"**

A deep striation may or may not necessarily be present.
The fracture mirror may be elongated along the outer
specimen surface.

(b) **elongated "coplanar parallel crack"**

Same as above except the  machining crack has linked with a natural flaw.
A step in the fracture origin emanates from the material flaw.

(c)  **"zipper crack"**

A type of parallel crack that is made up of a series of short semi elliptical cracks, which have linked.
A series of short tails, or "machining crack hackle," emanate
from the links or overlaps of the flaws and extend up into the fracture mirror.  These tails may be tilted to the left or right and help confirm that fracture originated in the central region of the set.   The short tails are telltale features of slightly misaligned or overlapping transverse machining cracks (or a scratch) and are often easier to see with an optical microscope with low angle lighting than with a scanning electron microscope.
The fracture mirror may be elongated along the specimen outer surface or it may have one or two prominent side lobes.
This origin type is common in transversely-ground rectangular
flexure specimens or scratched biaxial disk specimens.
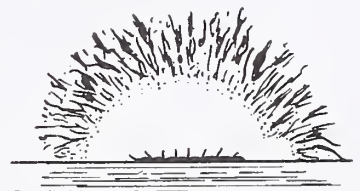
(d) **coarse "zipper crack"**

A type of parallel crack that is made up of a series of irregular, less coplanar semi-elliptical cracks.   Larger tails than in (c ) are created.   In severe cases, the tail may extend all the way to the mirror boundary. The fracture mirror may be elongated.
This origin is common in transversely ground or scratched specimens and the markings are sometimes termed "shark's teeth."
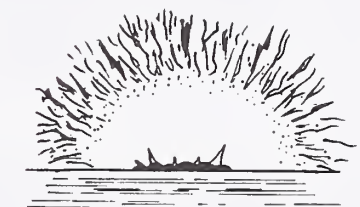
(e) **"V machining crack"**

The crack intersects the fracture surface at an angle.  Only a portion of the machining crack or crack series is exposed.  A pronounced step occurs in the fracture mirror.   One or two (shown) tails extend well up into the fracture mirror.  The machining direction is not quite perpen-
dicular to the specimen length and uniaxial stress axis due to grinding wheel cross feed.    This origin is common in cylindrical specimens prepared by centerless or cylindrical transverse grinding wherein the wheel and work piece displace axially relative to each other.

(f) **"coarse grinding parallel crack"**

The origin is a deep machining crack that extends along the entire surface. The origin is often bumpy since the origin is comprised of offset parallel cracks.  Thin bands of uniform depth extend along the specimen surface on either side of the fracture mirror.  The bands have the same depth as the grinding cracks.  Short tails, or "machining crack hackle" which may be in the thin bands are tilted away from the origin.   This origin type is common in coarse ground surfaces.

*Figure 55* Orthogonal machining cracks in longitudinally ground surfaces. Orthogonal machining cracks lie perpendicular to the grinding direction. They are much harder to detect than parallel cracks shown in the previous figure.
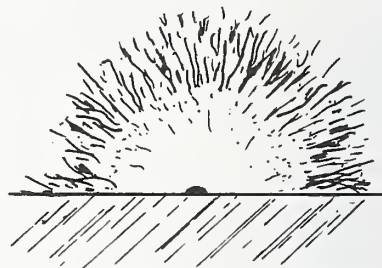
(a) **"orthogonal machining crack"**

A semi elliptical surface crack that extends well below the striation depths.
Depending upon the grain size and microstructure, the short semi elliptical cracks may be difficult to detect in polycrystalline ceramics since the cracks do not stand out clearly against the normal microstructure.
An origin location on the surface is a necessary requirement but <u>not</u> sufficient proof that the origin is machining damage.
In many instances, (particularly in beams in bending) natural material flaws may reside at the specimen surface.

(b) **"orthogonal machining crack"**

The same as above, except that an unusually deep machining striation is lined up with the machining crack.
Deep striations may aid interpretation, but they may not necessarily be present since final finishing may eliminate them.
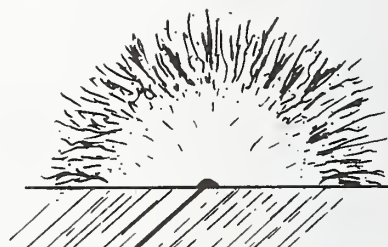
(c) **"orthogonal machining crack"**

The same as above except that the machining crack has linked up with a natural material flaw such as an agglomerate or pore.
The origin may be categorized either as an enlarged natural flaw or a hybrid natural flaw-machining damage.
The natural flaw may make the material more susceptible to machining crack damage in the immediate vicinity of the flaw .
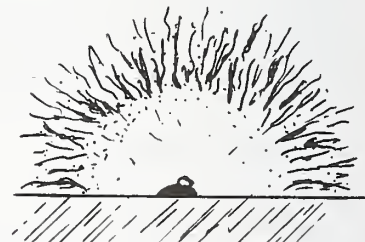
(d) **"orthogonal machining crack"**
The same as above, except that  the natural flaw created a bump or jog in the fracture mirror.   The irregularity at the origin created a step or curve in the fracture mirror that created a tail that extends well up into the mirror or even to its boundary.

84
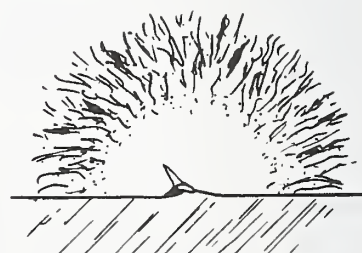
That routine post fracture optical microscopy of the fracture surface could be so effective was a surprise result of our project. In many cases, it was much easier to see the machining cracks in a stereo binocular optical microscope than in the SEM. We hope that fractographers and engineers will try low-angle illumination techniques and will consult these schematics. Indeed, while reviewing the technical and engineering literature about machining of ceramics and engine component preparation and testing, the lead author was struck at how many times these tell tale patterns showed up in old photographs, even in low quality photocopies. The same techniques should work on white translucent ceramics which are particularly difficult to analyze due to subsurface light scattering. A thin coating of gold-palladium or even staining the fracture surface with a common green felt tip pen may aid the examination.

We conclude by recalling some words written 33 years ago in connection with another study of the effects of machining damage upon strength. In 1970, Sedlacek et al. [98] pessimistically wrote: "To examine fragments of broken specimens is a futile exercise in microscopy which may, at the best, lead to only a subjective interpretation of the studied surfaces." A few years later (1974) Rice [99] more optimistically wrote: "Determination of flaws that are introduced by machining as well as surface chemical effects is progressing.... Unfortunately, flaw detection in ceramics has not advanced sufficiently to offer capabilities comparable with those of chemical characterization." We cannot agree with Sedlacek's assessment. We have made significant strides in the science of fractographic characterization of machining flaws, particularly for transverse grinding. We hope others will now search for machining cracks at fracture origins with more confidence. Subjectivity should be reduced. Processors and engineers should no longer have to guess whether machining damage is the cause of their woes.

## CONCLUSIONS

The flexural strength of rods and bars of a commercial, toughened SRBSN silicon nitride that were prepared by a variety of machining procedures were evaluated. Fractographic analysis was applied to every specimen and hundreds of machining cracks were characterized. The dominant factors in determining flaw severity were the abrasive wheel grit size and the direction of machining. The depth of machining cracks correlated strongly with the wheel grit. Cracks were as shallow as 12 μm for 600 grit ground surfaces to as deep as 80 μm for 80 grit transverse ground surfaces. A literature review indicated that 100 μm may be an upper limit for the depth of machining cracks in silicon nitride. Strength limiting machining flaws varied in size by as much as a factor of two in batches of identically prepared specimens. This variability matched the strength variability.

The SRBSN's "inherent material strength," whereby specimens nearly all fractured from material flaws, was obtained from rods ground longitudinally with a 320-grit wheel. Three shops matched or came close to matching this performance with 600 grit centerless or transverse cylindrical grinding.

Cylindrical and centerless grinding of rods may create similar, but not necessarily identical, flaws to those in surface ground flat bend bars. Strength limiting machining cracks sometimes were associated with striations that were not necessarily the deepest or most obvious on the ground surface. A single severe, "renegade" abrasive grit in a grinding wheel may control performance.

The evidence suggests that machining cracks and comparably sized artificial Knoop semielliptical flaws experience a resistance to fracture commensurate with plateau fracture toughness values. Evidently the benefits of the enhanced fracture toughness due to the interlocking grain microstructure occur during machining crack pop in or initiation. Subsequent stable crack extensions prior to fracture are small (5 $\mu$m – 15 $\mu$m).

Residual stresses had small or negligible effect upon fracture in the SRBSN.

Most other silicon nitrides had similar sized machining cracks as found in the SRBSN. Variations occur based upon material properties such as hardness, elastic modulus, and fracture toughness, upon the microstructure, and upon the energy and forces applied by the grinding machine. Toughened silicon nitrides may not necessarily have smaller machining cracks.

Damage maps for ground fully-dense silicon nitride were constructed. Hopefully these will aid machinists and engineers in appreciating the nature of machining damage and its effect upon performance.

Simple fractographic techniques may find parallel machining cracks on fracture surfaces. Their telltale markings are tabulated in a series of new schematic illustrations. These will help engineers and analysts find and characterize machining damage flaws with greater confidence. Orthogonal machining cracks, created by longitudinal grinding still remain difficult to detect.

## ACKOWLEGEMENTS

# Appendix A

## Fracture Origin Locations in Rods and
## Fracture Mirror Measurements for Rods and Bars

The stress at the origin site was used for computations of fracture toughness at the flaw location or for fracture mirror analysis. For the bar specimens, the origins were always at or very close to the tensile surface, and hence, the stress used was the same as the maximum stress in the beam, $\sigma_{max}$. This is the nominal value used for reporting strength and conducting Weibull analyses. On the other hand the rod origins sometimes were located in the interior or partway up the side surface. The stresses at the actual origin site, $\sigma_o$, were used for the fracture mirror calculations. From simple beam theory, stress decreases linearly with the origin's distance from the rod bottom to the neutral axis of the rod (which passes through the center of the rod): $\sigma_o = (2y/D)\, \sigma_{max}$ where D is the rod diameter and y is the distance from the neutral axis (**Figure A1**).

Fracture origin locations were determined by projecting the fracture surface image onto a television monitor that had a superimposed angular grid. The angular location of the fracture origin relative to bottom dead center (the maximum stress location) and the rod center in all the rod specimens was also measured. The specimen was tilted slightly so that the camera, which viewed the specimen through only one light path in the stereomicroscope, was perpendicular to the fracture surface. The angular location of the origin was measured to within $\pm\ 1^{\circ}$.[cc] The repeatability of this procedure was verified by multiple measurements on the same and the opposite fracture halves of several specimens. Nearly all specimens broke within $\pm\ 25^{\circ}$ of bottom center so that the stress at the origin site was 90% or more of the maximum outer fiber stress. **Figure A1** shows the distribution of fracture origin sites for two different sets of thirty rod specimens.

Fracture mirrors were measured with the stereo binocular microscope, while viewing at 30X – 63X through the eyepieces. Even though the microscope was capable of greater magnifications (205X), we found it optimal to not us such large magnifications, but to "step back" and view the fracture surface from a distance, so to speak. We viewed and measured the mirrors when they occupied about 1/3 to 1/2 of the field of view when looking through the stereo microscope.

Mirror constants are important properties that can aid in fractography interpretation of fractured components or lab test specimens. In general, stress and the mirror radius are related through the expression:

---

[cc] Type B estimate, 95% confidence level.

*Figure A1* Rod cross section views showing the distribution of origin locations. (a) is for a set of 30 specimens ground with a 320 grit wheel in the transverse direction. Stress decreases linearly with distance towards the neutral axis (mid plane). Nearly all specimens broke in the portion of the rod that experienced stresses 95% or more of the maximum stress near the bottom center of the rod. Most of the specimens broke from machining damage on the surface. A single large inclusion caused fracture in an unusually weak specimen and is marked as the hollow point that is well up the side of the rod. (b) is for a set of 30 specimens ground longitudinally with 320 grit wheel. More material flaws were activated in this set and several inclusions were well below the surface.
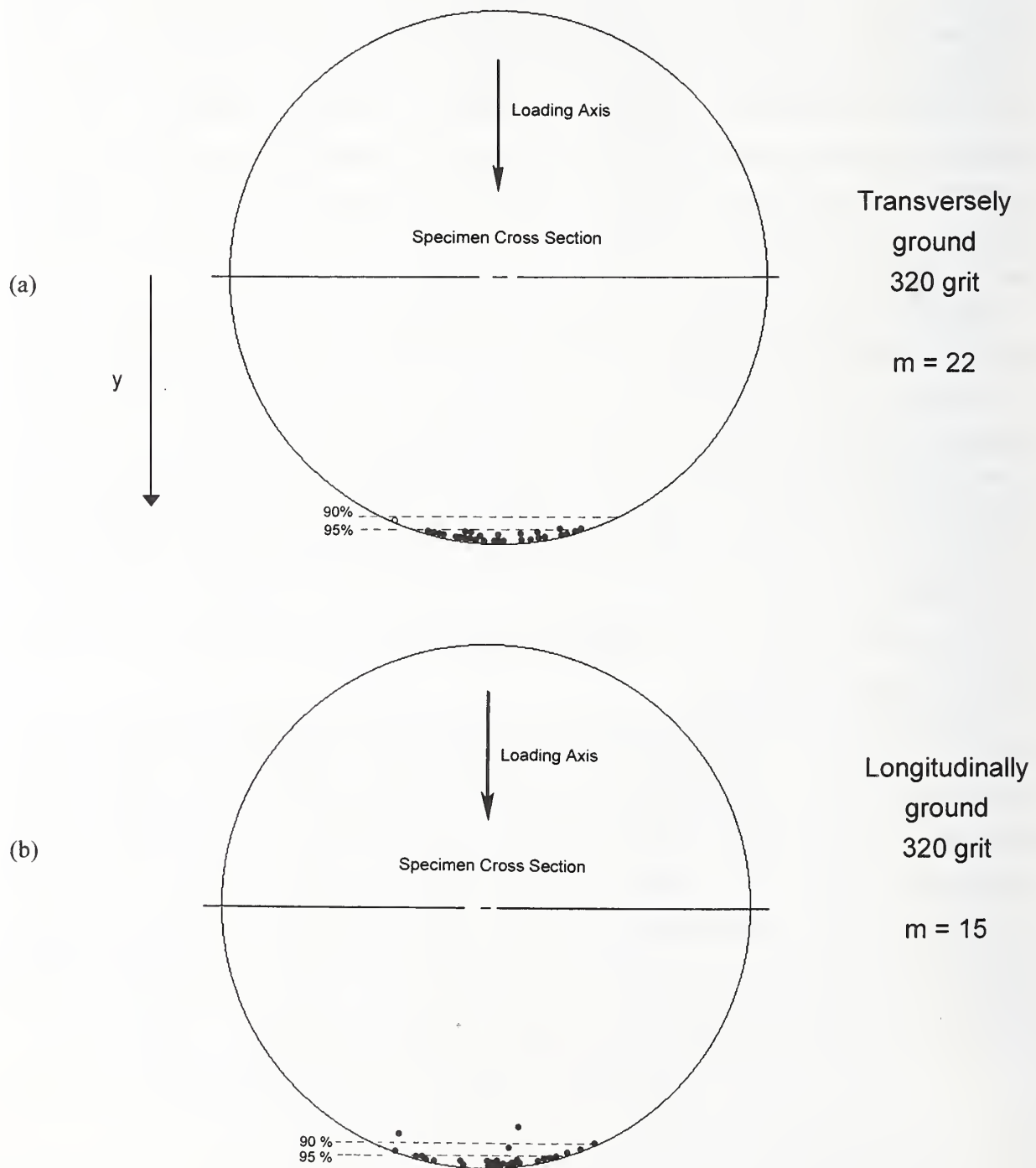
$$\sigma_f = \frac{A_o}{\sqrt{R_h}}$$

where $\sigma_f$ is the fracture stress at the mirror site, $R_h$ is the mirror radius (the mist-hackle boundary in this instance), and $A_o$ is the mirror constant.

Mirrors were plainly evident at low magnifications, but accurate assessment of their size was difficult. The mirror region itself was somewhat bumpy in this self-reinforced silicon nitride, so some judgment as to what was the mirror boundary was necessary. The criterion used in the present study was that the mirror boundary occurred at the point where hackle commenced and there was an obvious roughness change relative to the mirror. **Figure A2** shows schematics of the mirrors. The mirror size measurements were made while viewing the specimen with the binocular stereomicroscope. The microscope cross hair was used in conjunction with a micro positioning X-Y traversing stage on the microscope platform that read out to 0.001 mm. The fracture surface was positioned so that it was parallel to the traversing stage's axes of movement. Illumination was from a fiber-optic light source positioned at a low incident angle to the fracture surface. The mirror radii were calculated as follows. For the rectangular *bars,* the overall diameter $(R_1 + R_2)$ was measured on the tensile surface as well as the radius into the depth, $R_d$. An average radius $R_h$ was computed as $\{(R_1 + R_2)/2 + R_d\}/2$. All the origins on the rectangular bars were at or very close to the surface, so no stress adjustment was needed. For the cylindrical *rods,* the diameter on the surface $(R_1 + R_2)$ was measured as well as the radius into the depth, $R_d$, and an average mirror size computed as above. The two segments $R_1$ and $R_2$ were often unequal, especially for origins that were partway up a rod side. For origins located in the rod interior, the average of two orthogonal mirror diameters was used to compute the radius. The stress at the origin was corrected for the distance away from the bottom center for all rods for the fracture mirror size analysis. Bottom center was ascertained by viewing the entire fracture surface with special attention to the telltale cantilever curl on the opposite compression side of the fracture surface.

The fracture mirror data are shown in **Figure A3 and A4**. The graphs include data from many of the specimens in the study and cover a very broad stress and mirror size range. The mirror constant is the slope of the lines. The rod and bar data have slightly different (8.7 %) slopes. We cannot account for the difference at this time. The same eyes, same microscope, same illumination conditions, and similar averaging criteria were used in each case. There was no deviation from the overall trend for any data subset. All bar data fell on the bar line, and all rod data fell on the rod line. Potential residual stresses from machining extend only shallow distances into the depth, and are unlikely to affect mirror sizes.

**Figure A2** Schematics of fracture mirrors. In very fine grained or glasses materials, mirror boundaries are not too difficult to delineate as shown in a, where the mist hackle boundary is marked. The SRBSN in the present study had bumps and roughness even within the mirror region as suggested by (b) for bars and (c) for rods.

(a)

Glass

(b)

SRBSN
bars

$$R_h = \left[ \frac{\frac{(R_1 + R_2)}{2} + R_d}{2} \right]$$

(c)

SRBSN
rods

$$R_h = \left[ \frac{\frac{(R_1 + R_2)}{2} + R_d}{2} \right]$$
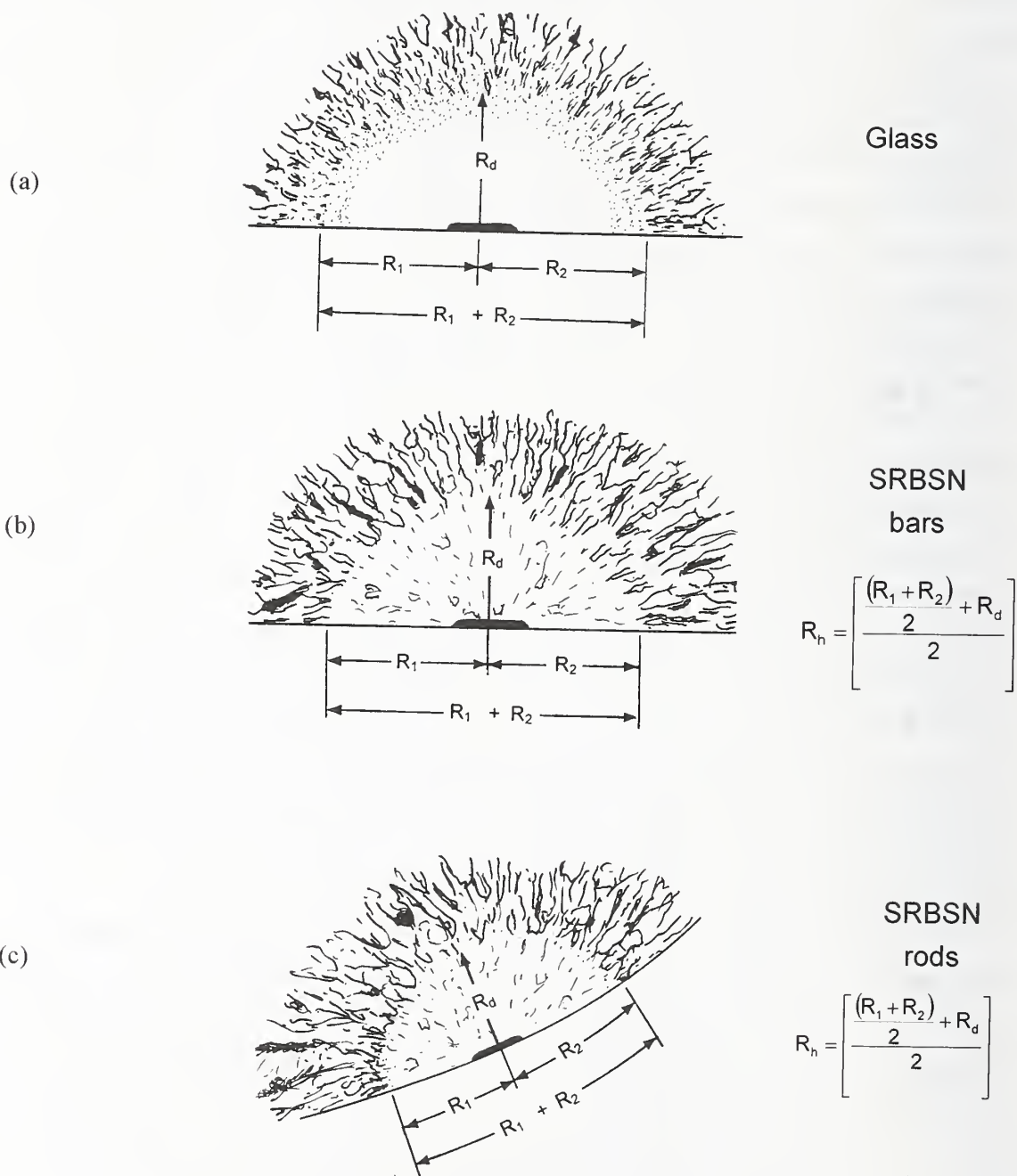
*Figure A3* Fracture mirror sizes for most of the rods tested in the study. The mirror sizes varied from test set to test set, but were in accordance with the general trend for this material. The slope of the line is the mirror constant $A_o$. Uncertainties for a single measurement are indicated by an error bar on the single rod datum at 587 MPa. The uncertainty bar corresponds to two limits for the datum: the minimum possible mirror size and absolute maximum size that in this case was the branching distance.
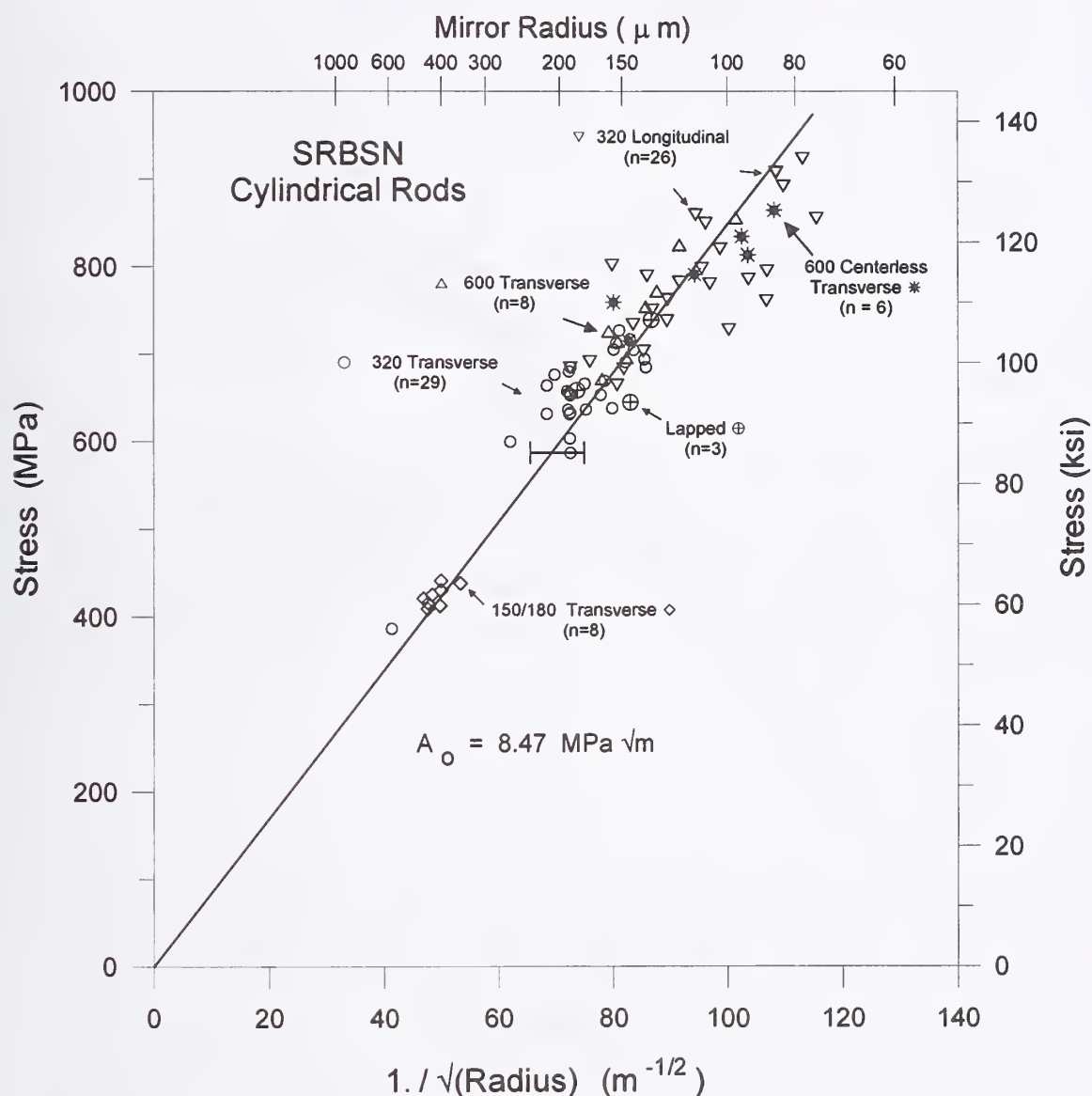
**_Figure A4_** Fracture mirror data for rods ○, and bars □. The solid lines show the linear regression lines with a zero intercept. The slopes of the lines are the mirror constants. The uncertainties, which are the standard deviation of the slopes of the line, are very small due to the large number of data points. The dashed lines are regressed lines with non zero intercepts. The intercept for the bars is 153 MPa, for the rods, 123 MPa.
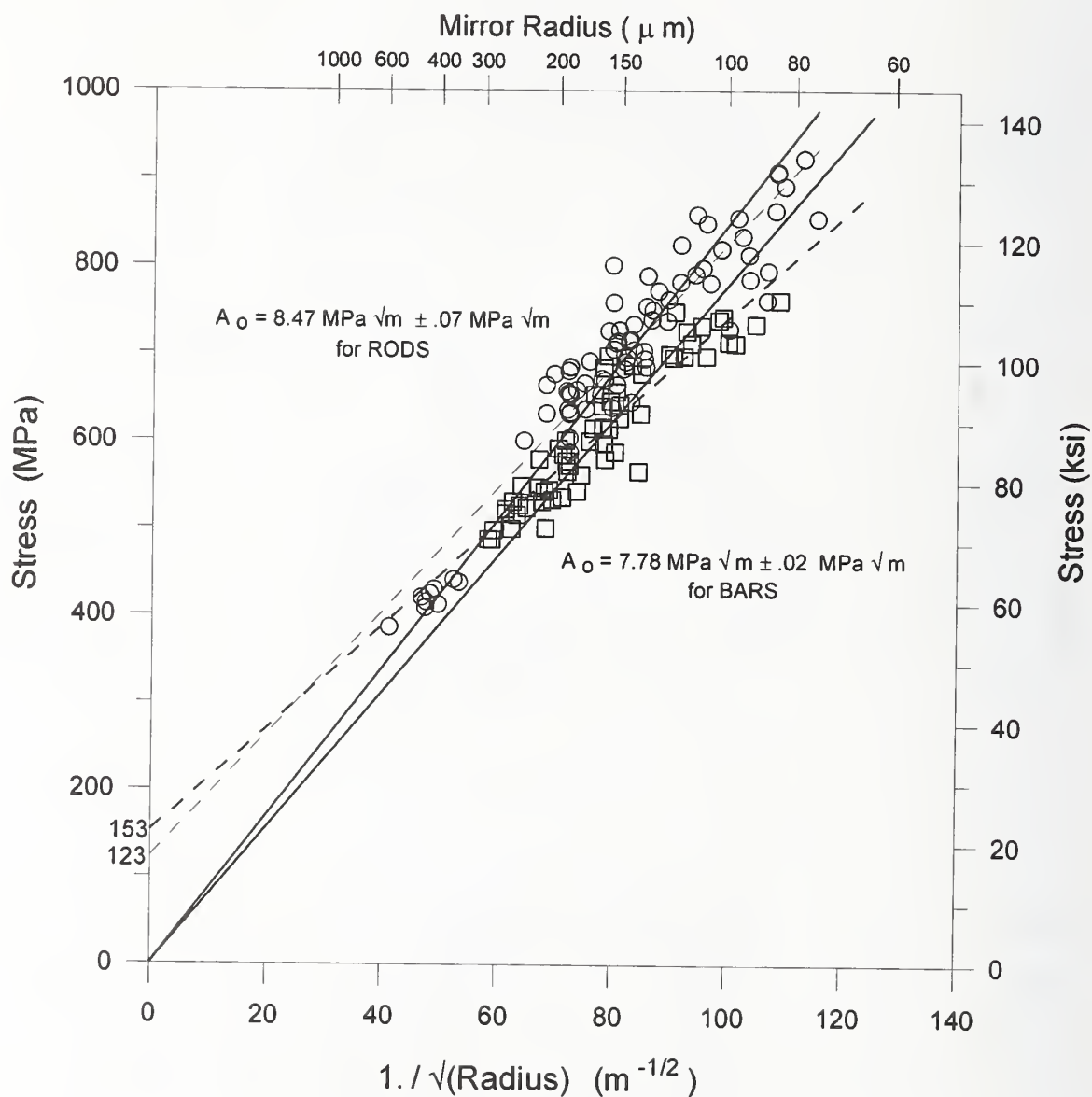
Kirchner and Conway[dd] noted that fracture mechanics stress intensity factors around surface connected semicircular and semielliptical flaws, could account for differences in mirror shapes in rods and bars. Hence, apparent mirror and branching constants from the two geometries could be slightly different.

One surprising observation was that the transversely ground bar specimens often had mirrors that were noticeably elongated along the specimen surface **(Figure A5 a-c)**. Elongations into the specimen *depth* are common in flexure specimens **(Figure A5 e,f)** and are due to the stress gradient, but the *lateral* elongation of the mirror dimension is noteworthy. The elongations were less noticeable in the rod specimens. The degree of mirror elongation along the bar specimen surface was directly related to the length and severity of the grinding flaws as shown in **Figure A6**. Weaker specimens had depth to width ratios much less than 1. Ellipticity is the ratio of the mirror radius into the depth to the radius along the surface. Weak specimens with shallow but very long surface cracks (e.g., "zipper cracks") had ellipticities as low as 0.68. From our experiences with the SRBSN and also with other glasses and ceramics, we conclude that flattened, elongated mirrors *are telltale signs* of scratches or transverse machining damage. We have even detected severely elongated and lobed mirrors in stress-free annealed glass disks. In some instances, a side lobe may even jut out from the side of the fracture mirror as shown in **Figure A5c.**

**Figure A7** illustrates two mechanisms by which elongated mirrors could form: either fracture unzips along the surface (a), or fracture starts and radiates outward from the two ends of the machining cracks. We believe the (a) is more plausible, especially since machining crack hackle lines on top of the "zipper machining cracks" **(Figures 31b and Appendix Figures C2c, d, f)** often "lean" or tilt to the left or right within the mirror. The tilts suggest that the origin crack unzips to the left and the right from the middle of the origin.

---

[dd] H. P. Kirchner and J. C. Conway, Jr., "Criteria for Crack Branching in Cylindrical Rods: I, Tension," *J. Amer. Ceram. Soc.*, 70 [6] (1987) 413-18.

*Figure A5*  Elongated fracture mirrors.   (a) – (c) show the lateral elongations that may arise from long machining cracks or scratches.   (d) – (f) shows the usual elongation patterns into the depth of the specimens as a results of the stress gradient in flexure specimens.  If the mirror is relatively small (high strength specimen or the specimen itself is large), the mirror will be semicircular (d).   If the specimen is smaller or is weaker, then the crack advances into a decreasing stress gradient as it penetrates into the depth. In such cases mirrors may be elongated in the depth direction (e) or may not form boundaries at all (f).



(a)

(b)

(c)

elongated

elongated

side lobe

(d)

(e)

(f)

semicircular

Flared into the depth and incomplete

Flared into the depth and incomplete
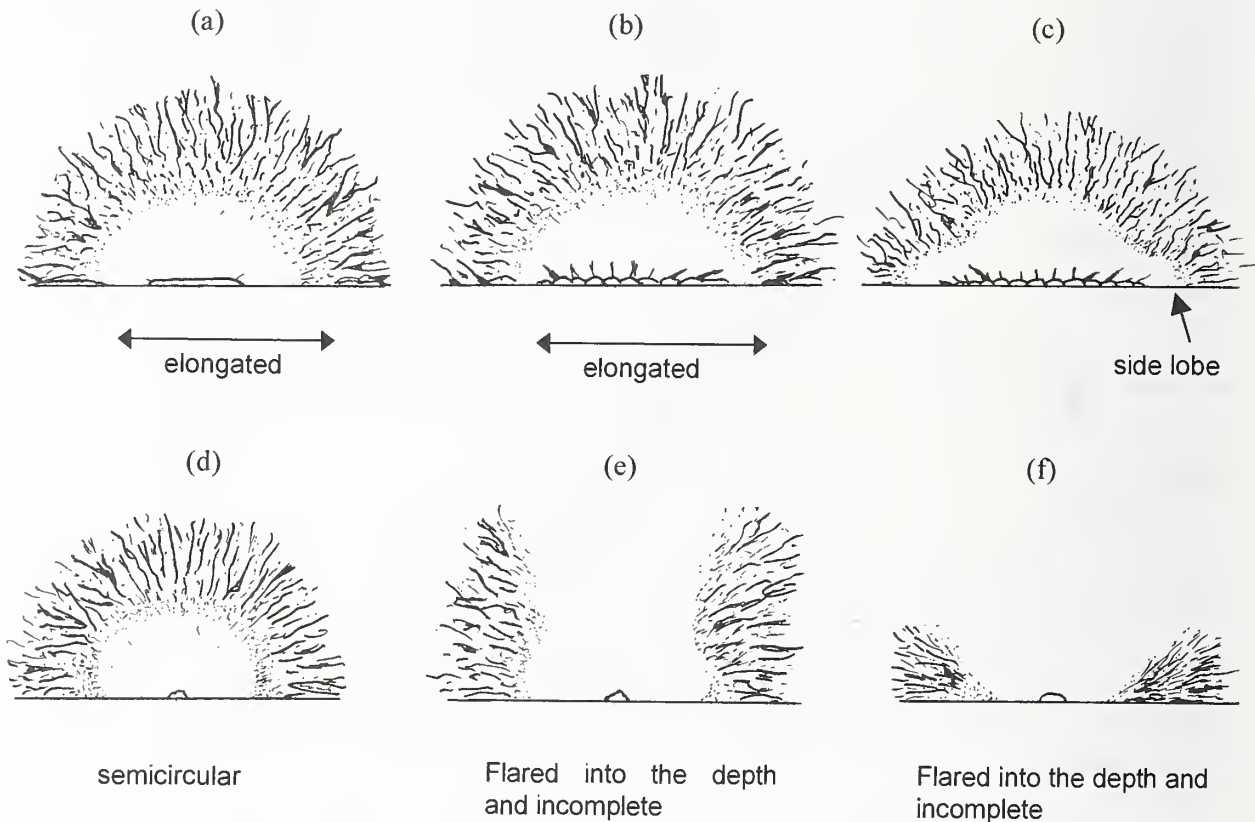
**Figure A6** Fracture mirror ellipticity for 30 rectangular bars with a 320 grit shop C transverse ground surface. The flaws were long shallow surface machining cracks in these specimens.
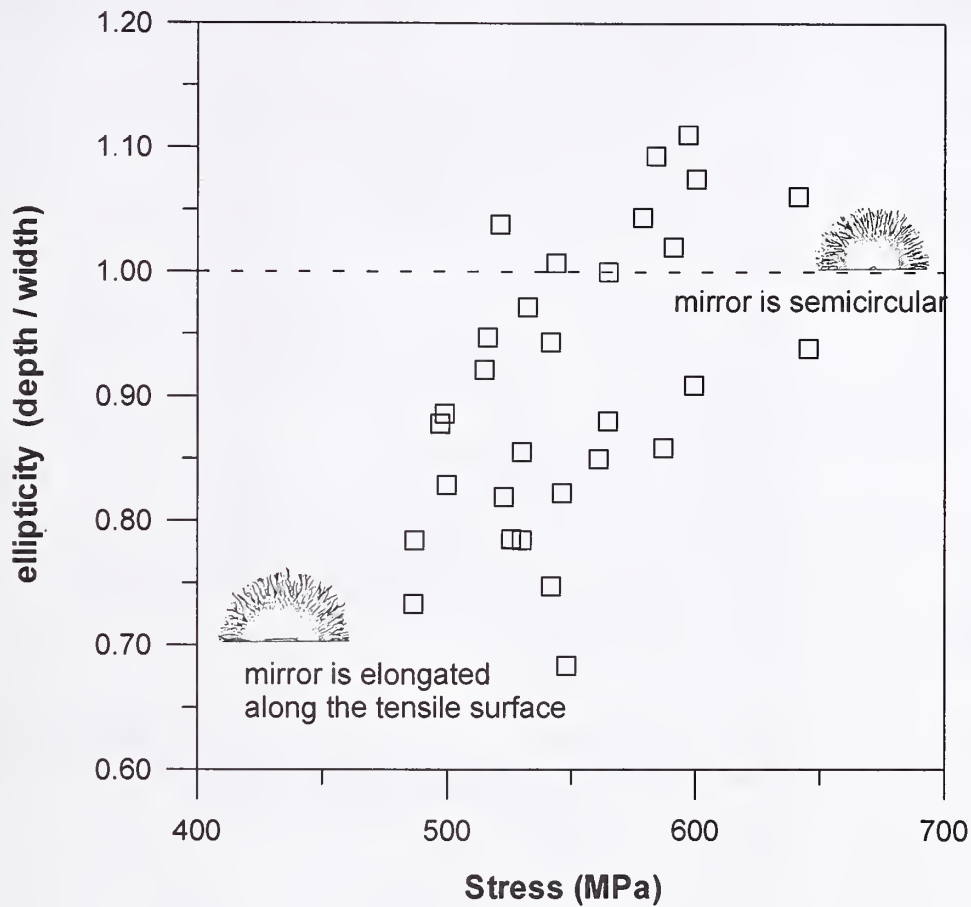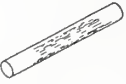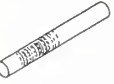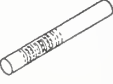


**Figure A7** Possible mechanisms to account for elongated mirrors associated with long surface scratches or machining cracks. (a) shows how crack propagation at the instant of fracture could commence from the flaw middle portion, but advance rapidly along the flaw ("unzip") before moving into the bar interior, or alternatively, (b), fracture could initiate simultaneously from both ends of the crack.
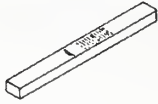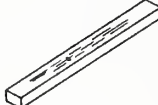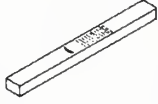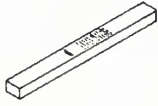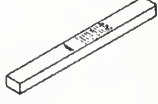
# Appendix B
## Machining Procedures

### RODS

| SHOP preparation | Machining Procedure |
|---|---|
| **C**<br>Longitudinal (Centerless)<br><br>320 grit | **Initial grinding;**<br>Conventional <u>Transverse</u> centerless grinding<br>Wheel: SD 320R100B, 12.7 mm wide, 203 mm diameter, resin bond<br>Rods ground down to 6.025 mm diameter by<br>Wheel depth of cut: 0.050 mm per pass<br>Wheel surface speed: 38.8 m/s (3650 rpm)<br>Workpiece rotation speed: 1100 rpm<br>Axial feed rate: 7.62 mm/s<br>Volumetric removal rate: 3.6 mm$^3$/s<br><br>**Finish grinding:**<br>Same wheel<br>Centerless Longitudinal Grinding<br>Wheel depth of cut: 0.005 mm for 5 passes<br>0.025 mm removal<br>Workpiece Rotation Speed: 2000 rpm<br>Axial feed rate: 3.6 mm/s<br>Volumetric removal rate: 0.17 mm$^3$/s |
| **N**<br>Transverse Centerless<br>600 grit | **Initial grinding:**<br>Wheel: D180-L100-B1/8, 19 mm wide, 254 mm diameter, resin bond<br>Wheel Surface Speed: 26.8 m/s (2015 rpm)<br>In feed: 0.050 mm per pass<br>Axial feed rate: 30 mm/s<br>Roughing final diameter: 7.05 mm<br><br>**Intermediate grinding:**<br>Wheel: ASD400B100B, 9.5 mm wide, 254 mm diameter, resin bond<br>Wheel Surface Speed: 32 m/s (2425 rpm)<br>In feed: 0.013 mm per pass<br>Axial feed rate: 30 mm/s<br>Workpiece rotational speed: 2890 rpm<br>Intermediate step final diameter: 6.3 mm<br><br>**Finish grinding:**<br>Total removal: .300 mm from diameter, .150 mm from each surface<br>Norton D10/20MIC-R75B619-1/8, 203 mm x 12.7 mm wheel, resin bond<br>Wheel surface speed: 25.8 m/s (2425 rpm)<br>In feed: 0.005 mm per pass<br>Axial feed rate: 23 m/s<br>Total removal: 0.300 mm from diameter, 0.150 mm from each surface |
| **W**<br>Transverse (cylindrical)<br><br>600 grit | **Initial grinding:**<br>Norton 6" x 12" chuck cylindrical grinder<br>320 diamond wheel, 100 concentration, 8" diameter x 1/2" wide, resin bond<br>Rods mounted on centers, plunge ground (no traverse)<br>Final roughing diameter: 6.305 mm – 6.356 mm<br><br>**Finish grinding:**<br>Cincinnati Milacron MD600-P100-B-1/8, 8" x 1/4" wheel<br>Surface speed: 18.6 m/s (1750 rpm)<br>Wheel in-feed: 0.025 mm per pass<br>Axial longitudinal feed rate: 4.2 to 5.1 mm/s (work piece)<br>Workpiece Rotational Speed: 950 rpm<br>Final finish diameter: 6.00 mm<br>Total removal: 0.300 mm from diameter, 0.150 mm from each surface |

| F<br>Transverse<br>600 grit | Details not reported. |
|---|---|
| **C**<br>Transverse<br>Centerless<br>320 grit | **Initial grinding;**<br>Conventional Transverse centerless grinding<br>Wheel: SD 320R100B, 12.7 mm wide, 203 mm diameter, resin bond<br>Rods ground down to 6.025 mm diameter by<br>Wheel depth of cut: 0.050 mm per pass<br>Wheel surface speed: 38.8 m/s (3650 rpm)<br>Work rotation speed: 1100 rpm<br>Axial feed rate: 7.62 mm/s<br>Volumetric removal rate: 3.6 mm$^3$/s<br><br>**Finish finishing:**<br>Same wheel<br>Wheel depth of cut: 0.005 mm for 5 passes<br>Work Rotation Speed: 680 rpm<br>Axial feed rate: 2.54 mm/s<br>Volumetric removal rate: 0.12 mm$^3$/s |
| **N**<br>Transverse<br>Centerless<br>220 grit | Wheel: Norton AD 220-R175B619-1/8, 12.7 mm wide, 203 mm diameter, resin bond<br>Depth of cut: 0.005 mm per pass<br>Wheel Surface speed: 30 m/s (2800 rpm)<br>Axial Feed Rate: 20 mm/s<br>Workpiece rotational speed: 2500 rpm<br>Removal rate: 0.94 mm$^3$/s<br>Total removal: 0.300 mm from diameter (final size 6.00 mm) |
| **S**<br>Transverse<br>Centerless then Lapped<br>30 μm grit | No details other than rods were centerless transverse ground<br>then lapped with 30 μm abrasive grit. |
| **F**<br>Transverse<br>150 or 180 grit? | Details not reported. |

# BARS

| SHOP | Specimen Preparation | Grit/ Depth of cut | Machining details |
|---|---|---|---|
| F | Transverse | 600 grit<br><br>5 μm? | Bars cut from Rods.<br><br>No details.<br>Probably ASTM C1161 standard procedure,<br>but with 600 grit resin bond wheel final finish added to only one 4 mm x 45 mm face.<br>Final removal with 600 grit wheel: 0.125 mm (specified) |
| C | Longitudinal | 320 grit<br><br>5 μm | Bars cut from Rods.<br><br>ASTM C 1161 multi-step sequence<br>Finish grinding with 320 grit longitudinal<br><br>Wheel: 320 grit, 100 concentration, 203 mm diameter, 12.7 mm wide<br>Wheel Surface speed 36 m/s (3400 rpm)<br>Wheel depth of cut: 0.005 mm per pass<br>Cross feed: 0.5 mm per pass<br>Table speed: 200 mm/sec<br>Volumetric removal rate: 0.5 mm$^3$/s |
| C | Transverse | 320 grit<br><br>5 μm | Bars cut from Rods.<br><br>ASTM C 1161 multi-step sequence<br>Except finish grinding with 320 grit wheel in transverse direction<br><br>Wheel: 320 grit, 100 concentration, 203 mm diameter, 12.7 mm wide<br>Wheel Surface speed 36 m/s (3400 rpm)<br>Wheel depth of cut: 0.005 mm per pass<br>Cross feed: 0.5 mm per pass<br>Table speed: 200 mm/sec<br>Volumetric removal rate: 0.5 mm$^3$/s |
| C | Transverse | 150 grit | Bars cut from 2 sets of SRBSN plates, not rods<br><br>Wheel surface speed: 30 m/s<br>Table speed: 0.025 m/sec<br>Down Feed: 0.050 mm per pass<br>Cross feed: 2.0 mm per pass |
| F | Transverse | 80 grit | Bars cut from 2 sets of SRBSN plates, not rods<br><br>Wheel surface speed: 30 m/s<br>Table speed: 0.025 m/sec<br>Down Feed: 0.050 mm per pass<br>Cross feed: 2.0 mm per pass |

## REFERENCES

1  S. Jahanmir, T. Strakna, G. Quinn, H. Liang, R. Allor, and R. West, "Effect of Grinding on Strength and Surface Integrity of Silicon Nitride: Part I," pp. 263-278 in *Machining of Advanced Materials*, ed. S. Jahanmir, Special Publication 847, NIST, Gaithersburg, MD, (1993).

2  S. Jahanmir, T. Strakna, G. Quinn, R. Kopp, S. Yoon, K. Kumar, "Effect of Grinding on Strength and Surface Integrity of Silicon Nitride: Part II," *idem,* pp. 279-294.

3  S. Jahanmir, L. K. Ives, L. Gill, and J. Filliben, "Effect of Grinding on Strength of a Sintered Reaction Bonded Silicon Nitride," *VDI Berichte*, 1276, (1996) 603-615.

4  L. K. Ives, S. Jahanmir, L. M. Gill, J. Filliben, "Effect of Grinding on Strength of a Sintered Reaction-Bonded Silicon Nitride," *Interceram*, 47 (3) (1998) 168-173.

5  H. K. Xu, S. Jahanmir, and L. K. Ives, "Material Removal and Damage Formation Mechanisms in Grinding Silicon Nitrides," *J. Mater. Res.*, 11 [7] (1996) 1717-1724.

6  T. J. Strakna, S. Jahanmir, R. L. Allor, and K. V. Kumar, "Influence of Grinding Direction on Fracture Strength of Silicon Nitride," *Trans. ASME, J. Eng. Mater. Techn.*, 118 (1996) 358-365.

7  G. D. Quinn, L. K. Ives, S. Jahanmir, and P. Koshy, "Fractographic Analysis of Machining Cracks in Silicon Nitride Rods and Bars," pp. 343 – 365 in *Fractography of Glasses and Ceramics IV,* Ceramic Transactions, Vol. 122, eds, J. Varner and G. Quinn, American Ceramic Society, Westerville, OH, 2001.

8  H. P. Kirchner, R. M. Gruver, and R. E. Walker, "Strength Effects Resulting from Simple Surface Treatments," pp. 353-363 in *The Science of Ceramic Machining and Surface Finishing*, NBS Special Publication 348, eds. S. Schneider and R. Rice, National Bureau of Standards, Gaithersburg, MD, 1972.

9  H. S. Starrett, "The Influences of Material Removal on the Strength and Surface of an Alumina," *idem*, 377 - 389.

10  R. H. Licht, S. Ramanath, M. Simpson, and E. Lilly, "Innovative Grinding Wheel Design for Cost-Effective Machining of Advanced Ceramics," Oak Ridge National Laboratories Final Report, ORNL/sub/93-SM037-1, 1996.

11  M. J. Andrews, A. A. Wereszczak, and K. Breder, "Predictions of the Inert Strength Distribution of $Si_3N_4$ Diesel Valves," *Ceram. Sci. and Eng. Proc.*, 20 (3) (1999) 555-563.

12  H. P. Kirchner, R. M. Gruver, and D. M. Richard, "Fragmentation and Damage Penetration During Abrasive Machining of Ceramics," pp. 23-42 in *The Science of Ceramic Machining and Surface Finishing II*, eds. B. J. Hockey and R. W. Rice, Special Publication 562, National Bureau of Standards Gaithersburg, MD, 1979.

13  M. Hakulinen, "Residual Strength of Ground Hot Isostatically Pressed Silicon Nitride," *J. Mat. Sci.,* 20 (1985) 1049-1060.

14  R. L. Allor and R. R. Baker, "Effect of Grinding Variables on Strength of Hot Pressed Silicon Nitride," Am. Soc. Mech. Engs. Paper 83-GT-203, ASME, NY, 1983.

15  R. L. Allor, R. K. Govila, and T. J. Whalen, "Influence of Machining on Strength Properties of Turbine Materials," *Ceram. Eng. and Sci. Proc.,* 3 (1982) 392-404.

16  C. A. Anderson and R. J. Bratton, "Effect of Surface Finish on the Strength of Hot-Pressed Silicon Nitride," pp. 463-476 in *The Science of Ceramic Machining and Surface Finishing II*, eds. B. J. Hockey and R. W. Rice, Special Publication 562, National Bureau of Standards, Gaithersburg, MD, 1979.

17  C. C. Wu and K. R. McKinney, "The Effect of Surface Finishing on the Strength of Commercial Hot Pressed $Si_3N_4$," *idem*, pp. 477–481.

18  K. Breder, A. A. Wereszczak, and M. J. Andrews, "Exploration of the Weibull Modulus as a Function of Surface Preparation and Flexure Testing Conditions," *Ceram. Eng. and Sci. Proc.*, 19 [4] (1998) 89-97.

19  M. Ota and M. Miyahara, "The Influence of Grinding on the Flexural Strength of Ceramics," 4th Int. Grinding Conference of the Society of Manufacturing Engineers, Vol. 2, paper # MR90-538, 1990.

20  R. L. Allor, T. J. Whalen, J. R. Baer, and K. V. Kumar, "Machining of Silicon Nitride: Experimental Determination of Process/Property Relationships," pp. 223-234 in *Machining of Advanced Materials*, ed. S. Jahanmir, Special Publication 847, NIST, Gaithersburg, MD, (1993).

21  J. E. Mayer, Jr. and G. P. Fang, "Diamond Grinding of Silicon Nitride Ceramic," *idem,* pp. 205-222.

22  J. E. Meyer, Jr. and G. P. Fang, "Effect of Grit Depth of Cut on Strength of Ground Ceramics," *Annals of the CIRP*, 43 (1) (1994) 309-312.

23  H. G. Wobker and H. K. Tonshoff, "High Efficiency Grinding of Structural Ceramics," pp. 171-183 in *Machining of Advanced Materials*, ed. S. Jahanmir, Special Publication 847, NIST, Gaithersburg, MD, (1993).

24  J. A. Salem, N. N. Nemeth, L. M. Powers, and S. R. Choi, "Reliability Analysis of Uniaxially Ground Brittle Materials," Trans. ASME, paper 95-GT-31, ASME, 1995.

25  M. B. Thomas, R. D. West, W. E. West, Jr. and K. Wyckoff, "Effects of Machining Parameters on the Surface Finish and Strength of Hot-Pressed Silicon Nitride," Therm Inc., Ithaca, NY, 1985.

26  K. E. Puttick, M. R. Rudman, M. A. Kirwan, R. Quinn, and G. Syers, "Machining Damage in Silicon Nitride," *J. Hard Materials,* 4 (1993) 55-76.

27  K. Li and T. W. Liao, "Surface/Subsurface Damage and the Fracture Strength of Ground Ceramics," *J. Mater. Proc. Technol.,* 57 (1996) 207-220.

28  T. Hollstein, W. Pfeiffer, M. Rombach, and B. Thielicke, "Analysis of Machining Damage in Engineering Ceramics by Fracture Mechanics, Fractography and X-Ray Diffraction," pp. 145-169 in *Fractography of Glasses and Ceramics, III*, Ceramic Transactions, Vol. 64, eds. J. Varner, V. Fréchette and G. Quinn, American Ceramic Society, Westerville, OH, 1996.

29  R. W. Rice and J. J. Mecholsky, Jr., "The Nature of Strength Controlling Machining Flaws in Ceramics," pp. 351- 378 in *The Science of Ceramic Machining and Surface Finishing II*, eds. B. J. Hockey and R. W. Rice, Special Publication 562, NBS, Gaithersburg, MD, 1979.

30  R. W. Rice, J. J. Mecholsky, Jr., and P. F. Becher, "The Effect of Grinding Direction on Flaw Character and Strength of Single Crystal and Polycrystalline Ceramics," *J. Mat. Sci.,* 16 (1981) 853-862.

31  J. J. Mecholsky, Jr., S. W. Freiman, and R. W. Rice, "Effect of Grinding on Flaw Geometry and Fracture of Glass," *J. of the Amer. Ceram. Soc.,* 60 (3-4) (1997) 114-117.

32  R. W. Rice, "Effects of Ceramic Microstructural Character on Machining Direction – Strength Anisotropy," pp. 223-234 in *Machining of Advanced Materials*, ed. S. Jahanmir, NIST SP 847, Gaithersburg, MD, (1993).

33  M. R. Foley, V. K. Pujari, L. C. Sales, and D. M. Tracey, "Silicon Nitride Tensile Strength Database from Ceramic Technology Program Processing for Reliability Project," pp. 3 -18 in *Life Prediction Methodologies and Data for Ceramic Materials*, ASTM STP 1201, eds. C. R. Brinkman and S. F. Duffy, ASTM, Westerville, OH, 1994.

34  V. K. Pujari, D. M. Tracey, M. R. Foley, N. I. Paille, P. J. Pelletier, L. C. Sales, C. A. Wilkins, and R. L. Yeckley, "Development of Improved Processing and Evaluation Methods for High Reliability Structural Ceramics for Advanced Heat Engine Applications, Phase I, Oak Ridge National laboratory Technical Report, ORNL/Sub/89-SB182/1, Aug. 1983.

35  G. D. Quinn, "Flexure Strength of Advanced Structural Ceramics: A Round Robin," *J. Amer. Ceram. Soc.,* 73 (8) (1990) 2374-84.

36  H. Richter, "From Ceramic Material to Ceramic Product," presented at the 7th European Ceramic Society Conference, Brugge, Belgium, Sept. 12, 2001.

37 ASTM C 1322-02, "Standard Practice for Fractography and Characterization of Fracture Origins in Advanced Ceramics," *Annual Book of Standards, Volume 15.01,* ASTM, West Conshohoken, PA 2002.

38 J. J. Swab and G. D. Quinn, "Fractography of Advanced Structural Ceramics, Results from the VAMAS Round Robin Exercise," VAMAS Report #19, National Institute of Standards and Technology, Gaithersburg, MD, February, 1995.

39 J. J. Swab and G. Quinn, "Results of a Round Robin Exercise on the Fractography of Advanced Structural Ceramics," *Ceram. Eng. and Sci. Proc.,* 15 (5) (1994) 867-876.

40 ASTM C 1421-99, "Standard Test Method for the Determination of Fracture Toughness of Advanced Ceramics," *Annual Book of Standards, Vol. 15.01,* 2001.

41 G. D. Quinn, J. J. Swab, and M. Motyka, "Fracture Toughness of a Toughened Silicon Nitride by ASTM C 1421," accept by *J. Amer. Ceram. Soc.,* 2002.

42 B. Mikijelj, private communication, 2000.

43 H. H. K. Xu, S. Jahanmir, amd L. K. Ives, "Effect of Machining Conditions on the Strength of Sintered-Reaction-Bonded Silicon Nitride," pp. 39 –52 in Proceedings of the 7th Program Review Meeting, NIST Ceramic Machining Consortium, Sept. 27-28, 1995 NIST, Gaithersburg, MD 20899.

44 T. Fett, D. Munz, A. B. Kounga, J. Rödel, and G. D. Quinn, "Bridging Stresses in Sintered Reaction-Bonded $Si_3N_4$ from COD Measurements," to be subm. *J. Amer. Ceram. Soc,* 2003.

45 A.B. Kounga, T. Fett, J. Rödel, and G. D. Quinn, "Crack-tip Toughness Measurements on a Sintered Reaction Bonded $Si_3N_4$," to be subm. *J. Amer. Ceram. Soc,* 2003.

46 ASTM C 1161-96, "Standard Test Method for Flexural Strength of Advanced Ceramics at Ambient Temperature," *Annual Book of Standards, Vol. 15.01,* ASTM, West Conshohocken, PA, 2001.

47 G. D. Quinn, "Weibull Strength Scaling for Standardized Rectangular Flexure Specimens," *J. Amer. Ceram. Soc.,* 86 [3] (2003) 508-511.

48 G. D. Quinn, "The Effective Volumes and Surfaces for Cylindrical Rods in Flexural Loadings," *J. Am. Ceram. Soc.,* idem, 475-480.

49 J. C. Newman and I. S. Raju, "An Empirical Stress Intensity Factor Equation for the Surface Crack," *Eng. Fract. Mech.,* 15 [1-2] (1981) 185-192.

50 G. D. Quinn, R. J. Gettings, and J. J. Kübler, "Fractography and the Surface Crack in Flexure (SCF) Method for Evaluating Fracture Toughness of Ceramics," pp. 107 - 144 in *Fractography of Glasses and Ceramics,* Ceramic Transactions, Vol. 64, American Ceramic Society, Westerville, OH, 1996.

51 ASTM C 1239-95, "Standard Practice for Reporting Uniaxial Strength Data and Estimating Weibull Distribution Parameters for Advanced Ceramics," *Annual Book of Standards, Vol. 15.01,* ASTM, 2001.

52 S. Malkin and M. Huerta, "Glass Grinding Mechanisms and Influence on the Finish Surface and Strength," pp. 93-106 in *The Science of Ceramic Machining and Surface Finishing II,* eds. B. J. Hockey and R. W. Rice, Special Publication 562, NBS, Gaithersburg, MD, 1979.

53 M. G. Schinker and W. Döll, "Plasticity and Fracture Induced by Scratching Optical Glass at High Speeds," pp. 115-133 in *Strength of Inorganic Glass,* ed. C. R. Kurkjian, Plenum, NY, 1985.

54 E. S. Alfaro, J. V. Guiheen, and J. R. Varner, "Insights Provided by Fractography in Strength Testing of Machined $Si_3N_4$ and Indented $Al_2O_3$," pp. 485-508 in *Fractography of Glasses and Ceramics, II,* eds. V. D. Frechette and J. R. Varner, Ceramic Transactions, Vol. 17, American Ceramic Society, Westerville, OH, 1991.

55 L. K. Ives, C. J. Evans, S. Jahanmir, R. S. Polvani, T. J. Strakna, and M. L. McGloufin, "Effect of Ductile-Regime Grinding on the Strength of Hot-isostatically Pressed Silicon Nitride," pp. 341-352 in *Machining of Advanced Materials,* ed. S. Jahanmir, NIST SP 847, Gaithersburg, MD, (1993).

56 D. B. Marshall, A. G. Evans, B. T. Khuri Yakub, J. W. Tien, and G. S. Kino, "The Nature of Machining Damage in Brittle Materials," *Proc. Roy. Soc. Lond., A* 385 (1983) 461- 475.

57  K. Mörgenthaler, "Damage Depths and Machining Removal Amounts, Example for NC 132 for a Particular Grinding Machine," Private Communication, 1989.

58  D. W. Richerson, T. M. Yonushonis, and G. Q. Weaver, Figure 6 in "Properties of Silicon Nitride Rotor Blade Materials," pp. 193-218, *Proceedings of the 1977 DARPA/NAVSEA Ceramic Gas Turbine Demonstration Engine Program Review*, Castine, Maine, eds., J. J. Fairbanks and R. W. Rice," Metals and Ceramics Information Center MCIC Report 78-36, Battelle, Columbus, OH, March, 1978.

59  G. D. Quinn, Unpublished Research, Watertown Arsenal, Watertown, MA, 1980.

60  S. Mizuno, N. Kobayashi, and K. Miyata, "Analysis of Sintered Silicon Nitride Grinding Damage," Society of Automotive Engineers paper 930163, March 1993, SAE, Warrendale, PA.

61  W. Kanematsu, M. Sando, L. K. Ives, R. Marinenko, and G. D. Quinn, "Determination of Machining Crack Geometry by Dye Penetration Technique," *J. Amer. Ceram. Soc.*, 84 [4] (2001) 795-800.

62  W. Kanematsu and L. K. Ives, "Propagation Behavior of Machining Cracks in Delayed Fracture," subm. to *J.. Amer. Ceram. Soc.*, 2002.

63  G. D. Quinn and J. B. Quinn, "Slow Crack Growth in Hot-Pressed Silicon Nitride," pp. 603 – 636 in *Fracture Mechanics of Ceramics*, Vol. 6, eds. R. C. Bradt, A. G. Evans, D. P. H. Hasselman, and F. F. Lange, Plenum, NY, 1983.

64  G. D. Quinn, "Fracture Mechanism Maps for Advanced Structural Ceramics, Part 1, Methodology and Hot-Pressed Silicon Nitride Results," *J. Mat. Sci.*, 25 (1990) 4361-4376.

65  A. J. Pyzik, D. F. Carroll, C. J. Hwang, and A. R. Prunier, "Self Reinforced Silicon Nitride – A New Microengineered Ceramic," pp 584-593 in *4th International Symposium on Ceramic materials and Components for Engines*," eds. R. Carlsson, T. Johansson, and L. Kahlman, Elsevier, New York, 1992.

66  A. J. Pyzik and D. R. Beaman, "Microstructure and Properties of Self-Reinforced Silicon Nitride," *J. Amer. Ceram. Soc.*, 76 [11] (1993) 2737-44.

67  G. D. Quinn, J. J. Swab, and M. D. Hill, "Fracture Toughness by the Surface Crack in Flexure (SCF) Method: New Test Results," *Ceram. Eng. and Sci. Proc.*, 18 [4] (1997) 163-172.

68  G. D. Quinn, K. Xu, R. J. Gettings, J. A. Salem, and J. J. Swab, "Does Anyone Know the Real Fracture Toughness? SRM 2100: The World's First Ceramic Fracture Toughness Reference Material," pp. 76-93 in *Fracture Resistance Testing of Monolithic and Composite Brittle Materials, ASTM STP 1409,* J. A. Salem, G. D. Quinn, and M. G. Jenkins, eds. ASTM, West Conshohocken, PA, 2002.

69  G. D. Quinn and J. J. Swab, "Comparisons of Calculated and Measured Flaw Sizes," pp. 175 – 192 in *Fractography of Glasses and Ceramics IV,* Ceramic Transactions, Vol. 122 eds, J. Varner and G. Quinn, American Ceramic Society, Westerville, OH, 2001.

70  G. D. Quinn and J. J. Swab, "Fractography and Estimates of Fracture Origin Size from Fracture Mechanics," *Ceram. Eng. and Sci. Proc.*, 17 [3] (1996) pp. 51 -58.

71  R. W. Rice, "Fracture Initiation in Ceramics, Challenges to NDE and Processing," pp. 1057-1064 in *Ceramic Developments*, 1988, eds. C. Sorrell and B. Ben-Nissan, Materials Science Forum Vols. 34-36, Trans Tech Publ., Switzerland.

72  T. Fett and D. Munz, "Evaluation of R-Curve Effects in Ceramics," *J. Mat. Sci.*, 28 (1993) 742-752.

73  L. K. Ives and S. Jahanmir, "Grinding Optimization for Advanced Ceramics," page 13 in *7th Program Review Meeting Proceedings, NIST Ceramic Machining Consortium*, September 27-28, 1995, NIST, Gaithersburg, MD 20899.

74  Private communication, R. Chand, Oct. 2002.

75  B. G. Koepke and R. J. Stokes, "Effect of Workpiece Properties on Grinding Forces in Polycrystalline Ceramics," pp. 75 – 91 in *The Science of Ceramic Machining and Surface Finishing II*, eds. B. J.

Hockey and R. W. Rice, National Bureau of Standards Special Publication 562, U. S. Government Printing Office, Washington, D.C., 1979.

76  H. H. K. Xu, N. P. Padture, and S. Jahanmir, "Effect of Microstructure on Material Removal Mechanisms and Damage Tolerance in Abrasive Machining of Silicon Carbide," *J. Amer. Ceram. Soc.*, 78 [9] 2442-2448.

77  H. H. K. Xu, S. Jahanmir, L. K. Ives, L. S. Job, and K. T. Ritchie, "Short-Crack Toughness and Abrasive Machining of Silicon Nitride," J. Amer. Ceram. Soc., *79* [12] (1996) 3055-3064.

78  D. B. Marshall, B. R. Lawn and R. F. Cook, "Microstructural Effects on Grinding of Alumina and Glass-Ceramics," J. Amer. Ceram. Soc., *70* [6] (1997) C139-C140.

79  H. P. Kirchner and J. C. Conway, Jr., "Mechanisms of Material Removal and Damage Penetration During Single Point Grinding of Ceramics," pp. 53 –61 in *Machining of Ceramic Materials and Components*, ed. K. Subramanian and R. Komanduri, Amer. Soc. of Mech. Eng., New York, 1986.

80  W. Pfeiffer and T. Hollstein, "Damage Determination and Strength Prediction of Machined Surfaces by X-ray Diffraction Techniques," pp. 235-245 in *Machining of Advanced Materials*, ed. S. Jahanmir, NIST SP 847, Gaithersburg, MD, (1993).

81  R. Samuel, S. Chandrasekar, T. N. Farris, and R. H. Licht, "Effect of Residual Stresses on the Fracture of Ground Ceramics," *J. Amer. Ceram. Soc.*, 72 [10] (1989) 1960-1966.

82  D. Johnson-Walls, A. G. Evans, D. B. Marshall, and M. R. James, "Residual Stresses in Machined Ceramic Surfaces," *J. Amer. Ceram. Soc.*, 69 [1] (1986) 44-47.

83  E. R. Shand, "Strength of Glass – The Griffith Method Revised," *J. Amer. Ceram. Soc.*, 48 (1) (1965) 43-49.

84  G. D. Quinn and G. Wirth, "Biaxial Stress Rupture of Silicon Nitride," *Mat. Sci. and Eng.*, A109 (1989) 147-152.

85  M. B. Thomas, R. D. West and W. E. West, Jr., "Grinding Hot Pressed Silicon Nitride for Optimum Surface Finish and Strength," unpublished private communication, 1986.

86  R. W. Rice, *Mechanical Properties of Ceramics and Composites, Grain and Particle Effects*, Marcel Dekker, New York, 2000.

87  R. W. Rice, "Effects of Ceramic Microstructural Character on Machining Direction – Strength Anisotropy," pp. 185-204 in *Machining of Advanced Materials*, ed. S. Jahanmir, NIST SP 847, Gaithersburg, MD, (1993).

88  H. H. K. Xu, L. Wei, and S. Jahanmir, "Influence of Grain Size on the Grinding Damage of Alumina," *J. Amer. Ceram Soc.*, 79 [5] (1996) 1307-1313.

89  W. Kanematsu, Y. Yamauchi, T. Ohji, S. Ito, and K. Kubo, "Formulation of the Effect of Surface Grinding on Strength Degradation of Ceramics," *J. Ceram. Soc. Japan,* 100 [6] (1992) 775-779.

90  K. Subramanian, T. K. Puthananyady, and S. Liu, "Diamond Abrasive Finishing of Brittle Materials – An Overview," Proceedings of the Supertech 1996 Conference, Lawrence Livermore Laboratories, November 1996, Publ. by the Diamond Association of America, Columbus, OH, 1996.

91  K. Subramanian, P. D. Redington, and S. Ramanath, "A Systems Approach for Grinding of Ceramics," pp 43 – 53 in *Machining of Advanced Materials*, ed. S. Jahanmir, NIST SP 847, Gaithersburg, MD, (1993).

92  MIL STD 1942 (MR) "Flexural Strength of High Performance Ceramics at Ambient Temperature," 21 Nov. 1983, U. S. Army Materials Research Center, Watertown, MA. (This standard was superceded by ASTM C 1161 in May 1998.)

93  ISO 14704 (2000) "Fine Ceramics (Advanced Ceramics, Advanced Technical Ceramics) – Test Method for Flexural Strength of Monolithic Ceramics at Room Temperature," International Organization for Standards, Geneva, SW, 2000.

94  ASTM F 417-75, "Standard Test Method for Flexural Strength (Modulus of rupture) of Electronic-Grade Ceramics," *Annual Book of Standards*, Volume 15.02, ASTM, West Conshohocken, PA, 2001.

95  ASTM C 1495-01, "Standard Test Method for Effect of Surface Grinding on Flexure Strength of Advanced Ceramics," *Annual Book of Standards*, Volume 15.01, ASTM, West Conshohocken, PA, 2001.

96  D. B. Marshall, "Failure from Surface Flaws," pp. 190 – 220 in *Fracture in Ceramic Materials: Toughening Mechanisms, Machining Damage, Shock,* ed. A. G. Evans, Noyes Publ. NY, 1984.

97  R. W. Rice, "Monolithic and Composite Ceramic Machining Flaw-Microstructure-Strength Effects: Model Evaluation," *J. Eur. Ceram. Soc.*, 22 (2002) 1411-1424.

98  R. Sedlacek, F. A. Halden, and P. J. Jorgensen, "The Effect of Grinding Variables on the Strength and Surface Finish of Alumina," pp. 391–398 in *The Science of Ceramic Machining and Surface Finishing*, Special Publication 348, NBS, Gaithersburg, MD, 1970.

99  R. W. Rice, "Machining of Ceramics," pp. 287-343 in *Ceramics for High Performance Applications,"* eds. J. J. Burke, A. E. Gorum, and R. N. Katz, Brook Hill Publ. Co., Chestnut Hill, MA, 1974.

The National Institute of Standards and Technology was established in 1988 by Congress to "assist industry in the development of technology . . . needed to improve product quality, to modernize manufacturing processes, to ensure product reliability . . . and to facilitate rapid commercialization . . . of products based on new scientific discoveries."

NIST, originally founded as the National Bureau of Standards in 1901, works to strengthen U.S. industry's competitiveness; advance science and engineering; and improve public health, safety, and the environment. One of the agency's basic functions is to develop, maintain, and retain custody of the national standards of measurement, and provide the means and methods for comparing standards used in science, engineering, manufacturing, commerce, industry, and education with the standards adopted or recognized by the Federal Government.

As an agency of the U.S. Commerce Department's Technology Administration, NIST conducts basic and applied research in the physical sciences and engineering, and develops measurement techniques, test methods, standards, and related services. The Institute does generic and precompetitive work on new and advanced technologies. NIST's research facilities are located at Gaithersburg, MD 20899, and at Boulder, CO 80303. Major technical operating units and their principal activities are listed below. For more information visit the NIST Web site at http://www.nist.gov, or contact the Publications and Program Inquiries Desk, 301-975-3058.

---

## Office of the Director
- National Quality Program
- International and Academic Affairs

## Technology Services
- Standards Services
- Technology Partnerships
- Measurement Service
- Information Services
- Weights and Measures

## Advanced Technology Program
- Economic Assessment
- Information Technology and Applications
- Chemistry and Life Sciences
- Electronics and Photonics Technology

## Manufacturing Extension Partnership Program
- Regional Programs
- National Programs
- Program Development

## Electronics and Electrical Engineering Laboratory
- Microelectronics
- Law Enforcement Standards
- Electricity
- Semiconductor Electronics
- Radio-Frequency Technology [1]
- Electromagnetic Technology [1]
- Optoelectronics [1]
- Magnetic Technology [1]

## Manufacturing Engineering Laboratory
- Precision Engineering
- Manufacturing Metrology
- Intelligent Systems
- Fabrication Technology
- Manufacturing Systems Integration

## Chemical Science and Technology Laboratory
- Biotechnology
- Process Measurements
- Surface and Microanalysis Science
- Physical and Chemical Properties [2]
- Analytical Chemistry

## Physics Laboratory
- Electron and Optical Physics
- Atomic Physics
- Optical Technology
- Ionizing Radiation
- Time and Frequency [1]
- Quantum Physics [1]

## Materials Science and Engineering Laboratory
- Intelligent Processing of Materials
- Ceramics
- Materials Reliability [1]
- Polymers
- Metallurgy
- NIST Center for Neutron Research

## Building and Fire Research Laboratory
- Applied Economics
- Materials and Construction Research
- Building Environment
- Fire Research

## Information Technology Laboratory
- Mathematical and Computational Sciences [2]
- Advanced Network Technologies
- Computer Security
- Information Access
- Convergent Information Systems
- Information Services and Computing
- Software Diagnostics and Conformance Testing
- Statistical Engineering

---

[1] At Boulder, CO 80303.
[2] Some elements at Boulder, CO.